Dynamic responses analysis for accidental collision scenarios of floating offshore wind turbine.

Yichi Zhang

A thesis submitted for the degree of

Doctor of Philosophy

School of Engineering

Newcastle University, United Kingdom

November 2021

Abstract

Offshore wind energy has been becoming one of the most attractive alternatives for fossil fuel energy in recent decades. Like all other offshore structures, offshore wind turbines are subjected to ship collision hazards as well. However, little attention has been paid to the ship-collision problem, especially for the floating offshore wind turbines (FOWTs). The FOWT is a typical rigid-flexible coupled multi-body system, and the investigation of the dynamic responses of FOWTs under ship collision scenarios is crucial and challenging. This thesis research conducts a comprehensive analysis on both external and internal dynamics of a Spar-type FOWT under ship collision scenarios, and two innovative methods are newly proposed.

Firstly, by combining an analytical model of ship collision and a FOWT simulation tool, DARwind, a novel integrated method for predicting global dynamic responses of FOWT is proposed. In this integrated method, the analytical model is an extended implementation of a ship collision model, based on the conservation of momentum principle. DARwind program is an aero-hydro-servo-elastic coupled nonlinear analysis tool for FOWTs. The integrated method can analyze and predict the global dynamic responses of FOWTs during the ship collision scenario, which include the 6DOF global motions, the tower vibration, the mooring tension, the blades tip deflection, and aerodynamic performance, etc.

Based on the development of the integrated method, cases of studies are conducted. Head-on collision cases in various environmental conditions are studied. The responses of global motions, mooring tensions, nacelle accelerations, blade tip deformation, and aerodynamic loads are investigated. It is found that the impact velocity can significantly influence motions and the mooring systems, especially in still water conditions. In wave conditions, the tower top deflection shows obvious change after ship collisions. Additionally, in wind-wave conditions, the edgewise blade tip deformation (inside the rotor plane) is found to be more sensitive than that in flapwise (outside the rotor plane). To further assess the safety of FOWT, the acceleration of the nacelle is examined, because the electric equipment might be sensitive to the axis

acceleration.

Secondly, for purpose of investigating the internal dynamics of FOWTs during ship collision scenarios, a novel fully coupled method based on the Nonlinear Finite Element Method (NLFEM) is also proposed. This method employs the user-defined subroutine in LS-DYNA code to model the hydrodynamic, aerodynamic, and mooring loads. These loads are varying over time during the simulation and are updated every 100 timesteps in LS-DYNA structural analysis to maintain accuracy and efficiency. The hydrodynamic loads are calculated in a specific way, with linear potential-flow theory, and the mooring loads are evaluated with a simplified linearized model while the aerodynamic loads are calculated based on a look-up table for thrust coefficients. This newly proposed method is able to calculate the external and the internal dynamics of FOWTs simultaneously under ship collision scenarios.

With the proposed fully coupled method, cases of studies have been conducted. The influences on the impact force and structural deformation from factors such as impact velocity, tower flexibility, deformability, and environmental loads are investigated and discussed. The external dynamic responses predicted by this coupled method are also compared with those from the integrated method described above. Good agreement has been achieved in low-energy impact scenarios. But for the high-speed energy impact scenarios with critical structural damage, the accuracy of the integrated method is not very satisfactory because some basic assumptions in the method are violated. This brings some further work.

In conclusion, two novel methods are newly proposed during the research of this Ph.D. project. The proposed methods are reliable to assess the dynamic performance of FOWTs under ship-FWOT collision scenarios considering the wave-wind effects. The results comprehensively reveal the responses of FOWTs under ship collision scenarios from the views of both external and internal dynamics, which could help to understand the ship-FOWT collision mechanisms better. Additionally, due to the lack of ship-FOWT collision studies, this work could supplement or benefit the engineering practice in the industrial fields, such as ship-FOWTs collision modelling, crashworthiness design, especially for the large-size FOWTs which enhance the maintenance challenges.

Acknowledgement

First and foremost, I would like to express the sincere gratitude to my supervisor, Prof. Zhiqiang Hu, for his valuable guidance and continuous encouragement through the Ph.D project. His professional vision and advice in ocean engineering have greatly support me to overcome difficulties and carry out my research project independently. Prof. Hu is a very kind teacher, who not only provided shows his expertise in academic, but also shows his positive attitude to life, which deeply inspires me.

I would like to thank my previous second supervisors, Dr. Xiangyin Meng and Dr. Do Kyun Kim, who have left the university and my current second supervisor, Dr. Simon Benson. I also wish to thank Dr. Yongchang Pu, Dr. Wenxian Yang, Dr. Narakorn Srinil for some valuable talks during my Ph.D study. The thanks are also extended to other staffs and our university for their efforts to support us for our research especially in the pandemic period of Covid-19.

During the second year of Ph.D study, I have got an exchange study and communication in Jiangsu University of Science and Technology, China. I would like to thank Prof. Kun Liu in Jiangsu University of Science and Technology and his students for providing warm help in my daily life, sharing valuable research experiences and providing supports for some software usage.

The thanks are also sent to my friends in Newcastle. Peng Chen has generously provided useful experiences on using the *DARwind* program when I conducted the first part of my research so that the research can go more smoothly. He not only provides useful discussions in academic, but also takes me out of the office to enjoy the natural scenery in Europe. The thanks are also sent to Yihong Li, Yerong Zhang, Fengshuo Xing, Xuhua Yan, Jianwen Xu, Dr. Shuai Sun, Dr. Baicheng Lyu, and all my office mates for filling my life in Newcastle with happiness.

Last but not the least, I would like to express my deepest gratitude to my parents, who have always supported me and encouraged me through my study and life abroad.

List of Publications

Journal Papers:

Zhang, Y., Hu, Z., Ng, C., Jia, C., & Jiang, Z. (2021). Dynamic responses analysis of a 5 MW spar-type floating wind turbine under accidental ship-impact scenario. *Marine Structures*, *75*, 102885.

Zhang, Y., Hu, Z., An aero-hydro coupled method for investigating ship collision against a floating offshore wind turbine. Submitted to *Marine Structures*. Under review

Conference papers:

Zhang, Y., & Hu, Z. (2019, June). Dynamic Responses Prediction for a Spar-Type Offshore Floating Wind Turbine Under Ship Collision Scenarios. In *International Conference on Offshore Mechanics and Arctic Engineering* (Vol. 58783, p. V003T02A009). American Society of Mechanical Engineers.

Zhang, Y. and Hu, Z., (2021). Investigation on the performance of an OC3-Hywind Spar-type floating wind turbine impact by an offshore service vessel. In 5th International Conference on Maritime Technology and Engineering, Lisbon. *Developments in Maritime Technology and Engineering* (pp. 537-544). CRC Press.

Zhang, Y. and Hu, Z., (2021). A nonlinear numerical simulation approach for the dynamic responses analysis of floating wind turbine under ship impact scenario. In 8th *International Conference on Marine Structures 2021.* In press.

Contents

List of Figures

List of Tables

Chapter 1 Introduction

1.1 Motivation of research

The exploration and utilization of renewable energy have flourished in the past decades to cope with the increasing demand for global energy consumption and lower CO2 emissions. Among the various types of renewable energy sources, wind energy is one of the most promising solutions as it is relatively easy for commercialization.

According to the latest global wind report (GWEC, 2021), the global wind power installed in 2020 is over 93 GW, which is a 53% growth compared with 2019, and the total global installed wind capacity reached 743 GW. Though onshore wind energy remains the most part of the total wind energy market, the offshore market has a significant growth in recent years. Figure 1-1 shows the historic development of the total installation of wind turbines worldwide. It is found that the installed offshore wind capacity occupied a percentage of 4.7% in 2020, while this value is just around 1.5% ten years ago in 2010.

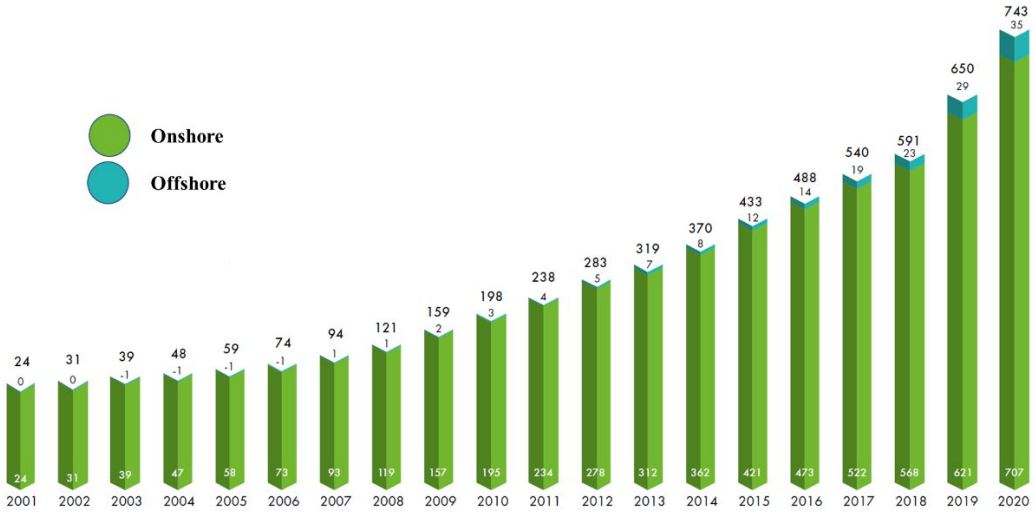

Figure 1-1. Historic development of total installations (GW), revised from the global wind report 2021 (GWEC, 2021).

The offshore wind farm has shown its potential and advantages compared with the onshore wind farms. Firstly, offshore wind turbines are less restricted by the space or infrastructures while these factors can limit the size and location of onshore wind turbines. Secondly, locating away from the land will lower the noise pollution concerned by many people. Additionally, the wind over the sea is much stronger and more consistent so that the offshore wind turbines could yield steadier power. Currently, Europe takes the lead of total offshore wind installations in the world and the cumulative offshore capacity in Europe has reached 24.8 GW (GWEC, 2021), providing 3% of Europe's electricity demand (Wind Europe, 2021).

However, with the rapid growth of offshore wind turbines, various challenges are found as well. Like other offshore structures, ship collision is one of the critical threats during the service life of an offshore wind turbine. As offshore wind farms could be located close to the traffic lanes, the potential collision risk of passing-by vessels should be evaluated and receive enough attention. Additionally, the offshore wind farms require regular check and maintenance, the collision hazard by service vessels shouldn't be neglected. As the cost of building or repairing an offshore wind turbine on site is very high. Once it is struck and damaged by the ship, severe economic loss could be caused. What's worse, it could lead to casualties.

An accidents list of offshore wind turbines can be found from the Caithness Windfarm Information Forum (CWIF, 2021), where several ship collision accidents are recorded. On 23rd Nov. 2012, five crew got injured after their vessel impacted against an offshore wind turbine at Sheringham shoal offshore wind farm, England. On 4th April 2014, there was a high-speed collision between a crew transfer vessel and a wind turbine in Kinmel Bay. Three technicians received injuries to varying extents. More recently, in Borkum Riffgrund 1 wind farm, in the German North Sea, three workers got injured, including one seriously, after the crew transfer vessel impacted against a wind turbine. Note that the list of the accidents from CWIF (http://www.caithnesswindfarms.co.uk) doesn't represent all recorded accidents. Though only several ship-OWT collisions are currently recorded

in CWIF, these recorded accidents could only be the 'tip of the iceberg' in terms of numbers of accidents and their frequency with the continuous increment of offshore wind farms. What's more, for the floating offshore wind farms, which are usually located in the farther sea to take advantage of the more consistent wind, the service vessel becomes larger and the floating offshore wind turbines are more exposed to ship collision hazard.

Therefore, it is necessary to consider the crashworthiness of offshore wind turbines in the early designing phase to improve wind farm safety, especially for floating offshore wind turbines (FOWT), which are subjected to more complex loading conditions. However, the research regarding the ship-FOWT collision analysis is still very few compared with those on conventional ship-ship collision problems. For floating offshore wind turbines, it is very important to understand the mechanism in ship collision scenarios.

1.2 Research aim and objectives.

The aim of this research is to investigate the comprehensive dynamic responses of floating offshore wind turbines under ship collision scenarios. To achieve this goal, a series of objectives are set as below:

a) To understand the characteristics of FOWT and the reason why previous ship collision analysis methods are not suitable for direct application on ship-FOWT collision.

b) To develop an efficient method for ship-FOWT collision analysis based on conventional collision analytical models and a FOWT analysis tool.

c) To investigate the 6DOF global motions of FOWT, the response of mooring systems in ship collision scenarios

d) To propose a more accurate simulation method based on Nonlinear Finite Element technology which addresses the external and internal dynamic

responses simultaneously.

e) To further analyze the responses of the rotor-nacelle assembly (RNA), such as the nacelle axial accelerations, the blade tip deformations, the aerodynamic performance in ship-collision scenarios. Additionally, the local structural behavior, collision force, and energy dissipation are also to be revealed.

f) To investigate the influence of tower flexibility, deformability of striking ship, and environmental conditions.

1.3 Thesis organization

The thesis contains seven chapters and the main research outcomes have been written in two journal papers. In this section, the summary of each chapter is introduced to outline the structure of the thesis.

Chapter 2 is a comprehensive literature review. It briefly introduces the development and characteristics of FOWTs and outlines the ship collision risk from previous studies. Additionally, the research methodologies for conventional ship collision analysis are thoroughly reviewed. Some general methods including analytical method, empirical method, numerical method, and model test are compared and discussed. The valuable references on how to consider the hydrodynamic aspects and structural aspects are summarized and the lack of methods for considering wind-wave loads in ship-FOWT collisions are pointed out.

Chapter 3 describes the proposed novel integrated method for quick assessment of ship-collision analysis. This method combined a 3-D analytical model and a FOWT analysis tool to conduct collision analysis. In this Chapter, the analytical collision model is firstly derived. Then the FOWT simulation tool, DARwind, with its background theory is introduced. Next, the methods on how to integrate them are described in detail, including some derivation of the transformation matrix used in the coupling and calculation process.

Finally, the method is verified by the comparison with a previous planar collision model.

Chapter 4 presents some cases studies based on the integrated method proposed in Chapter 3. The results in different environmental conditions are discussed. The external dynamic responses of FOWT during a long period after ship collision are analyzed. The global motions, mooring system response, tower vibration, nacelle axial accelerations are investigated in still water and wave only conditions. In addition to these aspects, the aerodynamic performance, and the blade tip deformation due to ship collision are investigated in wind-wave conditions.

Chapter 5 proposed a coupled numerical method of external and internal dynamics for ship-FOWT collision simulations. In this method, the LS-DYNA, a general finite element code is adopted to conduct the structural analysis. The hydrodynamic, aerodynamic, and mooring loads are added through the user-defined subroutine in LS-DYNA as these loads are uncertain before calculation but depend on the time and motions of models. In this chapter, the methods for evaluating these loads are firstly introduced and the algorithms of coupling them with LS-DYNA solver are then presented. For the hydrodynamic part, the potential-flow theory combined with linear wave theory is adopted. For the aerodynamic part, a simplified aerodynamic model based on a look-up table for the thrust force coefficient from a previous study is adopted, a point load is used to represent the whole wind loads acting on the blades. For the mooring part, it is linearly simplified as a restoring effect. This is a coupled method that can address the external and internal dynamics at the same time.

Chapter 6 presents the discussion on the simulation results from the coupled method described in Chapter 5. The structural responses, energy dissipation, and collision forces are analyzed. The influence of impact velocity, tower flexibility, the deformability of striking ships, and wind-wave conditions are investigated. Additionally, the results here are compared with some results from Chapter 4 to further investigate the advantages and limitations of these two methods.

Chapter 7 summarizes the whole thesis contents. Some key conclusions are made and some limitations from current work are discussed to make a recommendation for future research.

1.4 Contribution of work

The work intends to conduct a comprehensive dynamic responses analysis for FOWT under ship collision scenarios and the main contribution is summarized as:

a) Due to the lack of efficient methodologies and tools for analyzing ship-FOWT collision, an innovative integrated method is developed. The method can predict various global responses of FOWT such as global motions, mooring response, aerodynamic performances, etc.

b) Previous studies mostly focus on the external or internal dynamics in ship collision but ignore the possible coupling effects between them. What's more, most structural dynamic analyses cannot account for the hydro-aero loads. The coupled method in Chapter 5 models the hydro-aero loads in a detailed way so that the external dynamics and internal dynamics are coupled, and more accurate results can be obtained.

c) Based on the proposed methods, the dynamic responses of FOWT impacted by a ship are systematically investigated. The results could be valuable for the wind industry to consider the crashworthiness of FOWT in the early designing phase. Additionally, with the increasing sizes of FOWTs and OSVs nowadays, the optimization of crashworthiness design may need to be paid more attention to. The developed methods in this work and the research outcomes could supplement and benefit the industry for designing more reliable FOWTs in the future to lower the cost induced by ship collision accidents.

Chapter 2 Review on the development of FOWTs and ship collision analysis

2.1 Review on the development and challenge of FOWTs

2.1.1 Introduction to floating offshore wind turbines

Offshore wind turbines can be further divided into different types according to support structures. Figure 2-1 illustrated some common types of offshore wind turbines. In the shallow water area, the fixed-support offshore wind turbines are mainly adopted such as monopile OWTs or jacket OWTs. However, these fixed supports are no longer reliable or economic when the wind turbines come to a deeper water zone (deeper than 50 meters), then the floating platforms are developed. The most advantages of the floating offshore wind turbines are that in the deeper water zone, the wind is more consistent and the floating wind farms there can also reduce the environmental impact, less noise and invisible for people on the land (Henderson et al., 2003; Musial et al., 2004). Additionally, some types of floating platforms can be assembled in port and towed to wind farms, which is more efficient to install and maintain. It is expected that floating offshore wind turbines are more competitive in the future.

Nevertheless, the concept of floating offshore wind turbines is not a new idea, and it was first introduced as early as 1972, Heronemus (1972) proposed the concept of the floating offshore wind turbine, which consist of many small turbines and a hydrogen system on a floating platform, shown as Figure 2-2. The generated power was intended to be stored as hydrogen energy delivered to shore by pipelines. However, due to the limitations in manufacturing technology and cost, the floating offshore wind turbines were still in their infancy and cannot be commercialized until the world's first floating offshore wind farm (Stiesdal, 2009) is fully commissioned in Scotland in 2017. It has five 6-MW Hywind

floating wind turbines operated in the water depth from 95m to 120m, shown as Figure 2-3. The platform is a single floating cylindrical spar buoy that has ballast inside to help achieve hydrostatic stability. WindFloat Atlantic, another famous floating offshore wind farm, is located 20km off the coast of Viana do Castelo, Portugal, commissioned in 2020 and it has a total capacity of 25MW. This farm adopted the WindFloat, a semi-submersible platform (Roddier, et al., 2010), shown as Figure 2-4. The 'water entrapment plates' on the bottom of the three main pillars increase the hydrodynamic damping to optimize stability. The wind turbines are installed on one of the three main floating columns and the instability caused by the wind turbine under wind thrust force can be improved by the static and dynamic ballast system inside the three main columns. Besides, there are also other famous types of floating offshore wind turbines. HiPRwind (Bard, 2010; Quesnel, 2011), another semi-submersible FOWT, has a similar platform with WindFloat, but the wind turbine is installed at the centre of the platform, shown as Figure 2-4. The advantage is that the stability could be increased and the reliance on the ballast system can be reduced, so this kind of design is very popular later in other FOWT designs. IDEOL (Beyer et al., 2015), a barge-type floating offshore wind turbine, is featured for its simple manufacture and low cost of the concrete platform, shown as Figure 2-5. In addition to the above types of floating wind turbine, the TLP is also popular as it is the most stable platform and it less impacts the dynamics of the wind turbine. TLP is usually moored by several pairs of vertical tendons in tension and the stability is achieved by the combination of tension mooring lines and the reserved buoyancy. However, the TLP-type offshore wind turbines are still very few as there exist challenges on the mooring line designing and the high cost of installation. Some famous concepts of TLP offshore wind turbines can refer to Blue H TLP (Blue H Engineering BV, 2017), and PelaStar (Pelastar, 2013), etc.

Generally, according to the types of the dominant source to provide static stability for FOWTs, the above floating offshore wind turbines can be further categorized as ballast, buoyancy, and mooring system. A triangle diagram illustrated these categories as Figure 2-6. The Hywind spar-type floating wind turbine introduced above belongs to the ballast

category as it keeps stable mainly by the ballast inside the deep-draft slender structure. The TLP, as introduced above, has the most stability provided by the tension mooring system and excessive buoyancy and is the mooring type. Barge usually has a large water area plane and small draft to maintain so that the stability is guaranteed, so it is a buoyancy type. As per the semi-submersible FOWT, its stability is normally provided from multi-aspects, including ballast and mooring, thus it is placed in the middle of the triangle diagram in Figure 2-6.

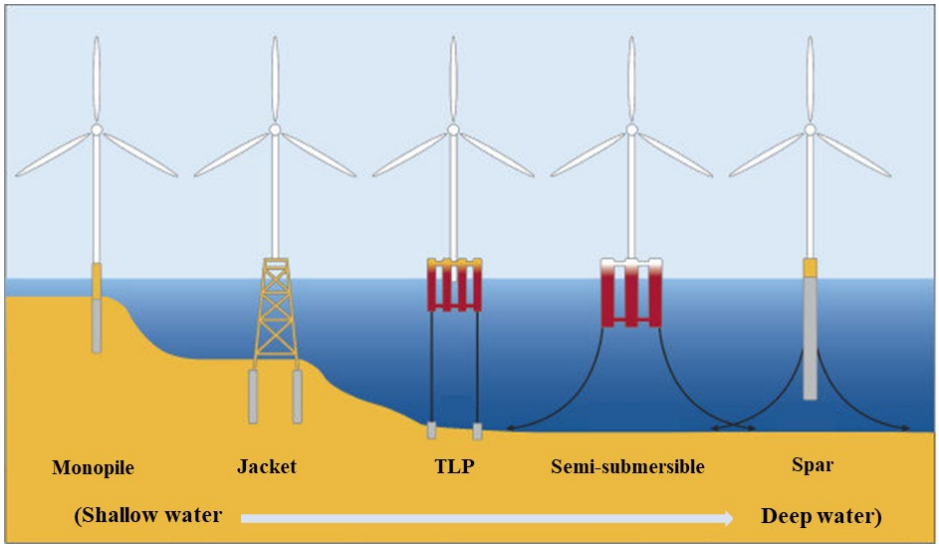

Figure 2-1. Common types of offshore wind turbine foundations, revised from Ref. (EWEA, 2013).

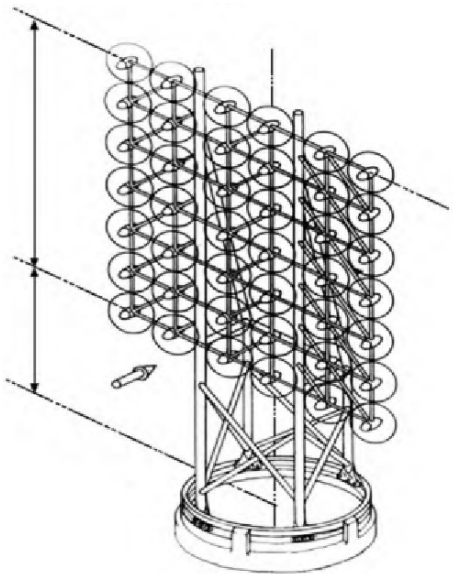

Figure 2-2. The concept of first floating offshore wind turbine proposed by Heronemus (1972)

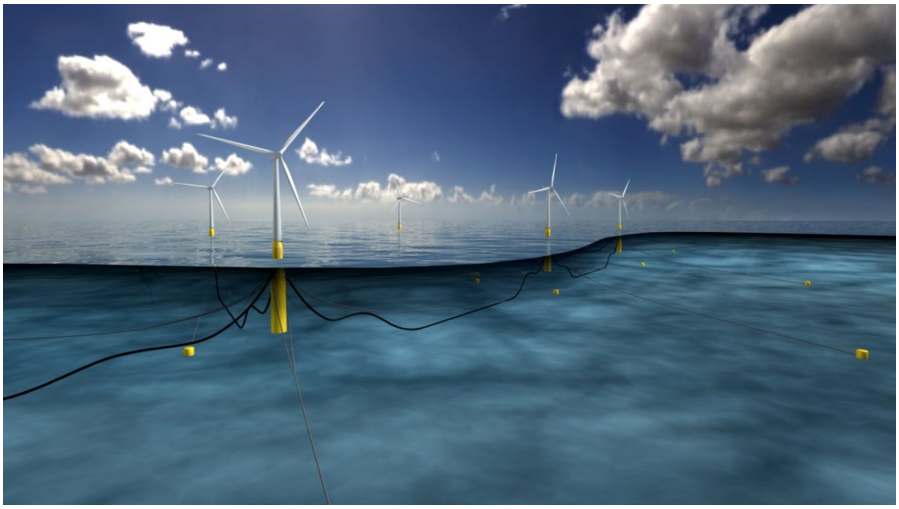

Figure 2-3. The Hywind Scotland illustration (Copyright © 2021 Equinor ASA, available from https://www.equinor.com/en/what-we-do/floating-wind/how-hywind-works.html)

Figure 2-4. WindFloat illustration. (Roddier et al. 2010)

Figure 2-5. Floating offshore wind turbine with the barge, IDEOL (Copyright © BW Ideol – 2021, available from https://www.bw-ideol.com/en/floatgen-demonstrator)

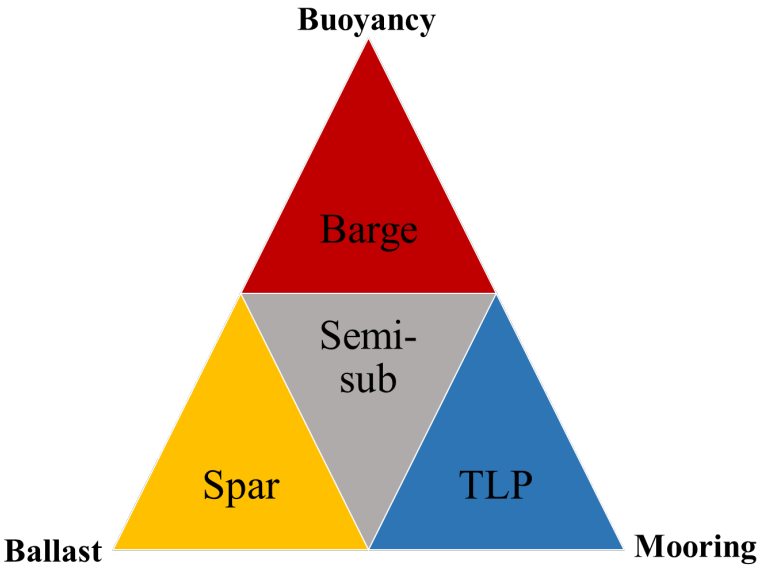

Figure 2-6. Different methods to achieve hydrostatic stability.

2.1.2 Development of studies on FOWT dynamics

The dynamics of FOWT is complex and involves multidisciplinary knowledge, including aerodynamics, structural dynamics, servo control strategies, hydrodynamics, and mooring system dynamics. When conducting integrated load analysis, the aero-elastic effect of wind turbines and the coupling effects between wind turbines and platform, mooring systems must be carefully considered, which bring big challenges. Currently, the

main analysis method of FOWT can be summarized as field measurement, scaled model test, numerical simulation.

The field measurement is one of the most significant approaches to investigate the dynamic responses of FOWT. Before the commercialization of a type of FOWT, the prototype is often established and in operation to record and analyze the data and performance. The on-site measurement brings the most direct and reliable results, which could help find some engineering problems. The Hywind Scotland, WindFloat Atlantic introduced in section 2.1.1 both have the prototypes before they are fully commissioned and other on-site measurement projects can refer to Ishida et al (2013), Forward (2014). These field measurement projects contribute a lot to FOWT optimization and help acquire valuable engineering experience and academic studies. However, the measurement work is expensive and time-cost, which may not be suitable in the design phase. Additionally, some characters cannot be directly observed from the prototype, thus the numerical studies and scaled model test are more performed in the past decades.

2.1.2.1 Numerical studies on the FOWT

Numerical simulation is an efficient approach compared with the field measurement and model tests, but it always relies on a powerful simulation tool. Thus, reliable simulation technology is of significance for obtaining accurate simulation results.

Currently, the numerical codes for FOWT analysis are also experiencing rapid development. FAST—Fatigue, Aerodynamic, Structure, Turbulence (Jonkman and Buhl, 2005) is originally an onshore wind turbine simulation tool developed by NREL. Jonkman (2007) added the modules of hydrodynamics and mooring systems to the old version of FAST to make it capable of simulating floating offshore wind turbines. Currently, FAST is an aero-hydro-servo-elastic coupled time-domain simulation tool, and the algorism structure for FOWT in FAST v8 is shown as Figure 2-7. The core modules include HydroDyn, MAP++, MoorDyn, FEAMooring, ElastoDyn, ServoDyn, InflowWind, and AeroDyn. HydroDyn calculates the hydrodynamic and hydrostatic loads

under the defined waves and current conditions while mooring dynamics evaluation has several optional methods. The ElasdoDyn is mainly for the structural dynamics analysis of the multi-body system. In the multibody system, the platform, nacelle, and hub are modelled as rigid bodies while the tower, blades, drive shaft are modelled as flexible bodies. The ServoDyn is used to apply the control strategies including blade pitch controls and adjusting the generator torque. The InflowWind is a module to process the wind-inflow and the AeroDyn is to calculate the aerodynamic loads acting on the blades and tower with the given inflow wind field. Other commercial software for FOWT simulation, such as Bladed (DNV-GL, 2015) and HAWC2 (Larsen and Hansen, 2019) are also very popular and widely used both in the academic and industrial fields. In addition to these FOWT simulation tools, some studies have combined the conventional numerical simulation tool with a specific program or module to conduct the FOWT simulation or use the CFD technology. Withee (2004) has developed a method to dynamically couple the AeroDyn, HydroDyn with ADAMS, a multi-body dynamic analysis program to conduct the fully coupled simulations of FOWT. Bachynski et al (2013) combined the SIMO, REFLEX, Aerodyn, and a servo control module written in java to conduct the fully coupled analysis and investigate the dynamic response of several types of FOWT during Pitch actuator fault, grid loss, and shut down. Some CFD analyses (Li et al., 2012; Tran and Kim, 2014; Liu et al., 2017) were also conducted, focusing on the aerodynamic performance of FOWT. The CFD method usually provides detailed and accurate results, but the computational cost is quite large.

To evaluate the feasibility of various FOWT simulation tools, IEA has funded the OC3 (Offshore Code Comparison Collaboration) project (Jonkman and Musial, 2010), OC4 (Offshore Code Comparison Collaboration Continuation) project (Popko et al., 2012; Robertson, 2013; Robertson, 2014) and OC5 (Offshore Code Comparison, Collaboration, Continued, with Correlation) project (Robertson 2015; Robertson 2017). The OC3 project conducts the code-code comparison for the given FOWT to investigate whether various simulation tools can accurately evaluate the dynamic responses of FOWT. However, many programs are established on a similar theory background, so the good agreement

between each simulation tool cannot completely imply that they can accurately simulate the FOWT dynamics. Thus, a series of model tests are encouraged in the OC4 project to conduct the comparison study between numerical simulation and model test. The results show that simulation tools can provide an overall true response while some drawbacks are found in correctly determining the hydrodynamic damping. The OC4 project has contributed numerous experiences and data regarding the model test of FOWTs and pointed out some limitations and challenges in current model test technology. For example, the Froude similarity and Reynolds similarity cannot be satisfied at the same time in the model test. Therefore, in the following OC5 project, researchers tried to adjust some parameters of airfoils to obtain the same aerodynamic performance in the original Reynolds number and then further validate the numerical simulation tools.

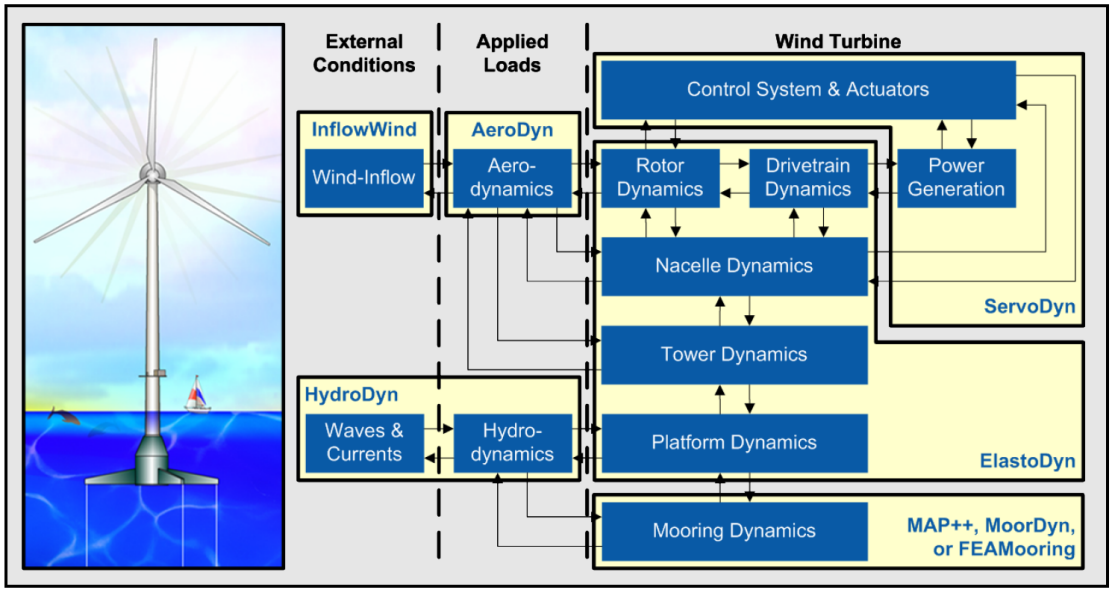

Figure 2-7. FAST control volumes for floating offshore wind turbines (Jonkman and Jonkman, 2016)

2.1.2.2 Experimental studies of FOWT

Compared with numerical simulation, the results from the model test could be closer to the real full-scale FOWT dynamics and they are often used to verify the numerical results. The key point for a FOWT model test is to accurately model the hydrodynamics, aerodynamics, and structural dynamics. Based on these principles, many model tests have

been designed and conducted.

Neilson et al (2006) has carried out model scale experiments for the Hywind concept and compared the model test with two different simulation models for integrated dynamic analysis. The model had a linear scale of 1/47 and was conducted at the Ocean Basin Laboratory at MARINTEK in Norway, shown as Figure 2-8. Various environmental conditions and control schemes were tested in the experiments, such as blade pitch control, which maintained the constant power. This model test was comprehensive, and it captured some features of FOWT dynamics which were not simulated in the numerical methods, providing valuable references in the development of FOWT. Later in 2010, Principle Power has conducted the scaled model test of WindFloat (Cermelli et al., 2010), a semi-submersible floating wind turbine which has been introduced in section 2.1.1. The 1/67 scaled physics model is shown in Figure 2-9. In this model test, it is found that a disc is placed instead of modelling the blades because the Froude-scale airfoil would lead to a different Reynolds number range compared with the prototype (the Froude similarity and Reynolds similarity cannot be satisfied at the same time). Additionally, establishing the control system in detail in this scaled model was difficult. To correctly represent the wind loads, The blades and control system were then simplified, and a disc was used to ensure the wind thrust force proportioned in this scaled model test. However, this method cannot capture the aerodynamic torque and gyroscopic moment. Duan et al. (2016a; 2016b) conducted basin experiments for an OC3 Hywind spar floating wind turbine. The physics model was built on a scale of 1/50 and to investigate the dynamic characteristics of FOWT, the experiment considered two types of rotor concepts, of which one is thrust-matched blades and the other one is geometry-matched blades, shown as Figure 2-10. Goupee et al. (2014) conducted model tests for three types of floating offshore wind turbine, Hywind (Spar), PelaStar (TLP), and DeepCwind (Semi-submersible) under the OC4 project to investigate the dynamic response of FOWT and validate the numerical simulation tools. Wan et al. (2015, 2016) innovatively proposed a concept of STC (Spar Torus Combination) which integrated the Hywind spar floating wind turbine and a wave energy converter and conducted the experimental studies of STC.

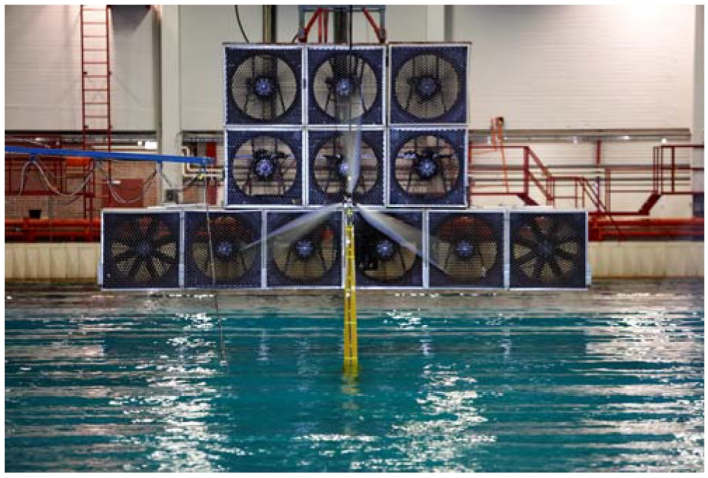

Figure 2-8. Experimental scale model (Neilson et al., 2006)

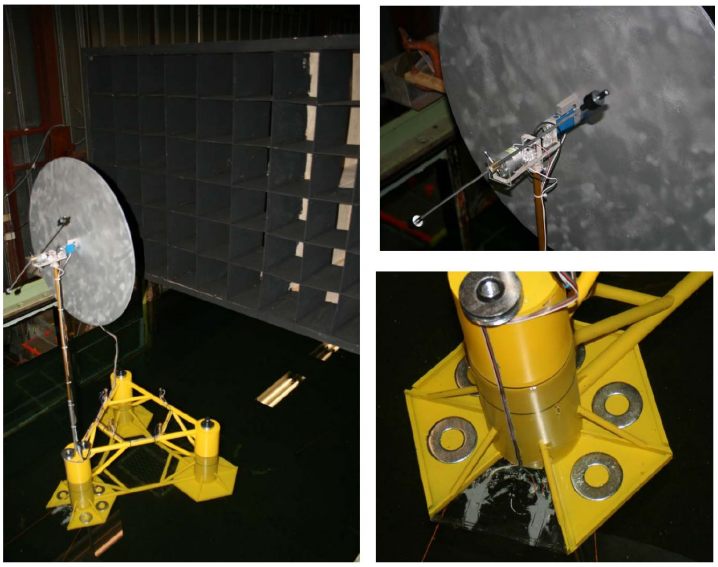

Figure 2-9. WindFloat model in front of the wind machine (left), top of tower instrumentation (top right), and strain gage setup on water0entrapment plate (bottom right) (Cermelli et al., 2010)

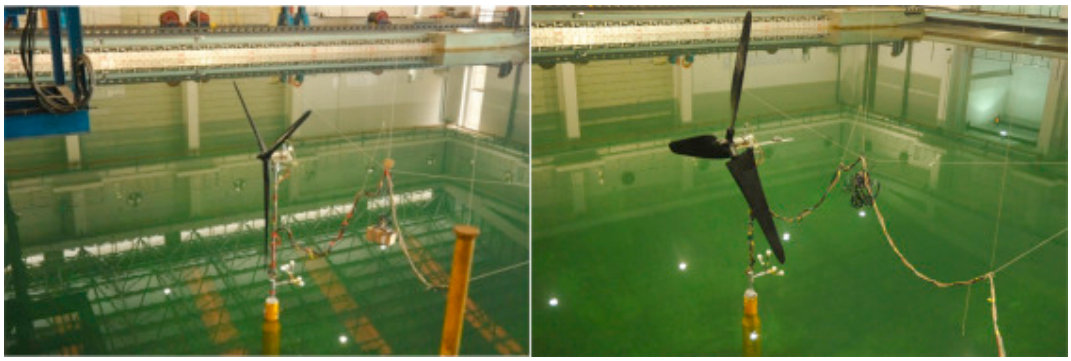

Figure 2-10. Geometry-matched blades (left) and thrust-matched blades (right) model in basin (Duan et al., 2016a).

In addition to those basin experiments of FOWT, some experiments were conducted under the wind tunnel to investigate the aerodynamic characteristics more accurately. The motions of floating platforms were then realized by placing a parallel kinematic robot on the bottom of wind turbines. Bayati et al. (2013) carried out a 2DOF (pitch and surge motion) experimental rig-HexaFloat (the kinematic robot on the bottom) at Politecnico di Milano Wind Tunnel to simulate a 1/25 scaled DTU 10-MW wind turbine. The HexaFloat has been expanded to 6DOFs (Bayatiet al.2014) and adopted in the following studies (Bayati et al., 2017; Belloli et al., 2020). The HexaFloat with a wind turbine set-up is shown in Figure 2-11.

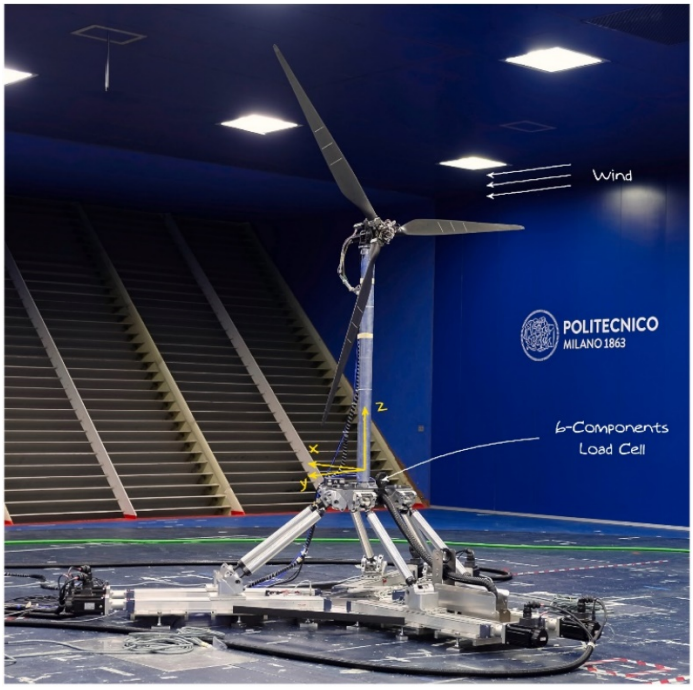

Figure 2-11. The HexaFloat with a wind turbine inside wind tunnel (Belloli et al., 2020).

2.2 Ship-FOWT collision risk analysis.

Currently, studies regarding the FOWT mainly focus on the integrated load analysis and global dynamic responses through numerical or experimental technology, as introduced above. However, the collision risk analysis for FOWT is very few due to the low quantity of floating offshore wind farms and the lack of ship-FOWT collision data, The risk analyses of FOWT can refer to the ship collision with some fixed-support offshore wind

turbines. In this section, several risk analyses will be reviewed.

As early as 2001, Christensen (2001) has established a model for calculating the collision frequencies for an offshore wind farm. The study intended to evaluate whether the location of the offshore wind farm is optimal from the view of ship collision risks and the flow chart of the calculation procedure is shown in Figure 2-12. In their model, the ship traffic and navigation routes, environmental conditions, the geometry of the wind farm, the failure scenarios were considered. It is found that the drifting ships (possibly resulting from the failure of propulsion machinery) contributes the most to the collision frequencies and two types of drifting collision, 'head and bow' and 'sideway', are worthy of investigation.

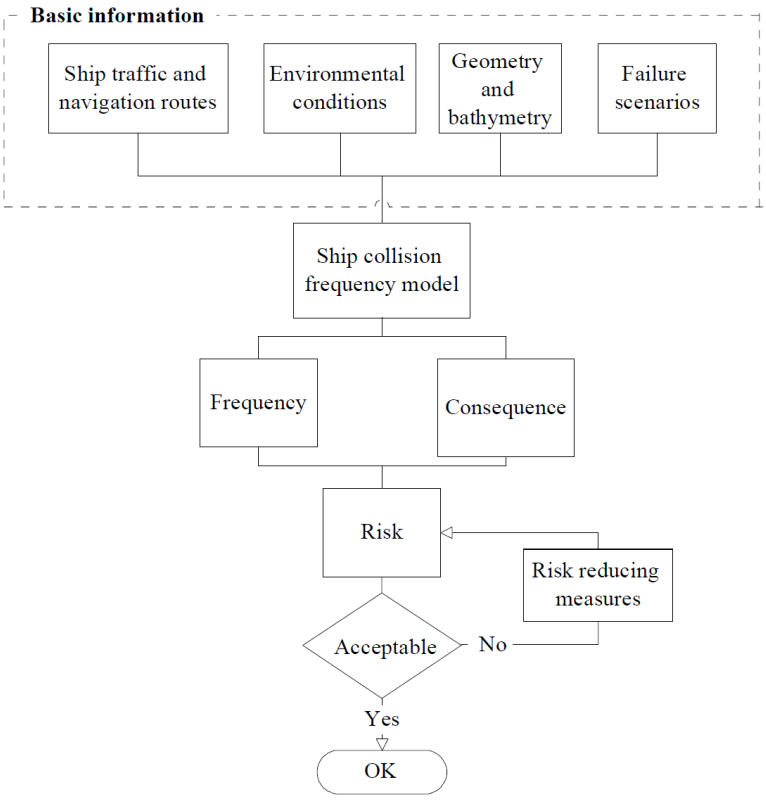

Figure 2-12. Flow chart of the calculation procedure (Christensen et al., 2001).

Later in 2006, Biehl and Lehmann (2006) carried out several simulations of ship collisions against OWTs and the results were then combined with some statistical data as well as probabilities of various scenarios occurrences to conduct the comprehensive

safety assessment. In the study, OWTs with three different foundations were chosen, monopile, jacket, and tripod. As for the striking ships, a double-hull tanker, a single hull tanker, a container vessel, and a bulker carrier were selected. The risk analyses showed that the monopile OWT has the lowest risk in case of collision. This work has also exhibited the dynamic responses of three types of offshore wind turbines impacted by large-size striking ships (the selected four types of ships had the length varying from 150m – 304m). In chapter 1, several real collisions accidents have been described and it is found that the striking ships are all service vessels (crew transfer vessels), implying that the collision risk of offshore service vessels might be more frequent.

Dai (2013) has carried out a risk analysis especially for collisions from service vessels. The study proposed a framework including six steps, which are summarized in Figure 2-13. In the first step, the objectives and boundary conditions for the risk analysis were established. Then the hazard was determined. Totally four types of service vessels and several typical collision scenarios were highlighted. In the probability analysis, the fault tree and event tree were made to identify the direct causes. Then some initial data was selected, and risk-influencing factors (RIF) were carefully selected. With the Bayesian networks, the probability analysis was finished. The consequence analysis was realized by conducting numerical simulation to assess the structural dynamic responses, such as energy dissipation, impact forces. With the obtained consequence and probability, the risk evaluation was finally finished. And some suggestions were made. However, in the analysis, there were no sufficient accidents records to support the probability analysis, some data from similar operations in the offshore oil and gas industries were adopted.

A similar risk analysis was also conducted by Presencia and Shafiee (2018) and the maintenance ship collision against offshore wind turbine was focused on. A risk evaluation model was proposed to quantify the collision risks associated with different ships under maintenance work on different components of offshore wind turbines. The model was tested under the scenarios including five types of ships and maintenance work on seventeen components. The results show that the replacement work in maintenance

has the most collision risk compared with other tasks.

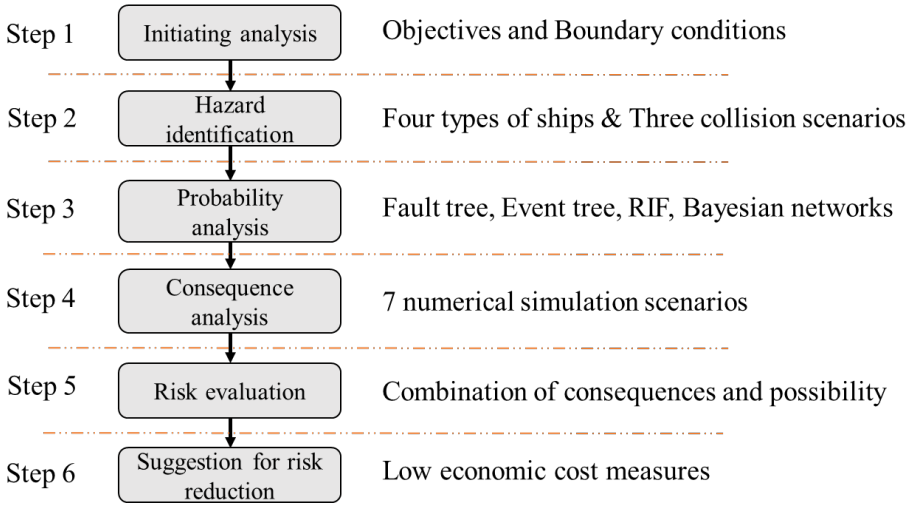

Figure 2-13. The risk analysis framework.

Through the review of ship-OWT collision risk analysis, it can be concluded that though few accidents have been recorded up to now, a clear collision hazard, especially from offshore service vessels, has been identified. For floating offshore wind turbines located further from the coast, larger offshore service vessels are required, and worse environmental conditions could exist, so the collision risk from offshore service vessels should be emphasized. In this thesis, the following work and analyses will also focus on the OSV-FOWT collision scenarios.

2.3 Review of research methodology in ship collision analysis

The ship-FOWT collision problem is an extension of the conventional ship collision problem. Though current ship-FOWT collision analyses are very few, the previous ship collision studies can provide valuable references. Generally, the ship collision is a highly nonlinear and transient process, including local structural deformation and global motions under various loads as well as conditions including impact force, hydrodynamic loads, and wind loads (mainly for OWT). It is usually difficult to consider all these effects in detail in one analysis. Thus, in the past decades, a common method for analyzing the collision problem is to decouple the collision process into two parts, the external

dynamics, and the internal dynamics (Minorsky, 1958). The external dynamics analysis mainly addresses the problems of predicting the global kinetic characters such as 6DOF global motions and the energy dissipation during the collision process while the internal dynamics analysis investigates the structural damage and how the energy is absorbed by introducing the plastic deformation theory. In this section, a comprehensive review of research methodologies of ship collision analysis will be made.

2.3.1 The decoupled methods used in ship collision analysis

2.3.1.1 External dynamics

The external dynamics is mostly analyzed through the theoretical model. In the theoretical model, the hydrodynamic effects are usually simplified as constant added mass factors, and the conservation of momentum principle is then adopted. When the velocities of the two ships before and after the collisions are obtained, the energy dissipation can be evaluated. Thus, the external theoretical model can provide very fast estimation with acceptable accuracy.

Pedersen and Zhang (1998) proposed an external dynamic model for ship collisions. In the study, the ship motions are limited in the horizontal water surface (2-D model). In the beginning, three different coordinate systems are established at the COG of each ship and the contact point, shown in Figure 2-14. Then the equations of motions for the striking ship are expressed as equations (2-1) to equations (2-3).

$$M_a(1+m_{ax})\dot{v}_{ax} = -F_\xi \sin\alpha - F_\eta \cos\alpha \tag{2-1}$$

$$M_a\left(1+m_{ay}\right)\dot{v}_{ay} = -F_\xi \cos\alpha + F_\eta \sin\alpha \tag{2-2}$$

$$M_a R_a^2(1+j_a)\dot{\omega}_a = F_\xi[y_c \sin\alpha - (x_c - x_a)\cos\alpha] + F_\eta[y_c \cos\alpha + (x_c - x_a)\sin\alpha] \tag{2-3}$$

In the equations, M_a is the mass of impact ship and $\dot{v}_{ax}$, $\dot{v}_{ay}$, $\dot{\omega}_a$ refers to the accelerations of the striking ship in the surge, sway, and yaw motions. R_a is the radius of gyration for the striking ship, and (x_c, y_c), (x_a, 0) are the coordinates of collision point and COG, respectively. The hydrodynamic effects are simplified by introducing the added mass coefficients m_{ax}, m_{ay}, j_a. The ratio between the collision forces parallel and perpendicular to the impact plane, F_η and F_ξ, is assumed to be constant, that is F_η=$\mu \cdot F_\eta$, where μ is the ratio of the impact impulses in two directions. Pedersen and Zhang (1998) further considered the two possible scenarios, the sticking and sliding of the two ships after the collision and give the analytical solution of energy dissipation for these two scenarios. This is a comprehensive study and it thoroughly discuss the external mechanisms of ship collision problems, but the limitation is that the model is limited to 2-D space and only the in-plane motions can be predicted.

Popov et al. (1969) has proposed an analytical collision model for the ship-ice collision. The model mainly studied the external dynamics of the ship-ice collision, and the impact impulse was assumed to apply along the normal direction at the impact point, and the friction between ship and ice is not considered. Then the problem is simplified to be a 1-dimensional problem. The hydrodynamic effects of ships were simplified as constant added mass factors obtained by some derived empirical equations.

To solve the 3D problem accurately, Stronge (2004) has proposed an analytical method to evaluate the dynamic responses for impact analysis of general items. A so-called local coordinate system was established at the collision point and calculations were finished under this coordinate system. The assumptions of short impact duration and small contact zone were made. This method was then further extended by Liu and Amdahl (2010) for ship collision analysis. The hydrodynamic effects were also simplified as the added mass as previous studies did. The coordinate systems of their model are shown in Figure 2-15 and Figure 2-16. The equations of motions were derived according to the theory from Stronge (2004). Liu and Amdahl (2010) further developed an analytical method for

energy dissipation evaluation with reaction impulse function for both sliding and sticking cases.

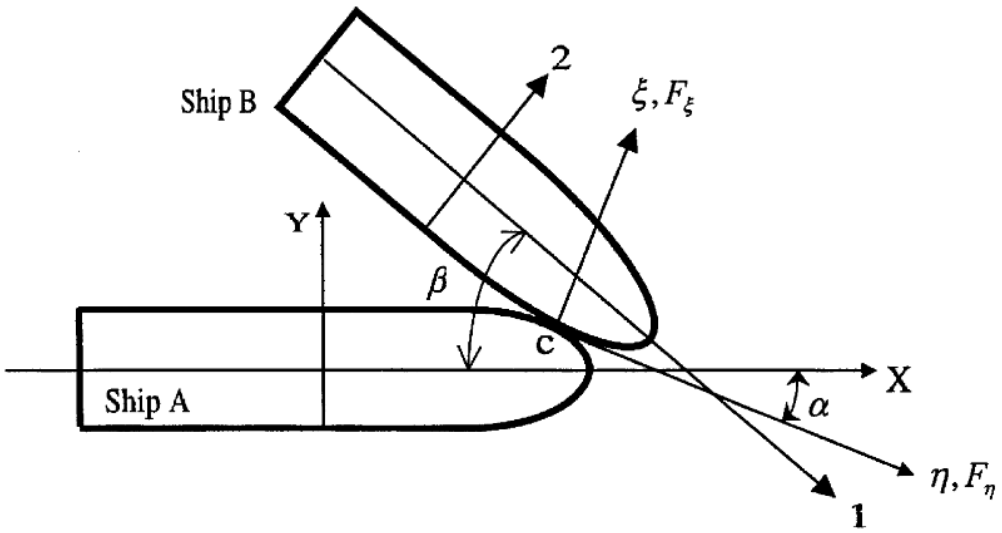

Figure 2-14. The coordinate system of ship-ship collision model (Pedersen and Zhang, 1998).

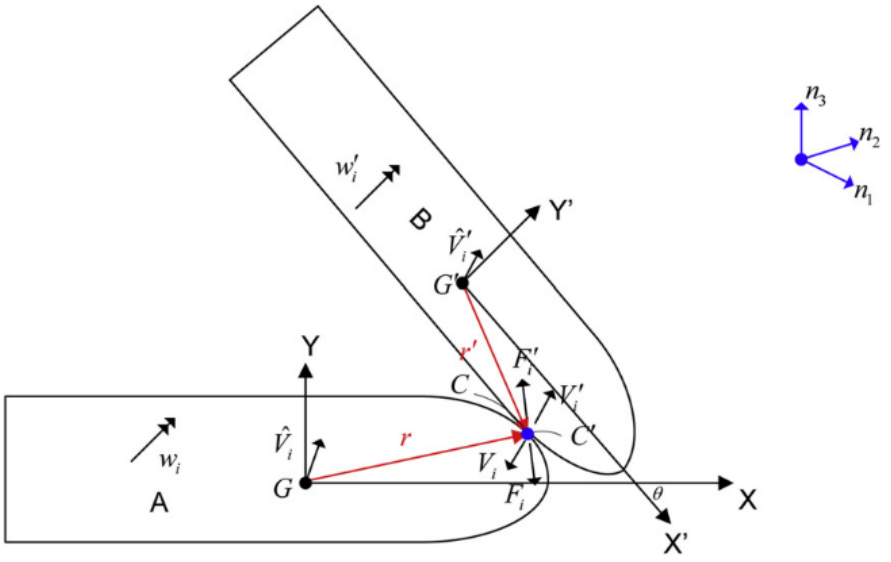

Figure 2-15. Illustration of the coordinate systems of ship collision model, by Liu and Amdahl (2010)

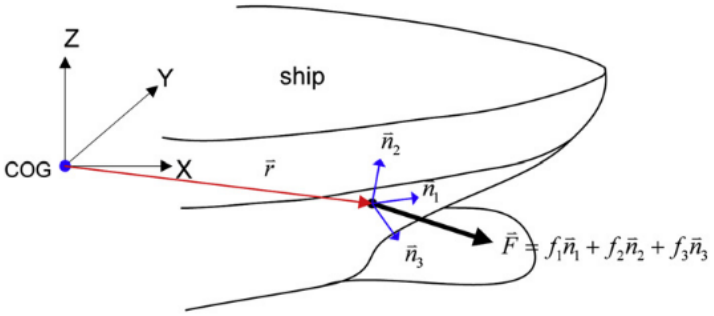

Figure 2-16. Geometry of collision point and local coordinate system, by Liu and Amdahl (2010)

Liu and Amdahl (2010) further discussed the difference between their 3D collision model and 2D model from Pedersen and Zhang (1998) and the energy dissipation ratio is compared as Figure 2-17. The results clearly show that the vertical eccentricity $\hat{r}_z$ can significantly influence the energy dissipation, particularly when the impact is in the middle of the ship (d/L=0). Because in the 3D model, the roll motion can be excited, and it can take a part of kinetic energy away, especially in the middle of the ship, where the vertical eccentricity is more obvious than the longitudinal eccentricity. Therefore, the energy dissipation from the 3D model is smaller compared with the 2D method in most cases. In conclusion, the features of capturing the vertical eccentricities can improve the accuracy of energy dissipation evaluation and can be also suitable for more cases, such as ship collisions against icebergs with irregular geometry, as illustrated by Liu and Amdahl (2010).

Other external dynamics analyses can be found in Hanhirova (1995), Mostofi and Bargi (2012), Pedersen (2013), Zhang et al (2017), Liu and Amdahl (2019), etc. Mostofi and Bargi (2012) studied the ship berthing impact against the floating piers with an analytical model and Pedersen (2013) analyzed the ship collision with some offshore structures, such as wind turbines, quays and bridge piers. Zhang et al (2017) further validated the robustness of the closed-form analytical solution proposed by Pedersen and Zhang (1998) by comparing 60 experimental results with the 2D analytical solution and a good agreement was reached. Additionally, a few improvements were made on the determination of some parameters and to enable the original model to consider the

effective mass of fluids with a free surface on board during the collision. Liu and Amdahl (2019) proposed another 3D collision model based on previous works (Stronge, 2004; Liu and Amdahl, 2010) and presented a so-called collision matrix to help better understand and calculate the external dynamics of ship collision.

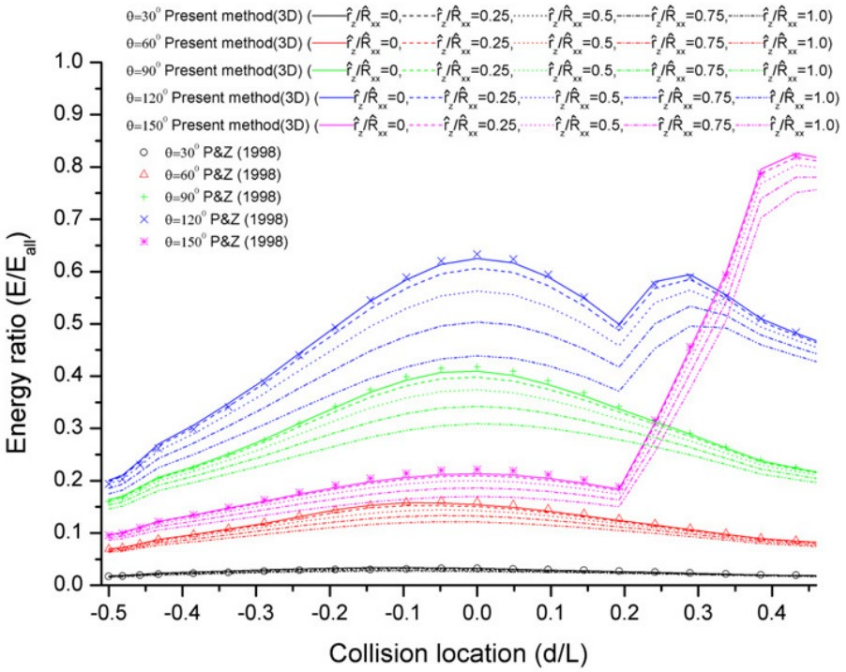

Figure 2-17. Energy ratio of total dissipated energy, by Liu and Amdahl (2010).

It is noted that for the external dynamics analysis with decoupled methods, the hydrodynamic effects are all simplified. Thus, the reasonable determination of the constant added mass factor is of great significance for the energy dissipation results. Minorsky (1958) firstly used the constant added mass $m_{ay} = 0.4m$ for sway motion in the external dynamic analysis. Later, Motora (1970) introduced the equivalent added mass to estimate the hydrodynamic forces in a more accurate way. The equations of three concepts of equivalent added mass were proposed, shown as equations (2-4) to (2-6). In the equations, M is the ship mass and m', m'', m''' are the equivalent added mass. $a(t)$, $v(t)$ represent the acceleration and velocity of the vessel at the end of the ship collision.

$$M + m' = \frac{f(t)}{a(t)} \tag{2-4}$$

$$M + m'' = \frac{\int_0^t f(\tau)d\tau}{v(t)} \tag{2-5}$$

$$M + m''' = \frac{\int_0^t f(\tau)d\tau}{0.5*v^2(t)} \tag{2-6}$$

It is shown that this equivalent added mass is not constant and could change with the collision duration. The equivalent added mass increases when the collision duration is longer. Only when the collision duration is short enough, the equivalent added mass is similar to the added mass of infinite frequency, as suggested by Minorsky (1958). Other similar studies on the determination of added mass factors can also refer to Popov et al. (1969), Jia and Moan (2010), and Zhao et al. (2020).

2.3.1.2 Internal dynamics

The internal dynamics mainly concerns about the local structural aspects, such as the structural deformation, and impact resistance, etc. The general methods for analyzing the internal dynamics include empirical methods, analytical methods, nonlinear finite element methods (NLFEM), and model tests. Liu et al. (2018) has summarized the features of these methods and the analysis procedure of structural crashworthiness in ship collision is shown as Table 2-1, and Figure 2-18, respectively. The symbol '*' means that the type of results can be addressed by the method.

Table 2-1. General methods for internal dynamics analysis, revised from Liu et al. (2018)

Method	Analysis		Result		
	Effort	Difficulty	Energy	Load	Stress
Experiment	Expensive, time consuming	Scaling effect	*	*	*
Empirical formula	Hand calculation	Lack validation	*		
Analytical formula	Hand calculation	Lack validation	*	*	
NLFEM	Specialty, time consuming	Definition of material fracture	*	*	*

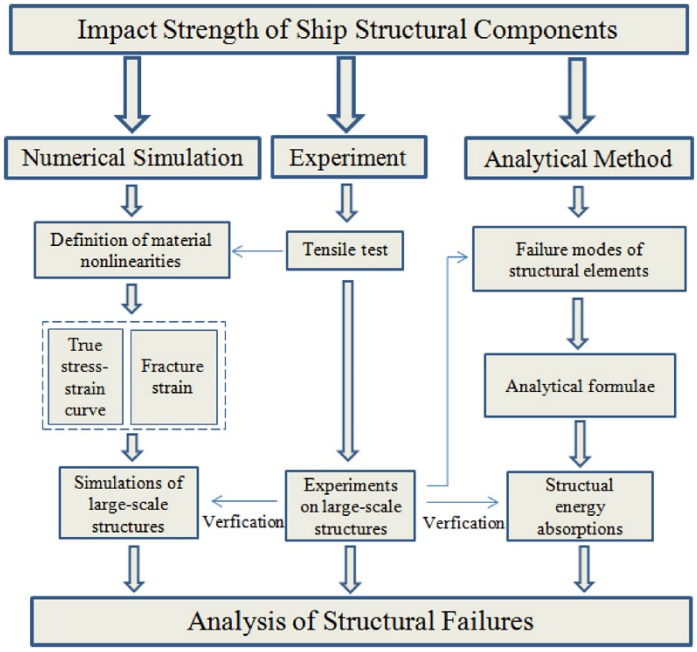

Figure 2-18. Analysis procedure of impact strength, from Liu et al. (2018)

■ Empirical method

Minorsky (1958) has proposed a well-known empirical formula, shown as equation (2-7), to predict the absorption of impact energy for nuclear powered ships based on the statistics of twenty-six actual collisions.

$$E = 47.2R_T + 32.7 \tag{2-7}$$

In the equation, E is the absorbed energy due to structural deformation, and R_T is the damaged structural volume of both striking and struck vessels. This empirical formula presented that the dissipated energy has a linear relationship with the damaged volume. The equation has been widely used by the industrial field in a period due to the fast calculation and the simple application. However, this method has its limitation that it is mainly appropriate for high-energy collisions which cause large extent of damage. For low-energy impacts with minor damage, Woisin (1979) later proposed the improved empirical formula,

$$E = 47.2R_T + 0.5\sum(h \cdot t_s^2) \tag{2-8}$$

where h refers to the height of broken or heavily deformed longitudinal members and t_s is the member thickness. More continued works on improving the empirical methods can also be found in Vaughan (1978), Woisin (1987), Pawlowski (1995), and Paik et al (1999), etc.

Pedersen and Zhang (2000) proposed another revised Minorsky's empirical method. As the original Minorsky's method only considers the damaged volume and doesn't distinguish the deformation mode of structures and material properties of the ships, the results would be still coarse in certain cases. Pedersen and Zhang (2000) refined the method and presented the newly revised empirical formula, which established the relationships between energy dissipation and different deformation mode, damaged volume, and structural material properties. Two main deformation modes were determined, plastic tension, crushing and folding. The formula is shown as equation (2-9),

$$E = \sum 0.77\sigma_0\varepsilon_f R_1 + \sum 3.50(\frac{t}{b})^{0.67}\sigma_0 R_2 \quad (2\text{-}9)$$

In the equation, E is the total energy dissipation. The first term on the right hand of the equation is the energy dissipation from plastic tension mode and the second term refers to the energy absorption from crushing and folding modes. This refined Minorsky's method was further re-validated through twenty model tests (Zhang and Pedersen, 2017) and very good agreements between the empirical formula and experiments were achieved.

■ Analytical method

Different from the empirical method, which is usually based on statistical studies, the simplified analytical method is developed based on the upper bound theory and some analytical deductions. It is very popular for predicting structural resistance and energy absorption during ship collision analysis. The analytical method usually considers that the different structural components contribute independently to the crushing loads and the possible interactions between them are ignored. Additionally, a key procedure is to

identify the deformation modes in advance and then it is represented through the simplified analytical model. Currently, some common structural deformation modes are identified as plate tension, folding/crushing, tearing/cutting and concertina tearing (Liu et al., 2018).

There are mainly two scenarios for ship structures to be evaluated, the bow collision and the side collision. For the bow collision, Amdahl (1983) has studied the crushing resistance of ship bows with analytical models. In the study, the bow structures were divided into L, T, and X type components. The total resistance was obtained by cumulating these independent component contributions. The analytical study on bow structures was also developed in the following decades by Pedersen et al. (1993), Wang (1995), Ocakli et al. (2004), Yamada and Endo (2005), etc. Yamada and Pedersen (2008) conducted a benchmark study on the axial crushing of the bulbous bows. The existing simplified methods were applied and compared with the experimental results to comprehensively evaluate the accuracy of these analytical methods.

For the side collision, the involved ship hull is generally a double shell plate with plate girders inside. This kind of structure can be further divided into various components such as shell plating, cruciform, web girder (Haris and Amdahl, 2012), shown as Figure 2-19. The total resistance is then obtained by summing up the contributions of each kind of component. The plate failure prediction has been analytically studied by Wang (1995), Simonsen and Lauridsen (2000), Haris and Amdahl (2012), Jones and Paik (2012), Jones and Paik (2013), and Liu et al., (2014), etc. In the study of Simonsen and Lauridsen (2000), the load-displacement curves were theoretically derived for plates and the energy absorption, as well as penetration, can be significantly influenced by plate geometries, impact location, and indenter radius. Liu et al., (2014) established an analytical model for predicting the plates behavior under low-velocity impact. Both aluminum and steel plates were included in the study and the structural failure was thought to start when the material necking behavior appeared. The results of the developed analytical model matched well with those of numerical simulation. Cho and Lee (2009) proposed the analytical method

to predict the stiffened plates responses under lateral impact loads as stiffened plates are common in the side and bottom structures of a ship hull. Similar analytical studies were also conducted by Liu et al. (2015). For other components such as cruciform and web girders, the analytical studies can refer to Santosa and Wierzbicki (1998), Abramowicz and Simonsen (2003), Hong and Amdahl (2008), Liu and Soares (2015). Gao and Hu et al. (2015) proposed an analytical method to predict the structural responses for side collision of a FPSO. In the study, the plate punching, perforating, denting, tearing and X-shaped structure (cruciform) crushing were identified as the main failure modes. Sun and Hu et al. (2015) also investigated the structural responses of the ship side under collision scenarios. The analytical model was for raked bow impact and both resistance, as well as energy absorption, were derived.

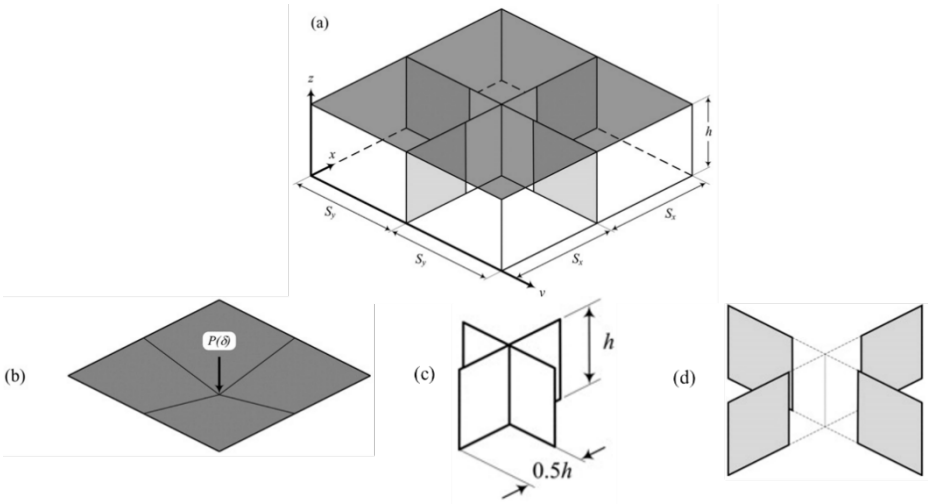

Figure 2-19. Illustration of: (b) shell plating, (c) cruciform, (d) web girder, revised from Haris and Amdahl (2012)

Generally, it is concluded that if the deformation modes of structural can be well expressed in the analytical model, the results from the analytical method are much more reliable. As the analytical method provides fast estimation on the crushing resistance in collision scenarios, it is very popular in the early designing phase.

- Model test

Model tests can be divided into two types, full-scale (or large scale) and small-scale tests,

respectively. The full-scale experiments can particularly provide the most direct insight and accurate results on the mechanism of structural responses in ship collision analysis, but it is not frequently conducted due to the high cost of building the model as well as the inspecting equipment. Small-scale tests can lower the cost and they are usually carried out especially for certain structural components, such as stiffened panels, web girders, and double hull structures to validate analytical methods. But there are still some drawbacks that the small-scale tests may not capture some details in real ship collision accidents, especially the initiation of fracture, because the scaling law is complicated.

In the last century (the 1990s), some large-scale collision tests have been carried out in Japan and the relevant details can be found from Vredeveldt and Wevers, 1993; Carlebur, 1995; Wevers et al. 1999). Akita et al. (1972), Jones (1978), Ellinas and Valsgard (1985) studied the model tests from 1962 to 1976 which were conducted in Italy, Germany, and Japan. These model tests were originally used to develop design formulae for collision-protective components on the side structures of the nuclear-powered vessels. Akita et al (1972) presented an analytical analysis based on these model tests. Both crushing resistance and energy dissipation were derived. Hagiwara et al. (1983) proposed a method for predicting ship collision damage, which relied on three joint experiments. The scaled bow models for a small-size ship (a cargo ship) and a large-size ship (an oil tanker) were established to investigate the crushing resistance. Amdahl (1983) also investigated the responses of ship bow structures through experiments. Totally 6 different straight bow models were included, and the experiment results were used to verify the simplified analytical method. Experimental studies on the straight ship bow structures can also refer to Endo et al. (2002), Yamada and Endo (2005), and Tautz et al. (2010). Yamada and Endo (2008), and Calle et al. (2017).

For double-hull structures, which are common in modern ship structures, collision experiments have been conducted since the last century. Ito et al. (1984) carried out model tests for double-sided hulls impacted by both raked and bulbous bows. Wang et al. (2000), Lehmann and Peschmann (2002) also experimentally investigated the dynamic behaviour

of the double-hull structures. In the study of Wang et al. (2000), totally nine tests were carried out for both grounding and collision scenarios and the test settings were shown as Figure 2-20. The different radius of the nose was set in the experiments to simulate the impacts of various kinds of ships. The test results show that the radius of impact cones and the impact location can significantly influence the structural responses of double-hull structures. Lehamann and Peschmann (2002) studied the collision model tests carried out by TNO. The scale ratio was about 1:3 and these tests were also reported by Vredeveldt and Wevers (1993), Carlebur (1995), and Wevers et al. (1999). Two inland waterway vessels were converted for use in the tests. The striking ship (NEDLLOYD 34) was equipped with a bulbous bow, while the struck model was installed into a frame, which was held on the side of another ship (AMATHA), illustrated as Figure 2-21. Karlsson et al. (2009) later also conducted experimental analysis for the bow collision on the side-shell ship structures.

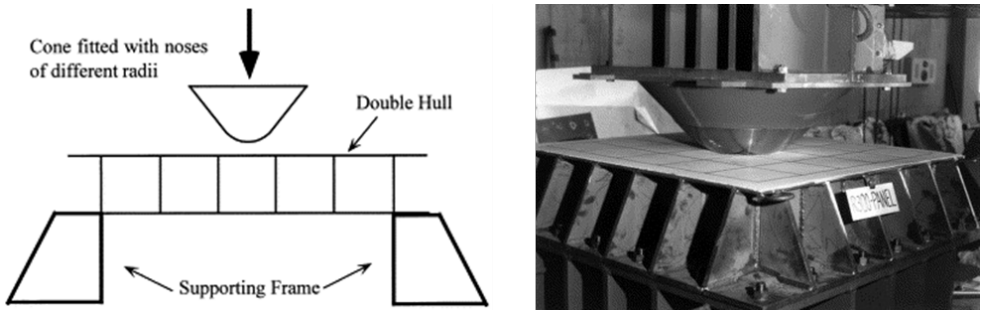

Figure 2-20. Illustration of impact tests of double-hull structures, from Wang et al. (2000)

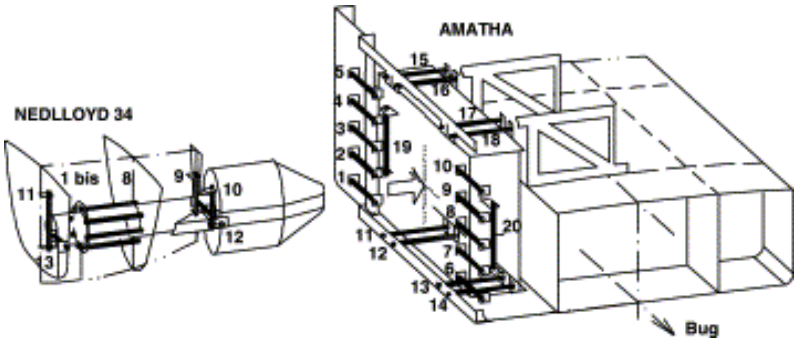

Figure 2-21. illustration of the ship collision settings, from Lehamann and Peschmann (2002)

In addition to these tests which investigated the entire ship bow and ship hull strengths,

many experiments were conducted to study certain structure components included in the bow or hull structures, such as shell plating and stiffened panels (Wierzbicki, 1995; Alsos and Amdahl, 2009; Cho and Lee, 2009; Choung et al., 2010; Villavicencio et al., 2014; Kim et al., 2016; Gruben et al., 2017), and web girders (Simonsen and Ocakli, 1999; Liu and Soares, 2016; Chen et al. 2019).

- Nonlinear finite element method

The nonlinear finite element method (NLFEM) has been very popular used as it can provide direct insight into the structural responses process and simulate the structural deformation and damage with high accuracy compared with empirical and analytical methods. Additionally, its cost is much lower than that of the model tests. With the rapid development of computers, the time cost of NLFEM has been significantly reduced and the maximum available elements are also increased, which allows the more complicated models to be calculated.

In the decoupled method, when calculating the internal dynamics with NLFEM, a common approach is to constrain the global motion of the struck structure and let the striking structure move in a prescribed path. When the area below the force-indention curve equals the energy absorption calculated by external dynamics, the penetration is obtained, and the structural damage can be evaluated.

Ohtsubo et al (1994) has conducted numerical simulations to study collision and grounding behaviour of oil tankers and proposed some improvements on accurately simulating the scenarios. Yamada and Endo (2008) studied the structural responses of ship bows in collision scenarios. A general-purpose NLFE code, LS-DYNA, was adopted to simulate the collision of an oil carrier. Other numerical simulations of ship collision can also refer to Ehlers et al. (2008), Ehlers et al. (2012), Storheim and Amdahl (2014), Calle et al. (2017), Sha and Amdahl (2019).

It should be noted that for numerical simulation technologies, the specialty of users is

required. the numerical simulation is parameter-sensitive and the suitable settings in the simulation software are significant to obtain reasonable results. The common challenges of conducting numerical simulation include the selection of mesh size, element type, boundary conditions, contact settings, modelling material properties, and some simplification on geometry models. The appropriate selection of these factors not only requires strong theoretical background but also needs rich experiences of IT operation and engineering judgment.

2.3.2 The coupled methods in ship collision analysis

The decoupled method has been widely used especially in the early period of ship collision analysis, but the drawbacks are also obvious. The coupled method can evaluate the global motions and local deformations at the same time, which captures the possible coupling effects between the global motions and the local penetration.

Petersen (1982) has proposed a coupled simulation method several decades ago. In the study, the global motions in the horizontal plane were considered and the hydrodynamic loads were applied using strip theory. The hydrodynamic forces (added masses and damping) on each section were calculated by an approximate method. The involved ships were modelled as overall rigid and only deformable with a small zone around the collision point. The deformable zone was further represented by four nonlinear springs, shown as Figure 2-22. This simulation was thought to be the earliest coupled study and the results agreed well with existing work (Motora, 1971). Though only 3DOF of motions were studied and the local deformation, as well as collision forces, were simplified, the study has provided valuable references on developing the coupling method in the future.

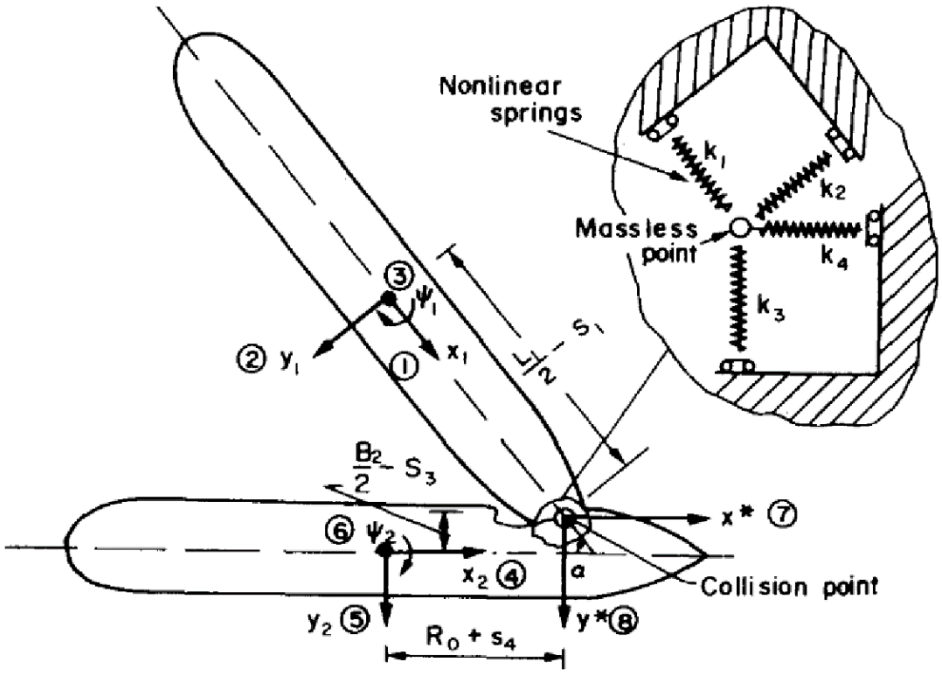

Figure 2-22. Coupled collision model, Petersen (1982)

Later, Brown (2002) employed a simplified collision model (SIMCOL) to study ship collisions. SIMCOL is essentially a coupled simulation tool, and the simulation process is shown as Figure 2-23. Step 1 and step 4 carry out the external dynamics analysis while step 2 and step 3 are for internal dynamics. Similar coupling methods were also described by Le Sourne (2001), Le Sourne (2007), Le Sourne et al. (2012). Le Sourne (2001) has conducted a coupled study for ship collision with a submarine. A new version of MCOL, a rigid body dynamic program, was coupled with LS-DYNA to conduct the collision analysis. In the simulation, the local impact force and deformation were calculated by LS-DYNA structural analysis solver, and the calculated crushing forces, as well as moments, were transferred to the subroutine MCOL to calculate the rigid body motions. The MCOL program considered the hydrodynamic loads in a very detailed way. The wave radiation force was calculated with linear potential-flow theory, and the viscous loads were considered by Morison's Equation. To increase the accuracy when calculating the large-rotational movements, the Eulerian angles and the corresponding transformation matrix were included as well. The MCOL program was also combined with the super-element method in the later studies (Le Sourne, 2007; Le Sourne et al. 2012) to conduct the coupled analysis. Tabri et al. (2008; 2009; 2010) experimentally and numerically studied

the symmetric and unsymmetric ship collision with various collision angles and proposed the numerical method coupling the external dynamics and internal dynamics in one model. Full 6DOF motions of ships can be predicted. The hydrodynamic forces were calculated with linear potential-flow theory and the impact force was obtained by integrating the surface tractions at the collision interface.

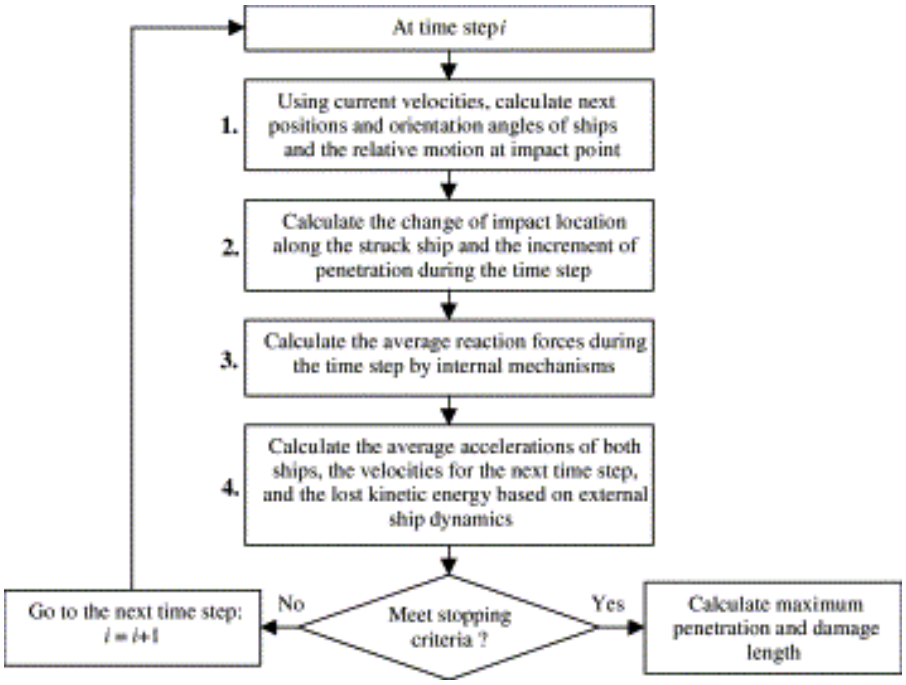

Figure 2-23. Calculation process of SIMCOL, from Brown (2002)

It is noticed that through the literature review above, the development of coupled methods has made great progression, especially on predicting the global motions and considering the hydrodynamic forces in a more accurate way. However, internal dynamics in the coupled methods seems to be simplified too much. For example, Petersen simplified the collision force with 4 springs at the contact point, Le Sourne (2007) and Le Sourne (2011) calculate the impact forces through the super element method, in which a simplified analytical model was adopted. Additionally, the detailed structural deformation cannot be captured. Pill and Tabri (2011) then proposed another coupled simulation method with finite element analysis code, LS-DYNA. In this way, the detailed structural deformation and collision force can be calculated at high accuracy. The challenge is how to consider the hydrodynamic effects. In the study, only the added mass was considered to represent

the hydrodynamic effects. The involved ship model is illustrated in Figure 2-24. A few discrete mass points including added mass were attached to a rigid bulb to simulate the striking ship. For the struck ship, a part of the side structure is modelled, and other parts were represented as a few added mass points or added mass blocks. The global motions were restricted in the horizontal plane.

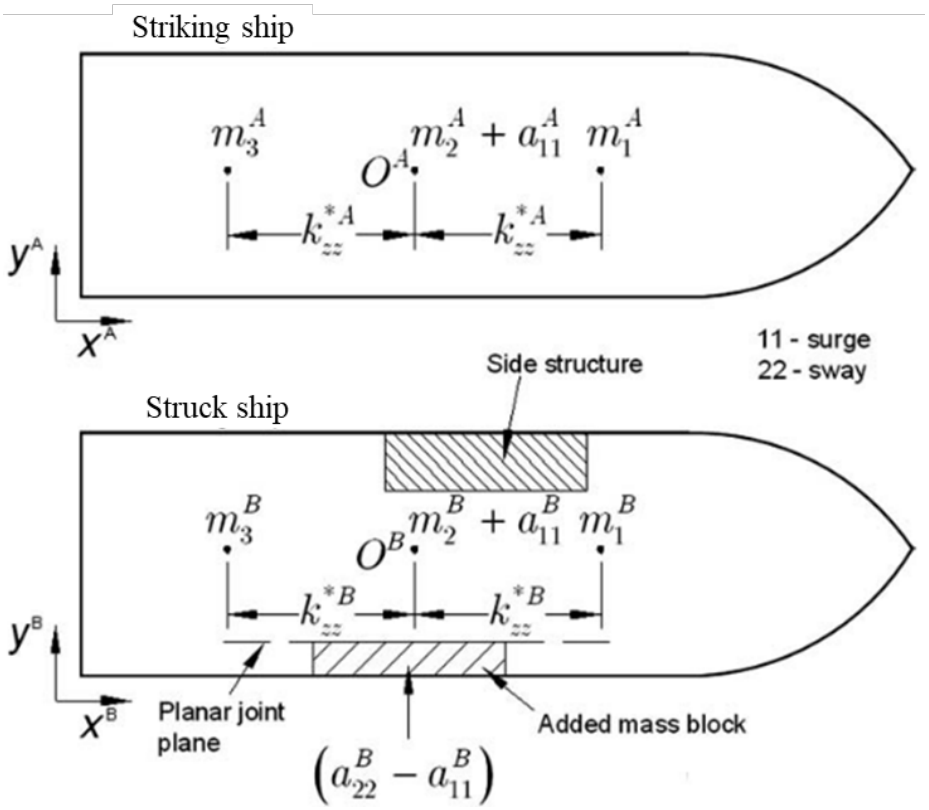

Figure 2-24. Illustration of the model in coupled simulation, from Pill and Tabri (2011)

Pill and Tabri (2011) though improve the accuracy of internal dynamics prediction in the coupled method, the external dynamics accuracy was reduced, i.e., only 3DOF can be predicted, hydrodynamic damping and restoring forces were not included. Yu et al. (2016), Yu and Amdahl (2016), Yu, and Shen et al. (2016) then developed a series of coupled methods that accurately represented the hydrodynamic effects and predicted the internal dynamics in detail. In these studies, the LS-DYNA code was adopted to conduct the structural analysis and the user-defined subroutine in LS-DYNA was employed to calculate the hydrodynamic forces, and totally three models were studied. In the study of Yu et al. (2016), the global motions were restricted in the horizontal plane, and the

hydrodynamic loads were estimated by a conventional maneuvering model. The method was then extended to 6DOF predictions (Yu and Amdahl, 2016), where the out-of-plane motions were simplified as three separate single degree of freedom spring-damper vibration subsystems. The method was verified with SIMO and the whole coupling algorithm is shown in Figure 2-25. In the study of Yu and Shen (2016), another hydrodynamic model, the linear potential flow theory, was adopted and the radiation forces were applied. With this method, the coupling analysis with high accuracy of both hydrodynamic effects and local structural responses can be conducted.

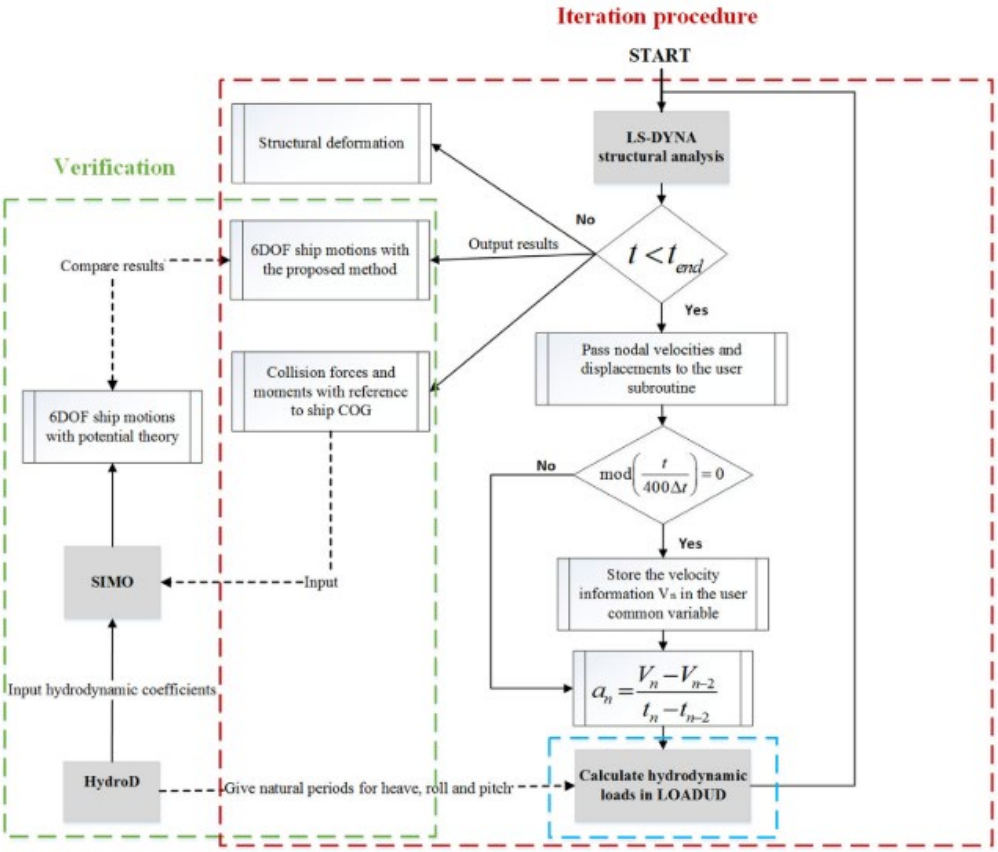

Figure 2-25. Illustration of the coupling algorithm of Yu and Amdahl (2016)

With the development of these coupled methods, the disadvantages of the decoupled method were found and discussed. Tabri (2012) compared the results from coupled and decoupled methods and found that the decoupled methods can predict right-angle collision with reasonable accuracy but for unsymmetric and oblique collisions, especially with small collision angles, a large error can be yielded on the prediction of structural

penetration. The comparison of coupled and decoupled methods was also discussed by Liu et al. (2017) and Yu et al. (2018).

In conclusion, developing and utilizing the coupled method in ship collision analysis should be more and more common in the future as it provides more accurate results by considering the interaction between local structural responses and global motions. However, the decoupled method should remain an amount of usage due to its fast estimation, especially in the industry and engineering practice.

2.4 Ship collision with offshore wind turbines

The classic ship collision analysis methods have been reviewed above, which provides valuable references for ship collision with floating offshore wind turbines because the current studies on ship-FOWT collision are very few. The features of FOWTs are quite different from ships. As they have floating platforms and slender structures with a lumped mass on the top. The global motions are more sensitive to the wave forces and the wind forces. It is important to consider these environmental loads during the collision analysis. Currently, the existing ship-OWT collision studies are most for fixed-support OWTs.

Biehl and Lehmann (2006) has conducted the numerical simulation on ship collision with several different types of OWTs, including the monopile, jacket, and tripod. The simulations were comprehensive and consider the wind loads, soil effects, gravity loads of OWTS. To avoid suddenly applying the gravity and wind loads to cause large amplitude vibration, a quasi-static analysis was conducted as the pre-calculation and the initial stress due to environmental loads were obtained. This was a coupled method, and the hydrodynamic loads of the ship were calculated by MCOL subroutine in LS-DYNA.

Other numerical collision analyses for the jacket, monopile and tripod OWTs can also refer to Le Sourne and Barrera et al. (2015), Moulas et al. (2017), Hao and Liu (2017), and Bela et al. (2017). Le Sourne and Barrera et al. (2015) studied the crashworthiness of a jacket foundation OWT struck by an OSV by means of nonlinear finite element methods

(NLFEM). Both rigid and deformable ships were modelled, and a series of factors, such as gravity loads, soil stiffness, were compared to conduct sensitivity analyses about the energy dissipation pattern and crushing force. The wind forces were not included in the collision analysis. Moulas et al. (2017) also employed NLFEM but mainly focused on evaluating the platform damage of OWT caused by OSV impact. The deformation pattern and damage modes of monopile and jacket type foundations in various collision scenarios were identified and discussed. Hao and Liu (2017) compared the crashworthiness of monopile, tripod, and jacket OWTs. In addition to the local structural responses of the platform, the acceleration at the nacelle was also analysed. Bela et al. (2017) studied the nacelle responses during ship collision on a monopile foundation OWT. In the study, the rotor-nacelle assembly was not modelled in detail, but it is represented by a lumped mass connected to tower top elements with rigid beams, shown as Figure, 2-26. Then the sensitivity of different parameters, such as impact velocity, impact location, wind effect, soil interaction, and deformability of striking ship was thoroughly discussed. The displacement, as well as accelerations at the nacelle of the monopile OWT, were compared and discussed in different scenarios.

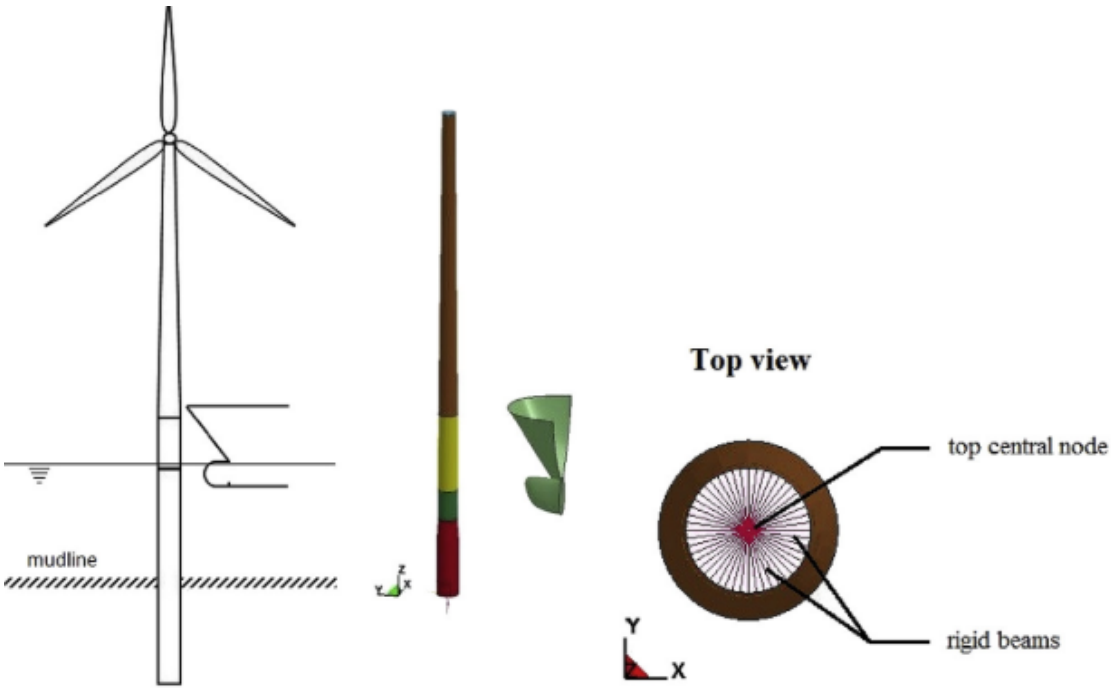

Figure 2-26. FE model of monopile OWT, from Bela et al. (2017)

It is noticed that the NLFEM is very popular in the ship-OWT analysis, but the high computational cost of time is not suitable for the early designing phase. Some analytical methods for ship-OWT analysis were proposed then. Le Sourne et al. (2016) developed analytical methods based on the upper-bound method (Jones, 2011) and Pire et al. (2018) further derived a series of formulae to assess dissipated energy at the bottom of wind turbine jacket foundation after a ship collision. Song and Jiang et al. (2021) developed a simplified analytical method for evaluating the energy absorption and impact force for monopile wind turbines. The aerodynamic damping effects were considered as well. The results of the analytical model were further verified by the numerical simulation with LS-DYNA. This study didn't simplify the wind thrust force as a constant but considered the changing of wind forces during collisions by means of the user-defined subroutine in LS-DYNA, shown as Figure 2-27, It provided a useful approach to model the varying wind force in ship-FOWT collision analysis.

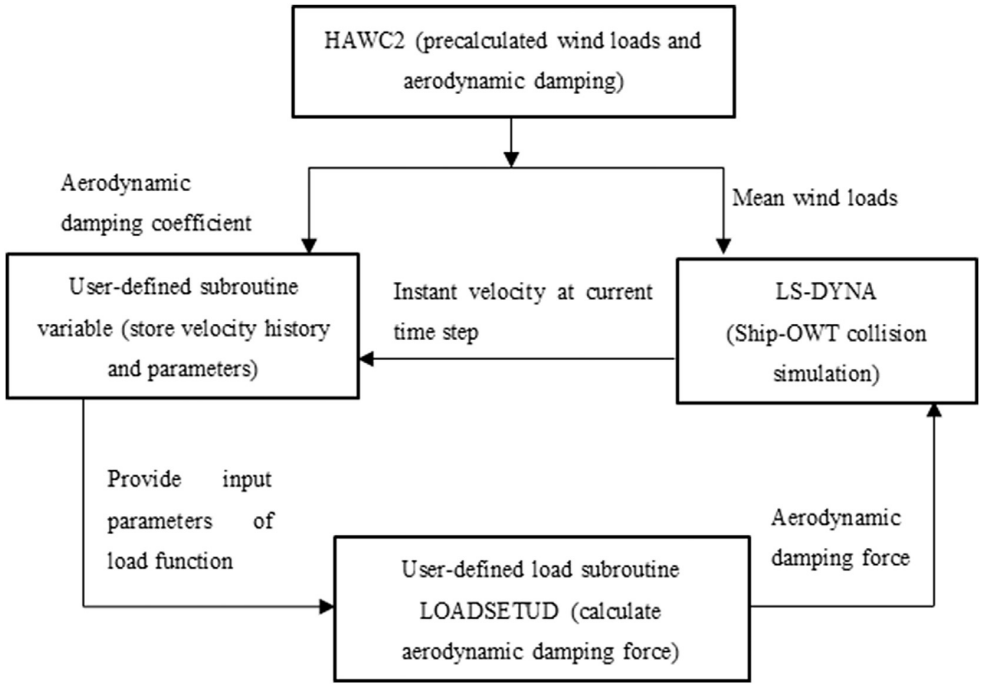

Figure 2-27. The algorithm for coupling wind effects in the numerical simulation with LS-DYNA, from Song and Jiang et al. (2021)

Some design standards of OWT regarding ship collision can be found from DNV-OS-J101 (2014), BSH (2007), DNV-ST-0473 (2016). The design of OWT against ship

impacts has been considered in ULS and ALS depending on whether the secondary or primary structure is damaged. It is noticed that these existing studies mostly focus on the offshore fixed foundation wind turbine, especially the internal dynamics.

Nevertheless, floating offshore wind turbines (FOWTs) still receive little attention on their crashworthiness design. FOWTs are normally exposed at further and deeper water zones where larger service vessels are required and could be located closer to the traffic line. Thus, the ship collision risk may increase. DNV-OS-J103 (2013) adopted the same requirements from DNV-OS-J101 (2014) regarding ship collision against fixed-bottom OWTs and applied them into floating wind turbines regarding ship collision but DNV-OS-J103 (2013) still pointed out that these requirements need to be more thoroughly discussed in the future due to some special and complicated features of the floating platform. There are a few but not adequate studies on ship collisions with floating wind turbines recently.

Echeverry et al. (2019) has studied the crashworthiness of a spar-type floating offshore wind turbine under ship collision by numerical simulation methods. Some parameters characterized to floating wind turbine were considered and discussed, such as hydrodynamic forces, ballast mass, and mooring line tension. The internal dynamic responses such as energy dissipation, collision force, and structural deformation modes were calculated with LS-DYNA while the external dynamics, such as 6DOF motions were predicted by MCOL. From the study of Echeverry et al. (2019), it is interesting to find that ship collision against floating wind turbines is quite different from the collision of fixed-foundation OWT. Due to more complicated loads and conditions including floating platforms, mooring, wave, etc. the FOWT doesn’t respond like a monopile or jacket foundation OWT which mainly gets serious structural deformation or collapse under the huge impact force. In addition to the structural deformation, the floating wind turbine has large translational and rotational motions in some directions as it is more flexible.

Though Echeverry et al. (2019) is a pioneer and made a contribution to the collision analysis of FOWT, it is still a preliminary study, because some significant loads were not included, such as wind and wave excitation force. For example, due to wind and wave excitation force, the FOWT would have got a certain displacement and velocity when ship collision occurs, and these scenarios are hard to be simulated in the previous studies. Thus, in this thesis, more comprehensive studies need to be presented for ship-FOWT collision analyses.

Chapter 3 An integrated method on external dynamics in Ship-FOWT collision

3.1 Introduction

In some cases where short-duration and non-critical impacts occur, the structural damage may not be serious and the FOWT system keeps intact. But the system working performance still needs to be checked, including global motions of the platform, the dynamic responses of mooring system, tower, and rotor-nacelle assembly (RNA).

In this chapter, a novel approach is proposed to analyze the global dynamic responses of FOWT system after ship-FOWT impact. The proposed approach contains two parts, one is a mathematical model for ship-FOWT collision scenario and the other is a method for pre-collision and post-collision analysis with the application of an aero-hydro-servo-elastic code, *DARwind*, an in-house programme developed by Chen & Hu et al. (2019), for fully coupled simulation of FOWT. In the following sections, the ship-FOWT collision analytical model and the fully coupled multi-body dynamic analysis tool, *DARwind* will be introduced, respectively, and then a description on how to integrate them will be presented. Finally, some verification works for the proposed method is conducted.

3.2 The novel mathematical model for Ship-FOWT collision scenario

For conventional 3-D collision analyses, a review has been made in Chapter 2. Stronge (2004) has proposed a 3-D impact dynamic model for rigid bodies and Liu & Amdahl (2010) further developed it for ship collision application. The ship-FOWT collision mathematical model presented in this section is a further development and implementation based on their methods. Some basic assumptions applied into the model are shown below.

- The collision duration is short and the global motions during collision process are small enough to be neglected.

- The collision force is much larger than other forces so that other external forces is temporarily neglected during the collision process.

- The striking position is on the supporting platform only and the structural deformations are limited to a small zone within the contact area of platform. In addition, the influences of structural damage of platform do not play a dominating role in this study.

- The operating performance of the FOWT is assumed remain unchanged during the collision as the change of operation order on FOWT is mostly a gradual process.

An offshore service vessel and a spar-type floating wind turbine are chosen as the reference targets, shown as Figure 3-1. Two global coordinate systems are used, of which the origins are located at the centre of gravity (COG) of a vessel and the FOWT at the beginning of the collision, respectively. A set of mutually perpendicular unit vectors $\overrightarrow{n_1}, \overrightarrow{n_2}, \overrightarrow{n_3}$ are used and the vectors $\overrightarrow{n_1}$ and $\overrightarrow{n_2}$ are in the common tangent plane at collision point C while $\overrightarrow{n_3}$ is normal to this plane. Then a local coordinate system $(\overrightarrow{n_1}, \overrightarrow{n_2}, \overrightarrow{n_3})$ is established. To distinguish the variables from different bodies, the prime mark *'* is used to indicates variables of the ship. Direction vectors from COG of each body to the collision point are represented separately as *r* and *r'*.

At the collision point C, the FOWT and ship are undertaken mutual impact forces F, F' so the impulses to each body are written as

$$\mathrm{d}P_i = F_i dt \tag{3-1}$$

$$\mathrm{d}P_i' = F_i' dt \tag{3-2}$$

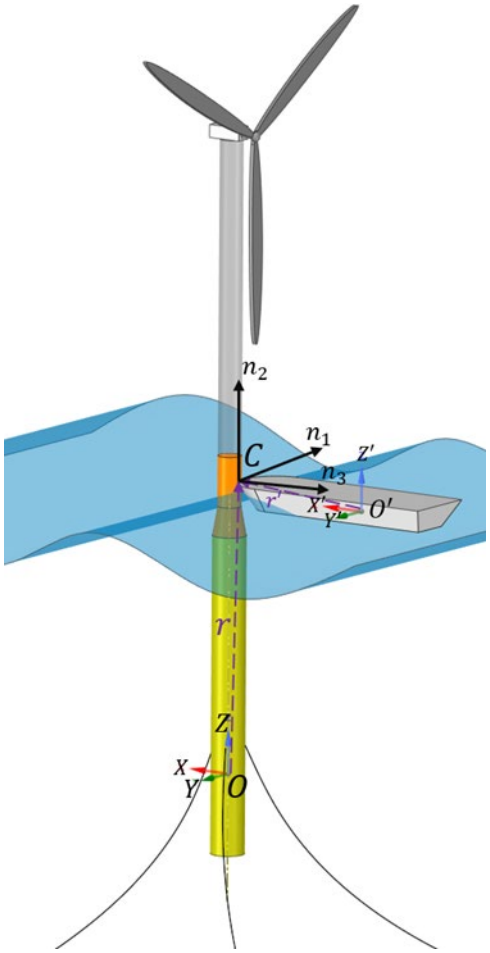

Figure 3-1. Coordinated systems definition in ship-FOWT collision model.

Thus, the equations for translational and rotational motions are expressed as

$$\mathrm{M}\mathrm{d}V_i = F_i dt \tag{3-3}$$

$$I_{ij} d\omega_j = \varepsilon_{ijk} r_j dP_k \tag{3-4}$$

and

$$\mathrm{M}'\mathrm{d}V_i' = F_i' dt \tag{3-5}$$

$$I_{ij}' d\omega_j' = \varepsilon_{ijk} r_j' dP_k' \tag{3-6}$$

where V_i and V_i' represent the velocities at COG of each body while ω_i and ω_i' are their angular velocities in the direction of $\overrightarrow{n_i}$ in the local coordinate system. Based on

the assumptions mentioned above, due to the large collision forces, all the other external forces can be neglected for being so that F, F' here only indicated the collision force. M, M$'$ and I_{ij}, I'_{ij} refers to the mass and second moment of FOWT and ship, respectively. To consider the effects of surrounding fluid, the added mass coefficient and added inertia coefficient are introduced to the mass matrices and inertia matrices. The above equations are written in Einstein summation convention and ε_{ijk} is Levi-Civita symbol and it equals to +1 if the indices are in cyclic order and -1 for anticyclic order and 0 if the value of any indices are the same. The subscript i, j of velocity and angular velocity refer to the i^{th} and j^{th} component of them.

Next, the velocities of these two bodies at the collision point *C* can be expressed as follows according to the velocity relationship between two points on a rigid body of supporting platform.

$$V_{ci} = V_i + \varepsilon_{ijk}\omega_j r_k \qquad (i,j,k = 1,2,3) \tag{3-7}$$

$$V'_{ci} = V'_i + \varepsilon_{ijk}\omega'_j r'_k \qquad (i,j,k = 1,2,3) \tag{3-8}$$

Then the relative velocity is obtained as

$$v_i = V_{ci} - V'_{ci} \tag{3-9}$$

As the deformation is assumed to be limited in a very small area at the collision point, the mass of the deforming part can be neglected. Therefore, the incremental change in the reaction impulses is equal in magnitude but in converse direction. Thus, it can be expressed as

$$dp_i = dP_i = -dP_i{}' \tag{3-10}$$

From equations (3-1) – (3-10), we finally have

$$\mathrm{d}v_i = m_{ij}^{-1} dp_j \tag{3-11}$$

where

$$m_{ij}^{-1} = (M_{ij}^{-1} + M'^{-1}_{ij}) + \varepsilon_{ikm}\varepsilon_{jln}(I_{kl}^{-1} r_m r_n + I'^{-1}_{kl} r'_m r'_n) \tag{3-12}$$

The change of relative velocity can be expressed as

$$dv_i = v_i^t - v_i^0 \tag{3-13}$$

where v_i^t refers to relative velocity in $\overrightarrow{n_i}$ direction when collision ends and v_i^0 indicates relative velocity when collision occurs. If we ignore the possible repetitive impacts and assume there's no sliding between FOWT and ship during the collision, then the relative velocity after collision can be expressed.

$$v_i^t = \begin{cases} 0 & i = 1 \\ 0 & i = 2 \\ -ev_3^0 & i = 3 \end{cases} \tag{3-14}$$

In the above equations, e is defined as coefficient of restitution and usually varies from 0 to 1. It equals to 0 when the perfect plastic collision occurs and equals 1 in the perfect elastic collision.

After obtaining the incremental change of relative velocity, the change of impulse can be calculated according to equation (3-11) and then the change of velocity as well as angular velocity of FOWT are obtained according to equations (3-5) and (3-6). Finally, the velocity and angular velocity of FOWT after collision can be expressed as

$$V_i^t = V_i + dV_i \qquad i = 1,2,3 \tag{3-15}$$

$$\omega_i^t = \omega_i + d\omega_i \qquad i = 1,2,3 \tag{3-16}$$

It is noticed that the calculations are conducted in the local coordinate system $(\overrightarrow{n_1}, \overrightarrow{n_2}, \overrightarrow{n_3})$. Thus, some transformation matrices need to be derived.

3.3 Fully coupled analysis methods for FOWT

DARwind is used in this study for the dynamic responses analysis of the system after impact. It is an intergrade programme based on fully coupled aero-hydro-servo-elastic methods for the simulation of offshore wind turbine developed by Chen and Hu. et al. (2019). The theoretical background will be introduced in this section.

In the programme, hybrid coordinate dynamical analysis method (Likins, 1972) and cardan angle methods (Tupling and Pierrynowski, 1987) are adopted to describe the kinematics of FOWT. Hybrid coordinate dynamical analysis method is for describing the translational motion of the rigid-flexible coupled multi-body system of FOWT. Two types of coordinate system are defined in this method, of which one is the global frame fixed on the earth and the other one is called local elastic body-fixed frame, also known as floating frame (Nada et al. 2010). The translational motion is described using the relative displacement between these two types of frames and the Cardan angles coordinate is used to describe the rotational motion. As a limited rotation of a body about one point can be decomposed as three limited angles corresponding to three different coordinated axes (Bauchau, 2010), the following steps are presented to define Cardan angles. As is illustrated in Figure 3-2, in the first step, the body fixed framed $e^{(0)}$ rotates an angle of α about its axis $e_1^{(0)}$ and then frame $e^{(1)}$ is obtained. Secondly, the frame $e^{(1)}$ will rotate about its axis $e_2^{(1)}$ for an angle of β to frame $e^{(2)}$. Finally, the frame $e^{(2)}$ rotates about axis $e_3^{(2)}$ to frame $e^{(3)}$ at an angle of γ. These three rotated angles are called cardan angles.

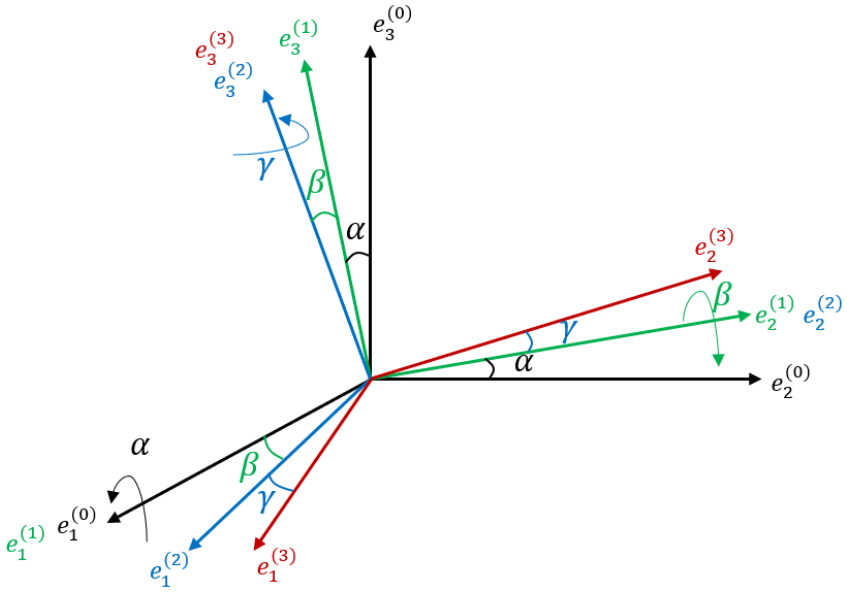

Figure 3-2. Cardan angles illustration

The platform is modelled as rigid and its motion in 6DOF are described using the methods introduced above. The kinematic reference point is located along the vertical central line of platform at the still water level (SWL). The flexible bodies such as blades and tower are modelled as Bernoulli-Euler beams, and they are discretized into structural elements. The deformations are calculated at the midpoint of the discrete elements using assumed mode method. (Morris, 1977)

In *DARwind*, aerodynamic loads at rotor plane are mainly calculated with Blade Element Momentum (BEM) method (Hansen, 2008) including some aerodynamic corrections, such as Prandtl's tip-loss and hub-loss corrections (Hansen, 2008), Glauert's corrections (Spera, 1994), dynamic wake corrections (Øye, 1991), etc. BEM method is essentially a combination of 1-D momentum theory and 2-D blade element theory. In 1-D momentum theory, the rotor is assumed to be a permeable frictionless disc and part of the momentum of the inflow will be lost when it passes through the rotor plane. In 2-D blade element theory, it is assumed that the blades are divided into many elements and the aerodynamic loads acting on these elements are calculated respectively. In addition, aerodynamic loads of the tower are calculated by summarizing the aerodynamic load at the midpoints of all discrete element

$$dF^T = \frac{1}{2}\rho C_d \delta L D (V_0^{wind} - V_{TE})\left|V_0^{wind} - V_{TE}\right| \quad (3\text{-}17)$$

where C_d is the drag coefficient, D is the diameter of section of the current element, V_0^{wind} is the upwind speed and V_{TE} is the velocity of tower element.

As per hydrodynamic loads, linear wave theory (Faltinsen, 1993) is used to model the wave. The diffraction, radiation as well as hydrostatic problems are considered. The required hydrodynamic coefficients to calculate hydrodynamic loads in *DARwind* code are obtained from a 3-D panel-based hydrodynamic analysis program, WAMIT. The total hydrodynamic loads thus can be written as:

$$F_H = F^W + F_{sec}^W + F^R + F^s + F^V \quad (3\text{-}18)$$

where F^W is the excitation force calculated by harmonic superposition method, F_{sec}^W is the second-order wave force consisting of sum-frequency and difference-frequency wave forces components. F^s refers to the buoyancy as well as hydrostatic restoring forces and F^V is the horizontal nonlinear viscous damping force calculated by Morison's equation. F^R is the linear wave radiation force with free-surface memory effects, given by

$$F_j^R(t) = -\sum_{k=1}^{6}\left\{\mu_{jk}(\infty)\ddot{x}_k(t) + \int_{-\infty}^{t} K_{jk}(t-\tau)\dot{x}_k(\tau)d\tau\right\}, \qquad j = 1, 2 \ldots, 6 \quad (3\text{-}19)$$

where $\mu_{jk}(\infty)$ is the added mass coefficient corresponding to infinite frequency and the second term on the right side is the potential damping.

In the mooring dynamics module, a catenary mooring system is modelled and quasi-static approach (Masciola et al. 2013) is employed in the code. The mooring lines are assumed to be in static equilibrium at any time with stretching force but some dynamical properties such as the inertia and damping are not considered. For conciseness, the formulae are not presented, and the detailed derivation can refer to Chen and Hu et al. (2019).

After introducing some key modules in *DARwind* code, the whole analysis procedures of *DARwind* are illustrated as Figure 3-3. As is presented in the flow chart, all types of loads are calculated at each time step firstly. Then Kane's equation method (Kane & Levinson, 1983) is applied to establish the dynamic equation for the multi-body system and generalized accelerations are then calculated. Finally, with the Runge-kutta method, the above calculation procedures are repeated until the terminative time set by the users.

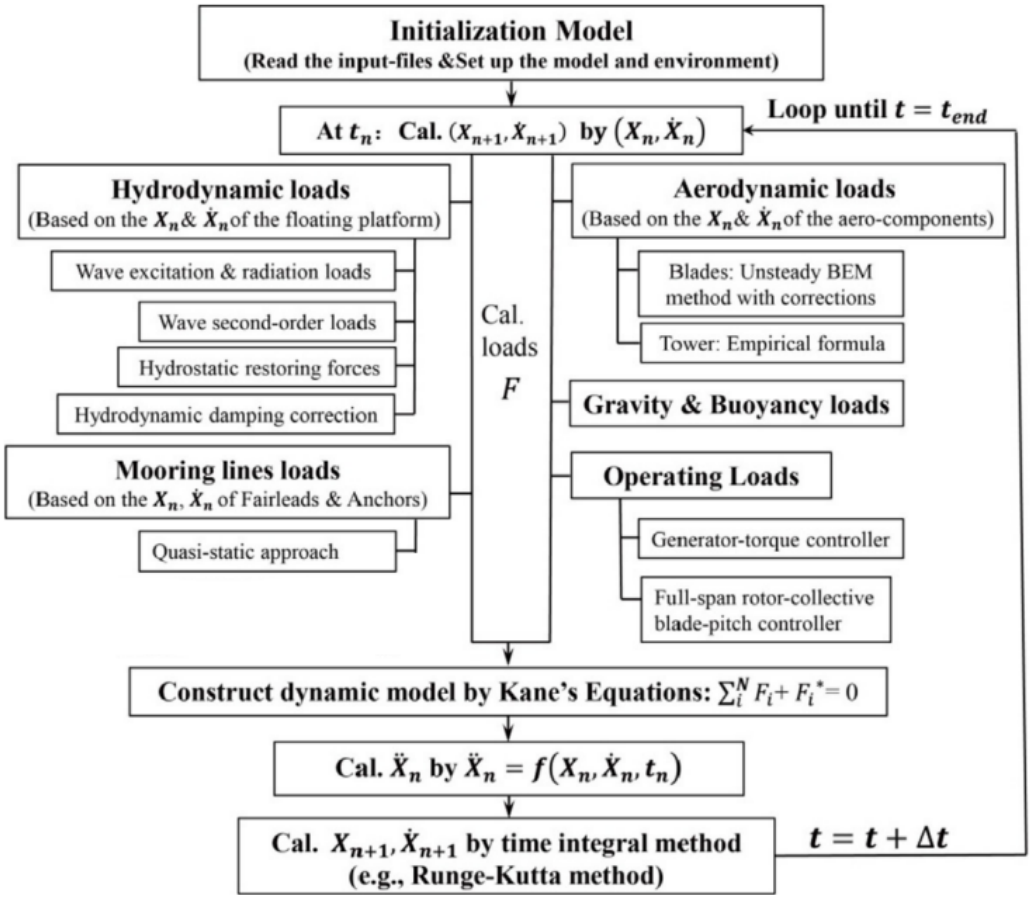

Figure 3-3. the illustration of analysis procedure of DARwind from Chen and Hu et al. (2019)

3.4 Integrated collision analysis methods

This section mainly introduces the procedure on how to integrate the above methods to obtain complete ship-FOWT collision analysis in wind-wave conditions. It should be noticed that the calculations of the transient collision model are conducted in the local coordinate system $(\overrightarrow{n_1}, \overrightarrow{n_2}, \overrightarrow{n_3})$, as described in section 3.2. Additionally, the kinematic

description of the FOWT in the transient collision model employs the centre of mass as the reference point, which is different from the kinematic reference point in *DARwind*. Thus, some transformation matrices need to be derived during the whole calculation procedures and they are derived in section 3.4.1.

3.4.1 Transformation matrix

As the calculation method of ship-FOWT collision is based on the local coordinate system but the velocities of ship and FOWT we described are in their own local frames. Thus, a series of transformation matrices need to be derived.

Also, if an FOWT is working under wave-wind condition, then before the moment of ship impact, FOWT may not be in an upright stance and could have some rotation motions. Thus, the derivation of transformation matrices for FOWT which have general rotational motions will be presented. According to description in section 3.2, the global and local coordinate systems set in collision model are illustrated as Figure 3-4. Figure 3-4(b) is the cross-section in XOY plane and α' is the angle that X-axis sweeps when it rotates about Z-axis to the projection of direction vector r in XOY plane.

By calculating the direction cosines between the axes of FOWT global and local coordinate systems such as

$$\cos\left(\vec{X}, \overrightarrow{n_1}\right) = cos\left(\alpha' + \frac{\pi}{2}\right) = -\sin(\alpha') \tag{3-20}$$

$$\cos\left(\vec{X}, \overrightarrow{n_2}\right) = 0 \tag{3-21}$$

$$\cos\left(\vec{X}, \overrightarrow{n_3}\right) = \cos(\alpha') \tag{3-22}$$

Then whole transformation matrix from FOWT global coordinates to local coordinates can be written as

$$T_{OL} = \begin{bmatrix} -\sin\alpha' & 0 & \cos\alpha' \\ \cos\alpha' & 0 & \sin\alpha' \\ 0 & 1 & 0 \end{bmatrix} \tag{3-23}$$

However, the velocities output from DARwind are in its global coordinate system and this is different from the global coordinate system in collision model. To distinguish them, a note will be added in the bracket following the coordinate system. For example, global coordinate system (DARwind), global coordinate system (collision).

The global coordinate system (DARwind) is fixed at the interface between the still water level and the initial centreline of the floating platform, and the global coordinate system (collision) indeed coincides with the body-fixed frame of floating platform, which rotates with the platform at the moment that collision occurs. Therefore, a transformation matrix from global coordinate system (DARwind) to global coordinate system (collision) needs to be derived.

As is introduced before, the cardan angles method is adopted to describe the rotational motion of FOWT in DARwind, the required matrix above is indeed the transformation matrix from frame $e^{(0)}$ to $e^{(3)}$, given by

$$T_{03} = T_{01}T_{12}T_{23} \tag{3-24}$$

where

$$T_{01} = \begin{bmatrix} 1 & 0 & 0 \\ 0 & \cos\alpha & -\sin\alpha \\ 0 & \sin\alpha & \cos\alpha \end{bmatrix} \tag{3-25}$$

$$T_{12} = \begin{bmatrix} \cos\beta & 0 & \sin\beta \\ 0 & 1 & 0 \\ -\sin\beta & 0 & \cos\beta \end{bmatrix} \tag{3-26}$$

$$T_{23} = \begin{bmatrix} \cos\gamma & -\sin\gamma & 0 \\ \sin\gamma & \cos\gamma & 0 \\ 0 & 0 & 1 \end{bmatrix} \tag{3-27}$$

Therefore, the transformation matrix from global coordinate system (DARwind) to local coordinate system at collision point C is obtained

$$T_{DL} = T_{03}T_{OL} \tag{3-28}$$

Next, let's focus on the transformation matrices for ship. To simplify the problem and only focus on FOWT, the ship is assumed to be in the upright floating position (no rotational motions) and only have forward speed before the collision. It's complicated to directly transform the data of ship from its global coordinate system to the local coordinate system, so it is divided into several steps to finish.

Firstly, we assume the FOWT at an un-rotated position, and then the transformation matrix from global coordinate system of ship to the body-fixed frame of FOWT at this moment can be obtained according to the illustration of Figure 3-5.

$$T_{SO} = \begin{bmatrix} \cos\theta & \sin\theta & 0 \\ -\sin\theta & \cos\theta & 0 \\ 0 & 0 & 1 \end{bmatrix} \tag{3-29}$$

Secondly, we will transform the data of ship from the body-fixed frame of FOWT at un-rotated position to the body-fixed frame of FOWT at its real position. This transformation matrix is given by T_{03} as well.

Finally, the data of ship will be transformed to the local coordinate system from the body-fixed frame of FOWT. The transformation matrix is the same as T_{OL}. Therefore, the final transformation matrix of ship from its own global coordinate system to the local coordinate system at collision point are obtained as

$$T_{SL} = T_{SO}T_{03}T_{OL} = T_{SO}T_{DL} \tag{3-30}$$

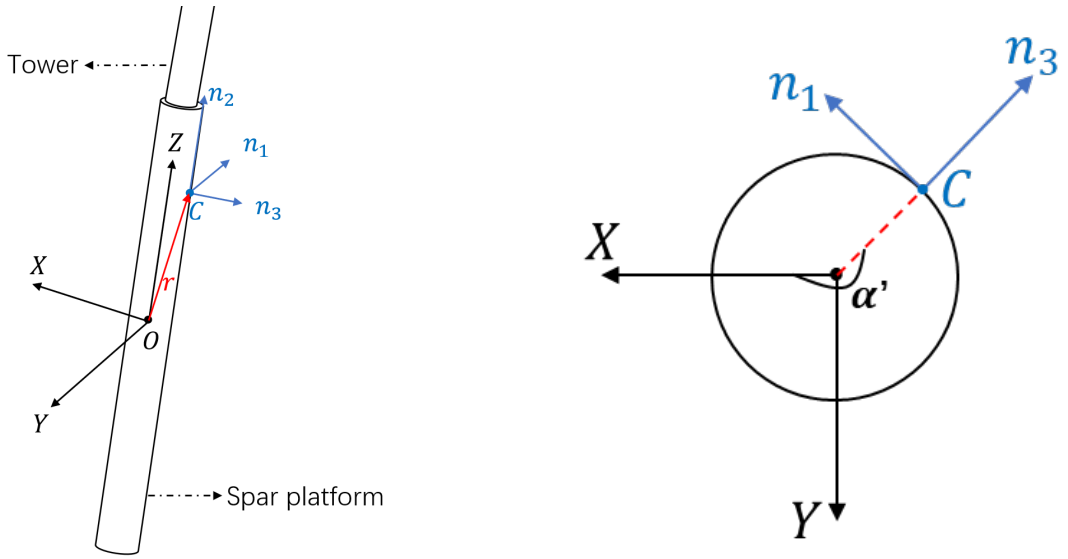

(a) Coordinate systems. (b) Cross-section view in XOY plane.

Figure 3-4. Illustration of coordinate systems and angles for FOWT.

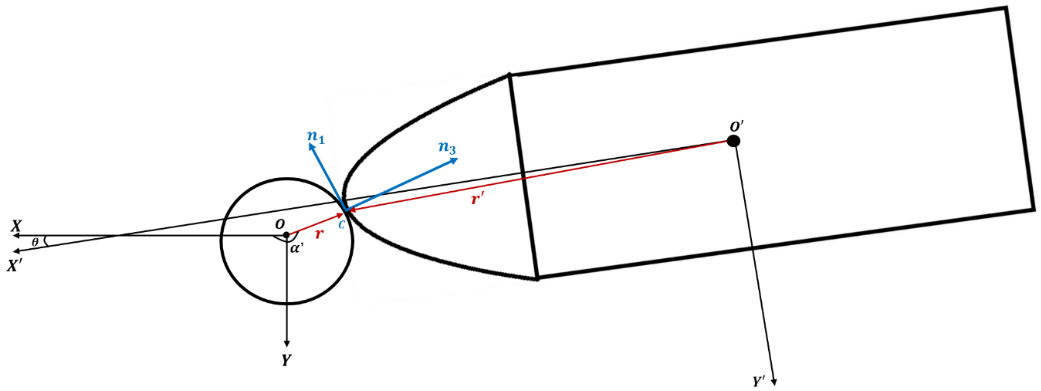

Figure 3-5. 2D Illustration of ship collision against an upright floating spar floating wind turbine.

As the transformation matrices have been derived above, some examples of using these transformation matrices are presented below. V_{global} refers to the velocities directly output from DARwind and other parameters are already expressed under the global coordinates in collision model, so the transformation matrix T_{OL} rather than T_{DL} is used for them

$$V_{local} = T_{DL}^{-1} \bullet V_{global} \tag{3-31}$$

$$r_{local} = T_{OL}^{-1} \bullet r_{global} \tag{3-32}$$

$$M_{local} = T_{OL}^{-1} \bullet M_{global} \bullet T_{OL} \tag{3-33}$$

$$I_{local} = T_{OL}^{-1} \bullet I_{global} \bullet T_{OL} \tag{3-34}$$

3.4.2 Integrating procedure of two models

In section 3.2, a mathematical model is built based on the 3D ship-OWFT collision scenario, but it only addresses the problem of kinematic characters at the collision moment. To have deeper understanding of the dynamic responses of FOWT during and after ship impact. The proposed mathematical collision model and *DARwind* programme are integrated as a new numerical tool. The main analyzing procedure is shown in Figure 3-6, and described below as well

Firstly, the input data is initialized and then a period of simulation for FOWT is conducted by *DARwind* until collision occurs at t_0. Following the step 2, the results during 0 - t_0 are saved and in the meantime, the dynamic responses output from *DARwind* at t_0 will be extracted. From the moment, t_0, the ship impact occurs, so the required data for collision calculation, including the current position and velocities of FOWT and ship in 6DOF, will be input to the 3D collision analysis program, as shown in step 4.

Afterwards, the velocities of FOWT after collision are calculated by the collision model and only the dynamic responses of FOWT are focused then. Due to extremely short collision duration, the moment before and after collision are districted as t_0^-, t_0^+. Only some kinematic parameters at t_0^+ are thought to be changed due to the ship impact while other parameters of FOWT at t_0^+, such as platform location, aerodynamic loads, power, etc. are thought to keep the same. Therefore, a series of new input data are formed following step 6 by combining the dynamic responses results at t_0^- and t_0^+.

With the new input file, a new period of t_1 simulation for FOWT will be conducted and

the results during this period can be output. Finally, in step 8, we integrate the results of $0 - t_0$ and $t_0 - t_1$ to obtain a complete time-domain results.

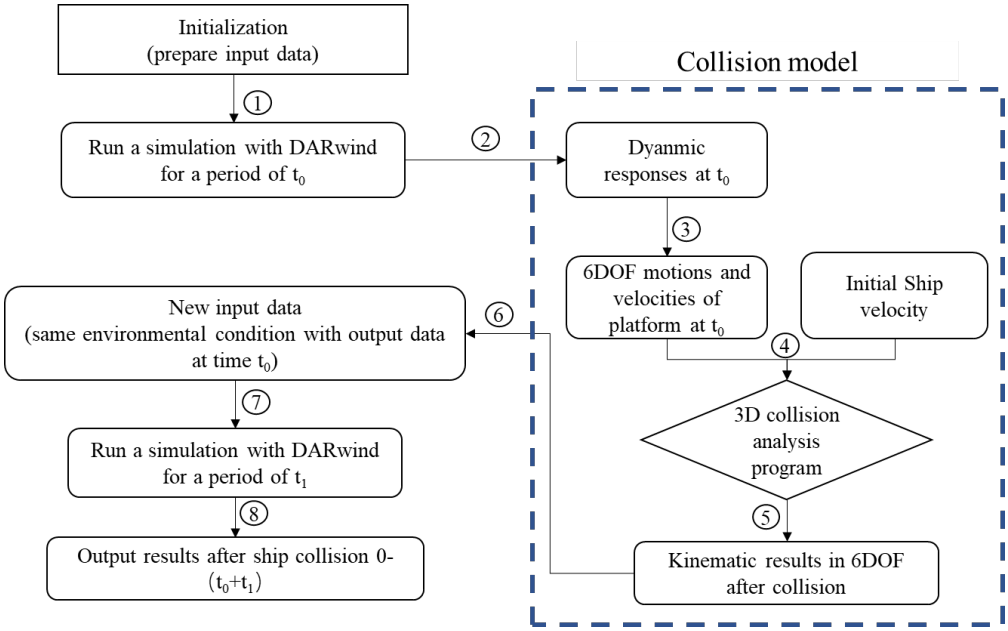

Figure 3-6. The overall flowchart for analyzing dynamic responses of FOWT impact by a ship.

3.5 Verification

The proposed method and code are verified in this section. As *DARwind* has been verified by code-code comparison and experiment validation (Chen & Hu et al., 2019), it is a reliable simulation tool for FOWT dynamic response analysis. Therefore, in this section, the ship-FOWT collision model is mainly verified by comparing the results with an analytical solution for ship-spar collision from Jonge and Laukeland (2013). As the velocities after ship collision can be obtained following the methods described in section 3.4.1, the energy dissipation can be estimated as

$$E_d = E_{total} - (E_{sk} + E_{fk}) \tag{3-35}$$

where E_{total} is the total impact energy before collision and E_{sk}, E_{fk} represent the kinetic energy of ship and floating wind turbine after impact, respectively. They are given as

$$E_{sk} = \sum_{i=1}^{3} \frac{1}{2} M'(1 + a_i')V_i'^2 + \sum_{i=1}^{3} \frac{1}{2} I_i'(1 + j_i')\omega_i'^2 \quad (3\text{-}36)$$

$$E_{fk} = \sum_{i=1}^{3} \frac{1}{2} M(1 + a_i)V_i^2 + \sum_{i=1}^{3} \frac{1}{2} I_i(1 + j_i)\omega_i^2 \quad (3\text{-}37)$$

Where M and I_i are the mass and inertia moment, a_i and j_i are the added mass coefficient and added inertia coefficient. The prime mark ' indicates the data of ship.

From Jonge and Laukeland's study (2013), for head on collision, the dissipated energy is calculated as

$$E = \frac{1}{2}\left[\frac{m_a(1+a_a){v_{a0}}^2}{1+\frac{m_a(1+a_a)}{m_b(1+a_b)}+\frac{m_a(1+a_a)R^2}{I_b}}\right] \quad (3\text{-}38)$$

where m_a, m_b are the mass of ship and spar, respectively. a_a, a_b are the added mass coefficients and v_{a0} is the initial impact velocity. R indicates the distance between collision point and CM (centre of mass) while I_b is the inertia moment around horizontal axis of spar including added inertia.

A 5-MW OC3 Hywind Spar-type floating wind turbine (Jonkman, 2009; Jonkman, 2010) and an offshore service vessel are selected, and the head-on collision are simulated. The parameters of FOWT and OSV required for the collision calculation are listed in Table 3-1 and Table 3-2

Table 3-1. Main properties of FOWT

Offshore floating wind turbine	
Total draft	120 m
Platform diameter at collision point	6.5 m
CM of whole FOWT below SWL	78 m
Total mass (including ballast, tower, nacelle, rotor, blades)	8066 tons
Ixx	6.8026E10 $kg * m^2$
Iyy	6.8023E10 $kg * m^2$
Izz	1.9157E8 $kg * m^2$
Ixy	9.9135E6 $kg * m^2$
Ixz	-8.6878E6 $kg * m^2$
Iyz	6.9659E6 $kg * m^2$

Table 3-2. Main properties of striking OSV

OSV	
Height	H=7.55 m
Length	L=72 m
Breadth	B=17 m
Draft	T=5.4 m
Mass	M=4000 t
Water plane coefficient	Cwp=0.8
Midship section coefficient	Cm=0.98

For FOWT, the added mass factors at the infinite frequency are chosen and these can also be found from Jonkman's study (Jonkman, 2010). The inertia properties presented in Table 3-1 are about the reference point which is located at the central line of platform at the SWL. It should be transformed to those about the CM (centre of mass) before the collision calculation because the motion equation in transient model is about CM (centre of mass) of the FOWT.

For the striking ship, the added mass is estimated based on previous studies. According to Petersen and Pedersen (1981), the constant added mass coefficients of ship used in the ship collision analysis depend on the impact duration and they also gave the empirical formula and varying range. For simplicity, $a_{11} = 0.05$ and $a_{22} = 0.7$ are selected for surge and sway motion. Pedersen et al. (1993) gave a value of $a_{66} = 0.21$ for added mass coefficient in yaw motion during collision. The other three added mass coefficients and the radius of gyration for ships used in collision analysis are estimated by the empirical formulae from Popov et al. (1969). They are given as

$$a_{33} = 2/3(BC_{wp}^2)/(TC_b(1 + C_{wp})) \tag{3-39}$$

$$a_{44} = 0.25 \tag{3-40}$$

$$a_{55} = B/(T(3 - 2C_{wp})(3 - C_{wp})) \tag{3-41}$$

$$R_{xx}^2 = C_{wp}B^2/(11.4C_m) + H^2/12 \quad (3\text{-}42)$$

$$R_{yy}^2 = 0.07C_{wp}L^2 \quad (3\text{-}43)$$

$$R_{zz}^2 = L^2/16 \quad (3\text{-}44)$$

Head-on collisions are conducted and the restitution coefficient e=0 is adopted in these verification cases, indicating that the collisions are purely plastic. The results under different impact velocities and at different collision height are compared in Table 3-3. It is found that the results from two methods match well, with only a slight difference about 1% error shown between the two methods, which implies that the present method has the capacity to evaluate the responses between ship and spar-type floating wind turbine. It is also interesting to find that the energy dissipation predicted from present method are less than that of the reference. This is due to the 3D model used in present method, 6DOF motions can all be predicted in the present method while motions in vertical plane are considered in Jonge and Laukeland's method (2013). The lack of motions in some degrees of freedom will result in smaller kinetic energy predicted after collision, so the dissipated energy will be larger than that of the proposed method.

Table 3-3. Comparison of results from current method and Jonge & Laukeland's method (2013)

Energy dissipation (MJ)								
Impact velocity / Impact height	1 m/s		1.5 m/s		2 m/s		2.5 m/s	
	Present	Jonge & Laukeland	Present	Jonge & Laukeland	Present	Jonge & Laukeland	Present	Jonge & Laukeland
3m above SWL	1.189	1.201	2.675	2.702	4.756	4.804	7.431	7.506
4m above SWL	1.181	1.193	2.657	2.684	4.724	4.771	7.381	7.455
5m above SWL	1.173	1.184	2.639	2.665	4.692	4.738	7.331	7.404

3.6 Summary

This chapter develops a method to evaluate the external dynamic responses of FOWT in the ship collision scenarios and gives some verification works. This method consists of

an analytical model and an aero-hydro-servo-elastic FOWT simulation tool, and various environmental conditions can be considered in the ship-FOWT collision.

The method is more efficient compared with the nonlinear finite element methods and can provide more results than the sole analytical method does. However, the method is established based on some assumptions, such as short collision duration, small contact area and slight structural damage. The method could lose accuracy when serious collision occurs. Additionally, the internal dynamic responses of FOWT in the ship-collision scenarios cannot be captured with this method. Therefore, a more comprehensive method including both internal and external dynamics needs to be considered.

Chapter 4 Cases of study on the integrated method

4.1 Introduction

An integrated method for investigating the external dynamics of FOWT in ship collision scenarios has been introduced in the last Chapter. With this newly developed method, the dynamic responses of FOWT can be predicted and analyzed.

In this Chapter, the 5-MW Hywind OC3 Spar-type floating wind turbine impacted by an offshore service vessel is selected as an example, and the global dynamic responses of FOWT after ship collision are analyzed, including the 6DOF motions, the responses of nacelle, blades, tower, and mooring system. Additionally, three different environmental conditions are considered in the collision scenarios.

4.2 The configurations of striking ships and Spar-type floating wind turbine.

The main scantlings of the 5MW-OC3 Hywind Spar-type floating wind turbine (Jonkman, 2009; Jonkman) and the striking OSV are shown as Table 4-1 and Table 4-2.

Table 4-1. Main scantlings of FOWT.

Offshore floating wind turbine	
Tower base above SWL	10 m
Tower top above SWL	87.6 m
CM of tower above SWL	43.4 m
Total draft	120 m
Platform top above SWL	10 m
Taper top below SWL	4 m
Taper bottom below SWL	12 m
Platform diameter above taper	6.5 m
Platform diameter below taper	9.4 m
CM of platform below SWL	89.9 m
Water depth	320 m
Number of mooring lines	3

Depth to fairleads below SWL	70 m
Radius to anchors from platform centerline	853.87 m
Unstretched mooring line length	902.2 m
Total mass (including ballast, tower, nacelle, rotor, blades)	8066 tons

Table 4-2. Main properties of OSV.

Offshore service vessel	
L.O.A	72.2 m
Beam	16 m
Depth	7.55/11 m
Draft	5.4 m
Displacement	4,000 tons

The evaluation of added mass factors of FOWT and OSV in the collision process can refer to the Section 3.5 and won't be introduced again. Note that the restitution coefficient $e=0.5$ is adopted in the following collision cases in this chapter, implying the collision includes both plastic and elastic structural deformation.

A brief case definition is listed as Table 4-3, where H and T are the wave height and wave period. Currently, only head-on collisions are applied. The ship impact, wave propagation and wind have the same direction, along the positive direction of surge motion of FOWT.

In still water case, the FOWT stays static and have no rotational or translational motions when collision occurs. According to the current designing standard (DNV, 2014), the impact velocity should be considered no less than 0.5m/s. Thus, in still water situation, the ship is given varying velocities from 1m/s to 3m/s to investigate the influence of impact velocity. For collisions in regular wave and wave-wind condition, the FOWT has got certain motions and velocities when collision occurs. In order to get general sight on the dynamic responses in these environmental conditions, ship collision is set up to occur when FOWT have different motions, corresponding to cases C1 – C4 and C5 – C9 in these two different environmental conditions.

Table 4-3. Collision scenarios and cases definition

Case number	Case types	*H (m)*	*T (s)*	Wind speed (m/s)	Ship velocity (m/s)

C0	Still water	-	-	-	from 1 to 3
C1 - C4	Regular wave (different initial motions when collision occurs)	4	10	-	3
C5 - C9	Wind and regular wave (different initial motions when collision occurs)	4	10	11.4	3

4.3 Analysis in still water condition

4.3.1 Response of 6-DOF motions

As the impact direction is along the positive direction of surge motion of FOWT, so the most obvious motion responses should appear in surge and pitch directions, shown as Figure 4-1.

For all pitch motions with different impact velocities, the same trends are found, shown as Figure 4-1 (a). It could be simple to understand that undertaking the ship impact, the FOWT gets considerable amount of kinetic energy, and the pitch motion is then excited due to the vertical eccentricity (vertical distance between COG and collision point). The motion responses after ship collision in the still water can be regarded as a free-decay trend with an initial velocity, which is given by ship impact. Therefore, the presented sinusoid of pitch motion can be explained.

For surge motions after collision, presented as Figure 4-1 (b), they show a quite different trend, not the sinusoid though they are regarded as free-decay motions with initial velocity. This is mainly caused by the coupling effects with pitch motion. As the dynamical reference point of the platform is set at the centre of section at still water level when it is un-moved, the pitch motion will no doubt result in the movement of dynamical reference point, which is reflected by the change of surge motion. Besides, the ship impact will result in pure translation motions in surge direction, which moves the dynamical reference point as well. When these two kinds of motions are coupled, the surge motion reflected in the figure are no longer sinusoid. it is interesting to find the surge motion curves have two crests during the first 40 seconds after collision and the time point of these two crests

(about 10th second and 40th second) almost corresponds to the time points, where the maximum pitch angles are reached. This indeed prove the coupling effects of pitch motion as well.

Though the different patterns of surge and pitch motion curves are found and discussed, the overall trend of them both shows periodically decay trends under the combined effects of the mooring system and hydro loads. Additionally, it is found that the impact velocities significantly influence the amplitude of motion responses, and they increase almost proportionally with the impact velocities rising. It is noticed that for impact velocity of 2m/s in still water, minor responses on platform motions are caused, less than 5m in surge motion and 1deg in pitch motion. For the largest impact velocity 3m/s, the maximum motion responses have obviously changed but are still in an acceptable range for a spar-type floating wind turbine.

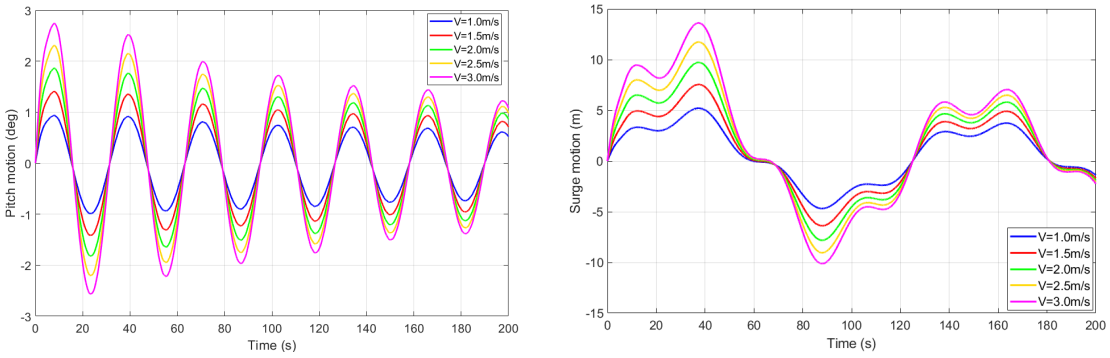

(a) Pitch motion response after collision. (b) Surge motion responses after collision.

Figure 4-1. Comparison of motion between collision scenarios with different impact velocities.

4.3.2 Responses of mooring system

Figure 4-2 illustrates how the mooring system responds after the ship impact and Figure 4-2 (a) presents the time-domain results of tension of fairlead #1 (the fairlead #1 is in XOZ plane and has the largest responses when undertake ship impact along the direction of surge motion) after the collision and Figure 4-2 (b) illustrates the mooring line responses. It is interesting to find that the fairlead tension shows a periodical decay trend after rapidly rising after ship impact. The mooring system is mainly used to protect the

platform from floating away so it should be sensitive to the translational motions of the platform, which are also proved by comparing Figure 4-1 (b) and Figure 4-2 (a). It is obvious that the overall trend of fairlead tension changes with surge motion (Figure 4-1 b) and the fairlead tension forces reach the peak where are also the maximum amplitude of surge motions reached.

For the mooring line forces shown in Figure 4-2 (b), the overall trend and pattern in these five scenarios are similar but in the scenarios with small impact velocity, the fluctuations of mooring line forces seem to be more obvious. It is found that the mooring line forces all increase rapidly though the curves are not so smooth in the scenarios with velocities from 1.5m/s to 3m/s. However, the forces in the scenario with an impact velocity of 1m/s show a slight fall before increasing. Additionally, it is found that the period of curves becomes larger in higher impact-velocity scenarios. It is concluded that the small-range motions caused by the low-speed impact will bring more fluctuations and lower responses period of mooring line forces.

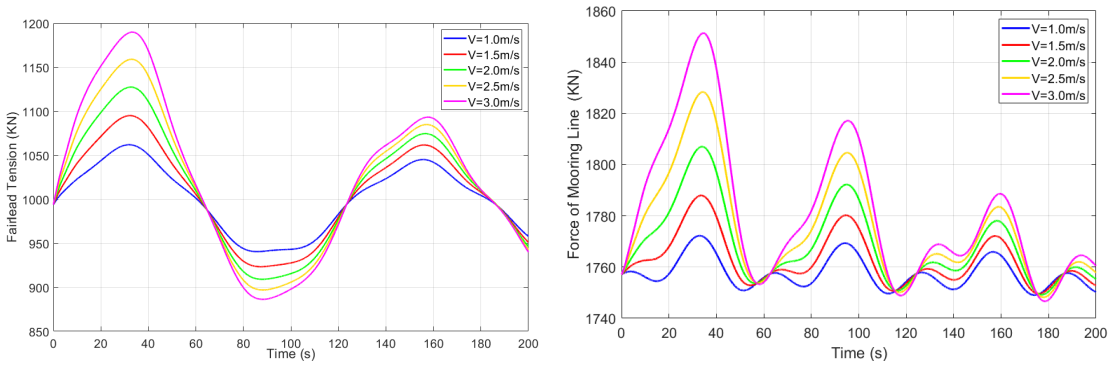

(a) Comparison of fairlead#1 tension. (b) Comparison of mooring line force

Figure 4-2. Comparison of tension of fairlead with different impact velocities.

4.3.3 Responses of rotor-nacelle assembly

Figure 4-3 (a) gives the motion responses at the tower top after a ship collision. It is interesting to notice that the tower top motions pattern in surge direction is similar with of platform surge motion, which is shown in Figure 4-1 (b) but the amplitude in Figure 4-3 (a) is much bigger, or in other words, comparing with the platform surge motion, the

crest and trough in the curves are enhanced. The enhanced crest and trough shown in the curves can be explained by considering the pitch motion coupling effects. As the tower is clamped on the floating platform, the surge motion of the platform will directly bring translation motions at the tower top, which explains the similar motion pattern between the tower top and the platform. In the meanwhile, due to the big height of the tower, a slight pitch motion of the platform can lead to considerable motion changes at the tower top. Thus, when these motions are coupled together, a similar trend with greater amplitude is then formed. Additionally, a very slight difference in period is found in each case. This could be explained by considering the flexible tower. Chen et al. (2019), Matha et al. (2010) found that the elasticity of the tower can influence the periods of surge and pitch motion modes. When impact occurs, the tower vibration will be excited and different impact velocities could cause different modes of vibration. The tower top motion is influenced by the coupling effects of platform motion and tower vibration, so it turns to have a little different period under different impact velocities.

The tower vibration can also be found in Figure 4-3 (b). After the ship impact, the static platform of FOWT gets a velocity and then has periodical decay trend due to the hydrodynamic damping effects. But some small fluctuations are found in Figure 4-3 (b), which exactly indicates the tower vibration phenomenon. Comparing the responses in different scenarios in Figure 4-3, the impact velocities are found to still have a significant influence on these aspects.

Figure 4-3 (c) gives a clear sight of acceleration histories, and it should be noted that the results presented here represent the pattern of the responses after the ship collision. The acceleration at t=0s, where ship collision ends, is not zero according to the figure. The ship collision is essentially an impulse acting on the spar platform, and the platform then gets increasing momentum. When the ship collision process ends, the contact force reduces to zero and the platform has gotten a certain velocity. This velocity leads to aerodynamic load on the blades, and hydrodynamic damping load on the Spar hull, which gives the initial non-zero acceleration value in Figure 4-3 (c). By considering the coupling

effects between platform velocity, the vibration of the flexible tower, and external forces including aerodynamic, mooring, and hydrodynamic aspects, the acceleration at this moment can be calculated by Kane's dynamic equation adopted in the DARwind programme. It should be noted that according to Figure 4-3 (c), the maximum magnitude of the acceleration is not at t=0s but at the next few seconds. At that moment, the nacelle already has a local deflection and keeps vibrating due to the flexible tower. Similar conclusions can also be found from Pedersen's study (2013), in which a ship collision against a fixed-support wind turbine was analysed. From the numerical simulation results in Pedersen's study (2013), the collision duration can be separated into two phases. In phase 1, the maximum contact force was reached and then fell but the maximum magnitude of acceleration at nacelle was found during phase 2 when the tower is moving back from the maximum nacelle deflection. In the current study, the scenario where maximum acceleration was reached is similar to that in phase 2 but current results could be a little conservative because the flexibility of the tower structure is neglected during the collision process. As for more transient details during a collision, they will be included in the coupling methods based on NLFE technology.

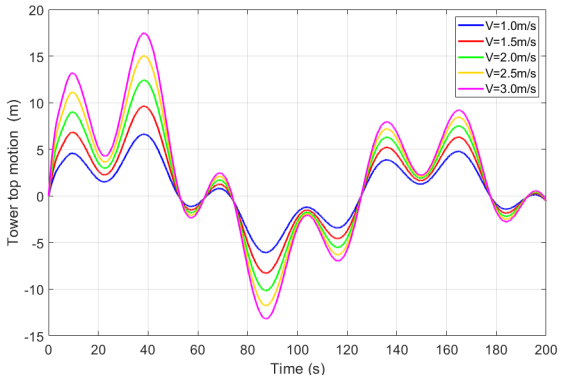

(a) Tower top (nacelle) motion in surge direction.

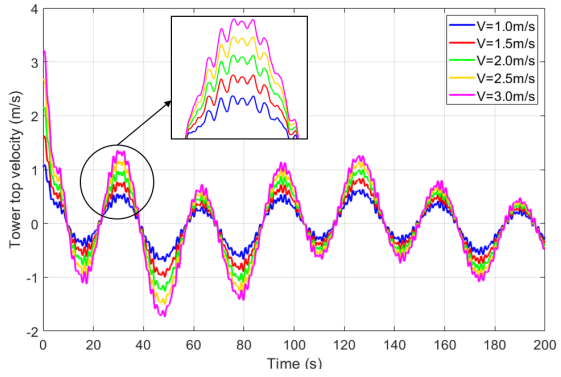

(b) Tower top (nacelle) velocity in surge direction.

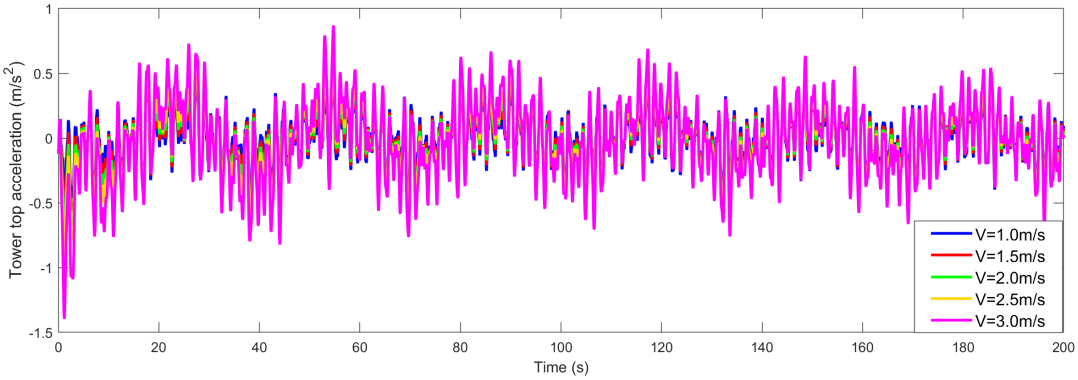

(c) Tower top acceleration along surge direction

Figure 4-3. The dynamic responses of nacelle under different impact velocities.

To further evaluate the safety of FOWT, the maximum tower tip deformation and acceleration along the impact direction are presented in Figure 4-4. The maximum tower tip deformation here indicates the purely elastic deformation, and it clearly shows a slow growth with the increment of impact velocity when impact velocities are less than 2.5m/s. Due to the large mass of rotor-nacelle assembly (RNA), the sudden change of platform motion caused by ship impact will lead to a large inertia force at the tower top, subsequently resulting in a structural deformation.

For the maximum acceleration values shown in Figure 4-4, it appears to have a non-linear rise with impact velocity increasing. The increasing speed also becomes faster at higher impact velocity. The non-linear behaviour is mainly caused by the flexible tower. The acceleration result is obtained from the integrated collision analysis model (collision model + DARwind). In the DARwind programme, the FOWT is modelled as a rigid-flexible coupled multi-body system. Due to the sudden motion change of platform caused by ship impact, the vibration of the flexible tower will be excited and bring considerable acceleration. The tower top acceleration depends on the coupling effects of tower vibration as well as the platform motion. This becomes the source of nonlinearity in the relationship between tower top acceleration and impact speed. The acceleration at the nacelle needs more attention when the crashworthiness of FOWT is taken into consideration during the early designing phase as some equipment in the nacelle might be sensitive to it.

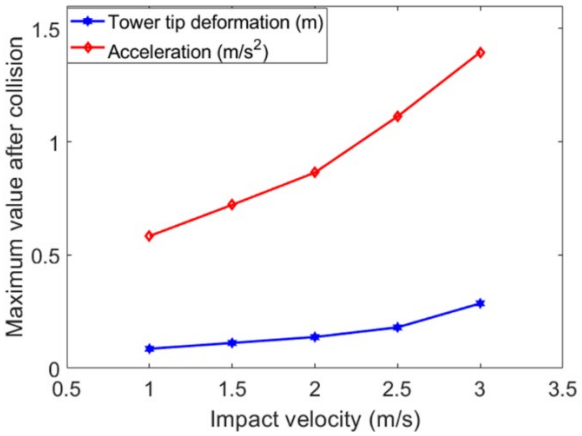

Figure 4-4. Responses at tower top (nacelle) vs. impact velocity

4.4 Collision analysis in wave-only condition

Wave, as a common environmental condition, will bring new loads for the FOWT. Thus, the dynamic responses due to ship impact in this type of condition need to be investigated. Figure 4-5 gives time-series results of surge motion in wave-only conditions without ship collision. In order to have a general insight on how the ship impact influences the dynamic responses of FOWT, four typically different points are chosen as the ship impact moment, named C1, C2, C3, C4, respectively. The 6DOF motions of FOWT at these impact moments are extracted from Figure 4-5 and listed in Table 4-4. Other parameters of these cases have been defined in Table 4-3.

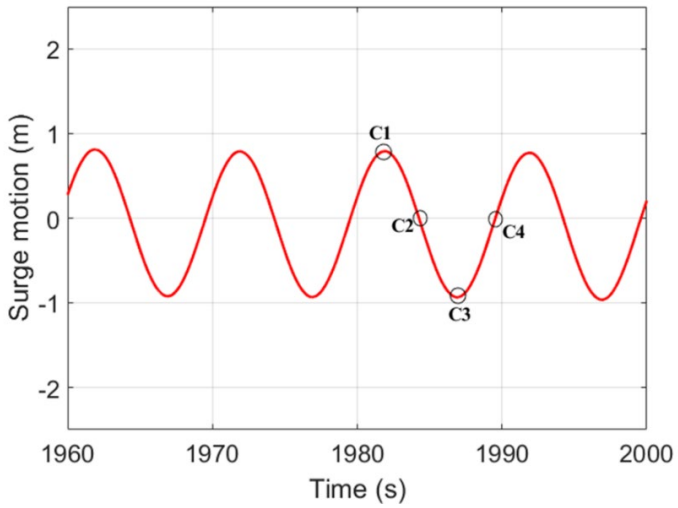

Figure 4-5. The surge motion in wave-only condition and the definition of impact moments

Table 4-4. Initial 6DOF motions of FOWT at the impact moment of collision scenarios

Case Number	Surge(m)	Sway(m)	Heave(m)	Roll(deg)	Pitch(deg)	Yaw(deg)
C1	0.7904	-0.0384	-0.2458	-0.0035	0.4021	-0.0016
C2	0.0000	-0.0124	-0.4903	-0.0029	-0.0251	0.0142
C3	-0.9338	0.0231	-0.4323	-0.0014	-0.4784	-0.0101
C4	0.0000	0.0547	-0.2518	-0.0001	0.0205	-0.0024

4.4.1 Responses of 6-DOF motions

The whole time-series results of platform motion responses, including those before and after a collision, are shown in Figure 4-6 and Figure 4-7. It is noticed that in the first few seconds, the ship collision hasn't occurred, so both the surge motion and pitch motion of FOWT is in the periodical oscillation caused by the regular wave. Due to the sudden ship impact, the platform of FOWT then has a sudden change in its velocity, causing obvious translation (surge) and rotational motions. In the meanwhile, the regular wave still acts on the platform forcing it to oscillate in a small range. For surge motion shown in Figure 4-6, it is noticed that after the collision, though the overall trends are similar, the detailed motion responses, including amplitude and pattern of small fluctuations, are quite different. The most overall motion pattern is mainly caused by the ship impact, and the small spikes shown on the curve are due to the coupling effects of regular wave and pitch motion. For pitch motion responses presented in Figure 4-7, similarly with the surge motion, obvious motion increments in pitch direction after ship impact are found and a lot of spikes exist in their motion curves due to the regular wave as well.

Though the ship velocity and wave condition are defined as the same in these four cases, the FOWT has different motions with different velocities at the moment of collision, which leads to different relative impact velocities (total impact energy) and will surely cause different values of motion responses accordingly. It is interesting to find that the gap of surge motions in the four cases is slight (the maximum values are all around 5m) compared with that of pitch motion. Obviously, the maximum amplitude of pitch motion responses in case C2 is much smaller compared with those of the other 3 cases. This

indicates that in the wave-only condition, responses of surge motion due to ship impact are less affected by the initial state of FOWT while pitch motion responses of FOWT could also be influenced by its initial state when ship impact occurs. Additionally, by comparing Figure 4-2 with Figures 4-6, 4-7. Another interesting finding is that for the same ship impact velocity, 3m/s, the maximum amplitudes of both surge and pitch motions in wave-only conditions are generally less than those in still water. The regular wave brings additional resistance during the motion of FOWT after ship collision, which takes more kinetic energy away

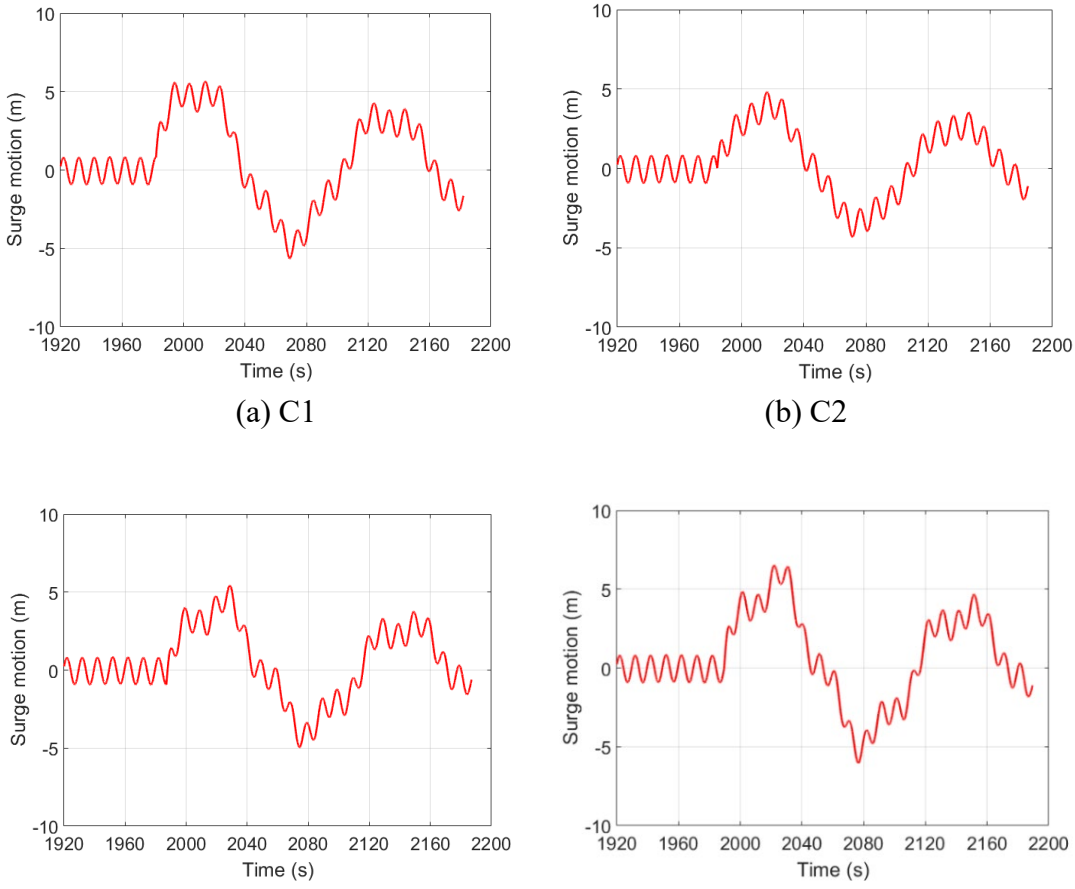

(a) C1 (b) C2

(c) C3 (d) C4

Figure 4-6. Surge motion for four collision scenarios in wave-only condition.

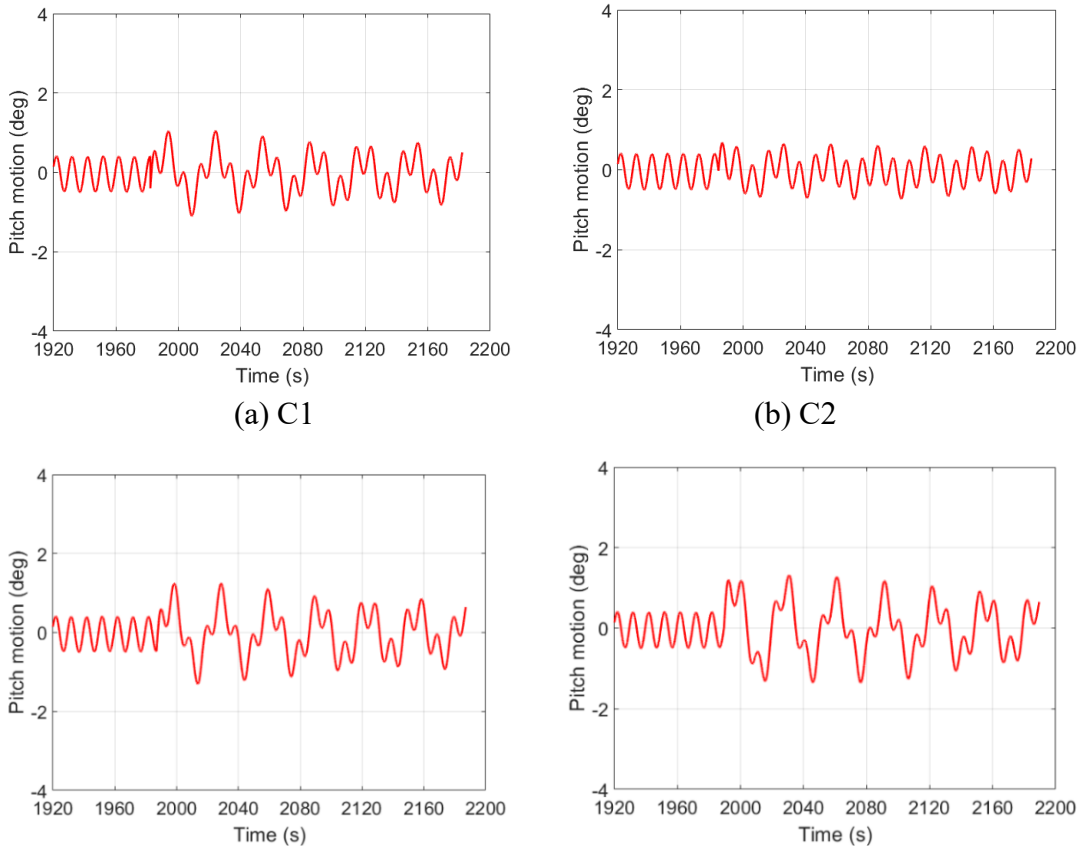

(a) C1 (b) C2

(c) C3 (d) C4

Figure 4-7. Pitch motion for four collision scenarios in wave-only condition.

4.4.2 Responses of rotor-nacelle assembly

As for the responses at tower top in wave-only condition, the comparisons of maximum deformation before and between collision is presented, shown in Figure 4-8. As is analyzed before, the elastic deformation is mainly caused by tower vibration and the large inertia force at the tower top. Due to ship collision, the platform has a sudden change of motion, enhancing the tower vibration. The increasing rates of tower tip deformation after collision are read as 54.2%, 51.2%, 62.7%, 77.3%, respectively. Considering the tower vibration and platform motion, the maximum acceleration after the collision is calculated and presented in Table 4-5. These values in different cases don't show an obvious gap and are all less than the suggested safe line 0.2-0.3g, where g is the gravitational acceleration. In general, the nacelle is thought to be safe and can withstand this kind of ship impact. More attention needs to be paid to structural responses in the future.

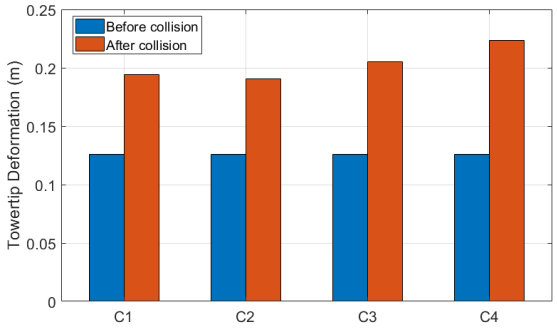

Figure 4-8. Comparison of maximum tower tip deformation.

Table 4-5. The maximum accelerations at tower top after ship impact.

Impact scenarios	C1	C2	C3	C4
Maximum acceleration (m/s^2)	1.0495	1.1412	1.4334	1.3065

4.4.3 Responses of mooring system

Mooring system mainly provides the restoring forces for a floating platform to keep them stable. As the platform has obvious growth in its motions after the collision, the responses of mooring line forces and fairlead tension need to be compared, shown as Figure 4-9. The maximum tension at fairlead rises more apparently and rises by 11.99% on average while the maximum tension of the mooring line has a slight average increment rate of 1.11%. It is noticed that the maximum values for both fairlead and mooring lines appear in case C4, where the most obvious motion changes occur after the collision. For the safety evaluation, these peak values are still in a normal range and don't need extra attention.

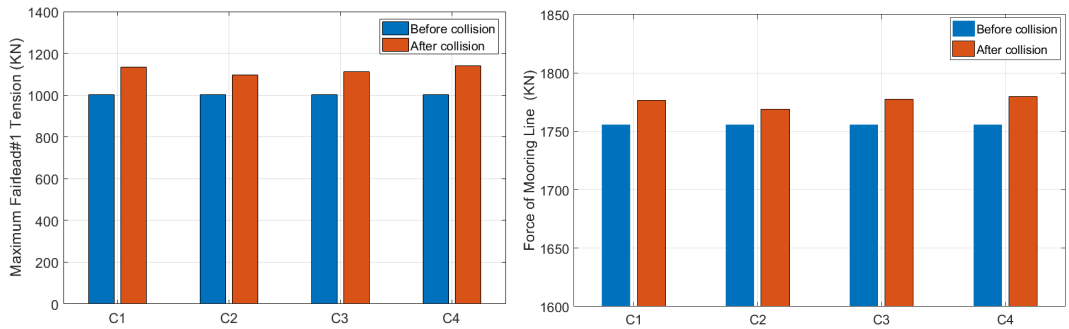

(a) Comparison of maximum tension at fairlead #1. (b) Comparison of maximum mooring line force.

Figure 4-9. Comparison of mooring system.

4.5 Collision analysis in wind-wave condition

Wave-wind combined condition is common for FOWT but also brings new challenges for the investigation of dynamic responses of collision scenarios. The impact loads are more complicated, and the dynamic responses might be more difficult to predict. In this section, in order to investigate the general features of FOWT in wind-wave condition under ship collision, a certain period of fully coupled simulation by DARwind was conducted firstly and 5 typical cases, C1-C5, which indicated different collision moments, are selected from a period, shown as Figure 4-10. The detailed motion in 6DOF at the collision moment are listed in Table 4-6 and other parameters of environmental condition are defined in Table 4-3.

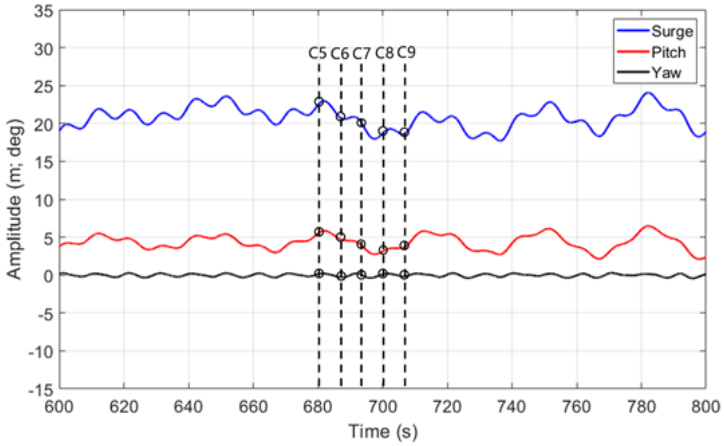

Figure 4-10. Motions in wind-wave combined condition.

Table 4-6. Initial 6DOF motions of FOWT at the moment of collision

Case Number	Surge(m)	Sway(m)	Heave(m)	Roll(deg)	Pitch(deg)	Yaw(deg)
C5	22.4308	-0.2099	-0.2593	0.0853	5.4883	0.1490
C6	20.8388	-0.4088	-0.7080	-0.2709	4.7906	-0.2773
C7	20.2062	-0.4589	-1.1465	0.3241	4.0128	0.0804
C8	18.6727	-0.3033	-0.8146	0.1751	3.1094	0.0887
C9	18.5813	-0.1346	-0.7132	0.0141	3.6518	-0.1935

4.5.1 Responses of 6-DOF motions

The motions in wave-wind conditions without ship collision are set as a reference to help us have direct insight on how platform responses after the collision and the comparison

between collision case and reference are presented in Figure 4-11. As the wind loads are introduced in these four cases, it is noticed that both surge and pitch motion keep periodically moving around a certain value rather than zero and the small fluctuations are mainly due to the regular wave. It is interesting to find that the yaw motion is also obvious in addition to the surge and pitch motion, and this is affected by the so-called gyroscopic moments. As the wind was considered in this section, the rotor of FOWT then had rotational motion. The rotational rotor combining the platform pitch motion will then excite the gyroscopic moments and enhance the yaw motion of the platform.

After the collision, it is observed that no matter in which case, surge motions, and pitch motions all have obvious increment along the ship-impact direction immediately after ship impact. But it is interesting to find that the maximum values of pitch motions after collision in some cases, such as C6, C7 are less than the reference. In other words, after the collision, though the pitch motions rise immediately compared with those in scenarios without collision, they cannot reach the largest pitch motion that they should have reached without collision. This could be explained by considering the aerodynamic loads. As the impact suddenly enhances the pitch and surge velocity of the platform, the velocities at the rotor plane changes accordingly, then the wind loads acting on the rotor plane change as well, so the pitch moment induced by wind varies. If the motion effects caused by ship impact cannot offset the loss of wind loads, then the pitch motion in a collision scenario may not reach the maximum value in a non-collision scenario even though the pitch motion will increase during a short time after the collision

It is interesting to find that the yaw motions also change after collision though the ship impacts along the surge direction, and this can be understood by considering the change of gyroscopic moments. Ship impact along the surge direction shouldn’t have influenced the yaw motion of FOWT directly, but as a rigid-flexible coupled multi-body, the loads and structures always have interaction. The change of platform motions due to ship impact influence the motion of rotor-nacelle assembly, subsequently affecting aerodynamic loads. Finally, the combined effects of the change from aerodynamic loads,

mooring loads as well as pitch motions result in the varying gyroscopic moments.

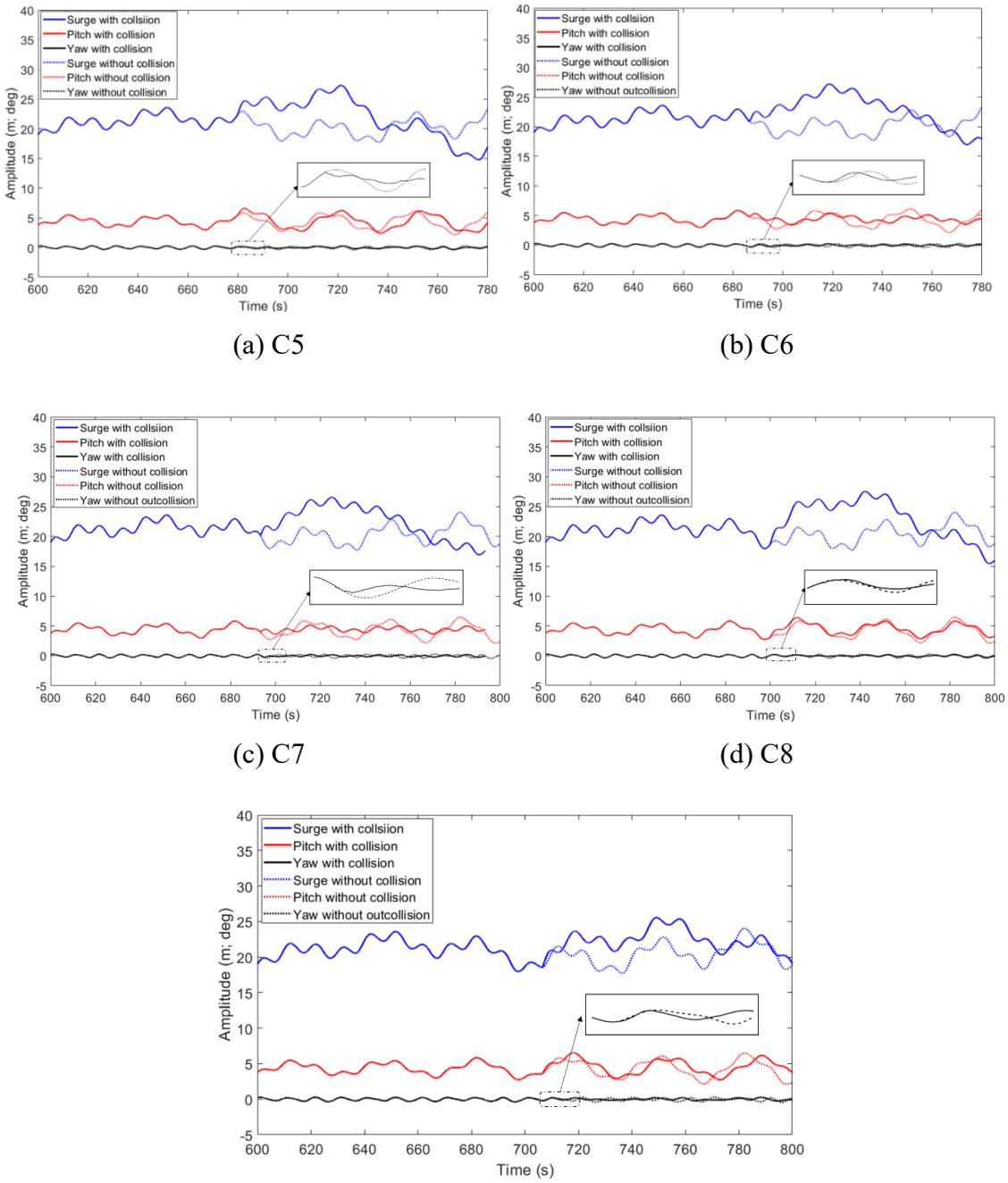

(a) C5 (b) C6

(c) C7 (d) C8

(e) C9

Figure 4-11. Motions comparison between collision scenarios and reference scenarios for case C5-C9.

4.5.2 Responses of mooring system

The maximum fairlead tension, as well as mooring line force before and after collision in wave-wind condition, are compared as Figure 4-12. These forces from the mooring

system are mainly governed by platform translation motions. The largest change occurs in case C8, where the surge motions also increase the most. Because of the combination of wave and wind, the surge and pitch motions are already kept at a relatively high value, where large tension forces exist at the fairlead and mooring line. Thus, the increment due to ship impact is not so obvious. The average increasing rate for fairlead tension and mooring line force is found at 5.76% and 3.72%. the maximum fairlead tension and mooring line forces reach around 1410 kN and 2092 kN respectively, which are much larger than those in still water and wave-only condition. Though they are in an acceptable range in the current cases (with impact velocities of 3m/s), the mooring strength after ship collision in wave-only condition still needs more attention as the typical impact velocity for an OSV could reach 5m/s.

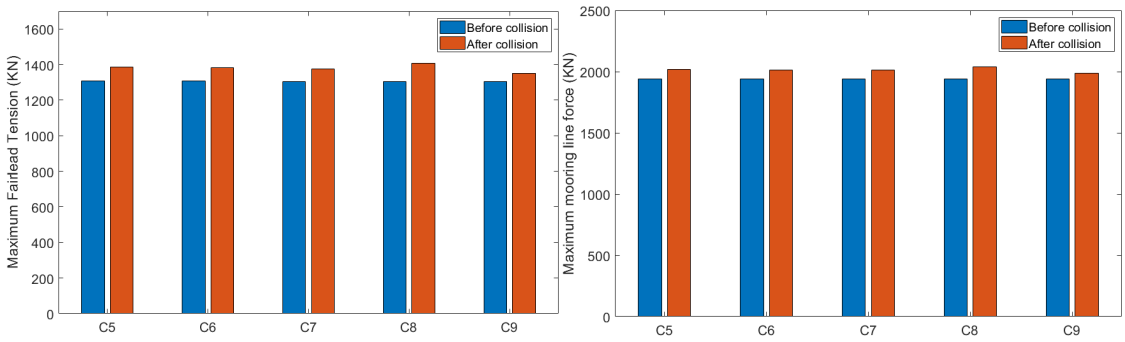

Figure 4-12. Comparison of maximum responses of mooring system before and after ship collision.

4.5.3 Influence on the aerodynamics

Aerodynamic thrust loads on the rotor in these five cases are presented in Figure 4-13. It is interesting to find that the rotor thrust force in each case shows a regular pattern with respect to the time before the collision. The rotor thrust force pattern before a collision could be different by using the different simulation tools. For example, in some other common simulation tools for FOWT, such as FAST (Matha et al., 2010), the rotor thrust force could be constant and this is due to the different control strategies. In FAST, the generator-torque controller and the blade-pitch controller are combined to work together in order to maintain the power above the rated condition. However, in the DARwind code, a typical-variable control scheme is used when above the rated condition. In that case, the

generator-torque controller will maintain the nominal value of torque and only the blade-pitch controller works to regulate the rotor speed. This will bring varying power and aerodynamic load on the rotor, but it could help reduce the fatigue damage of the shaft due to the constant generator torque.

After ship impact, the sudden reduction of the thrust force mainly results from the change of motion and velocity at the rotor plane. The analyzing program adopted BEM methods (Hansen, 2008) to evaluate the aerodynamic load, and in this method, the thrust force acting on each blade element depends more on the relative incident velocity. Due to the ship impact, the platform motion and velocities in surge and pitch direction will immediately rise along the ship impact direction. As is connected by the tower to the platform, the rotor-nacelle assembly will then get growth on its velocity, which is along the same direction as the wind speed. As a consequence, the relative velocity at blade elements decreased in a short time after the collision and results in the transient fall of rotor thrust force. Later, due to the control strategy and coupling effects between each component, the thrust force at the rotor plane will get adjusted and gradually recover to its normal responses pattern.

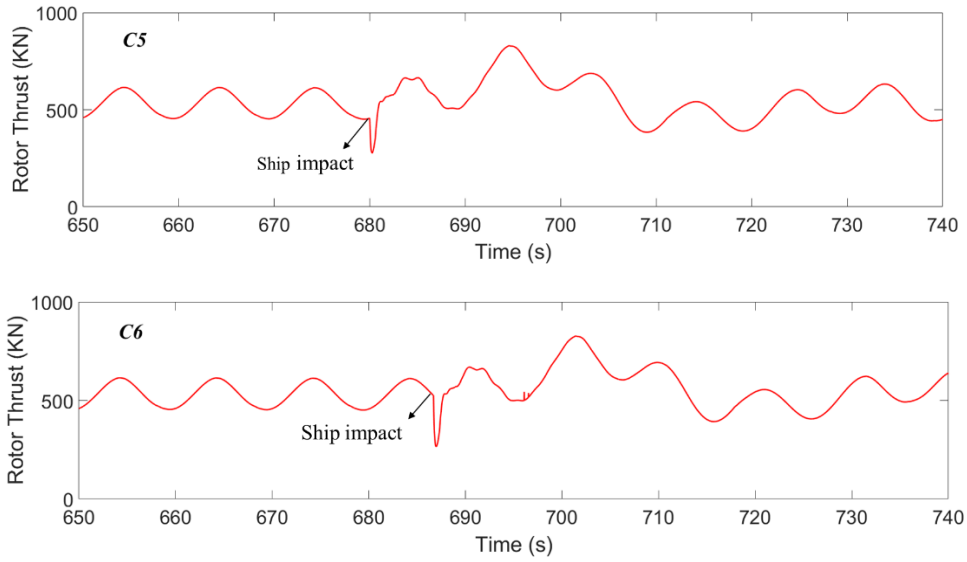

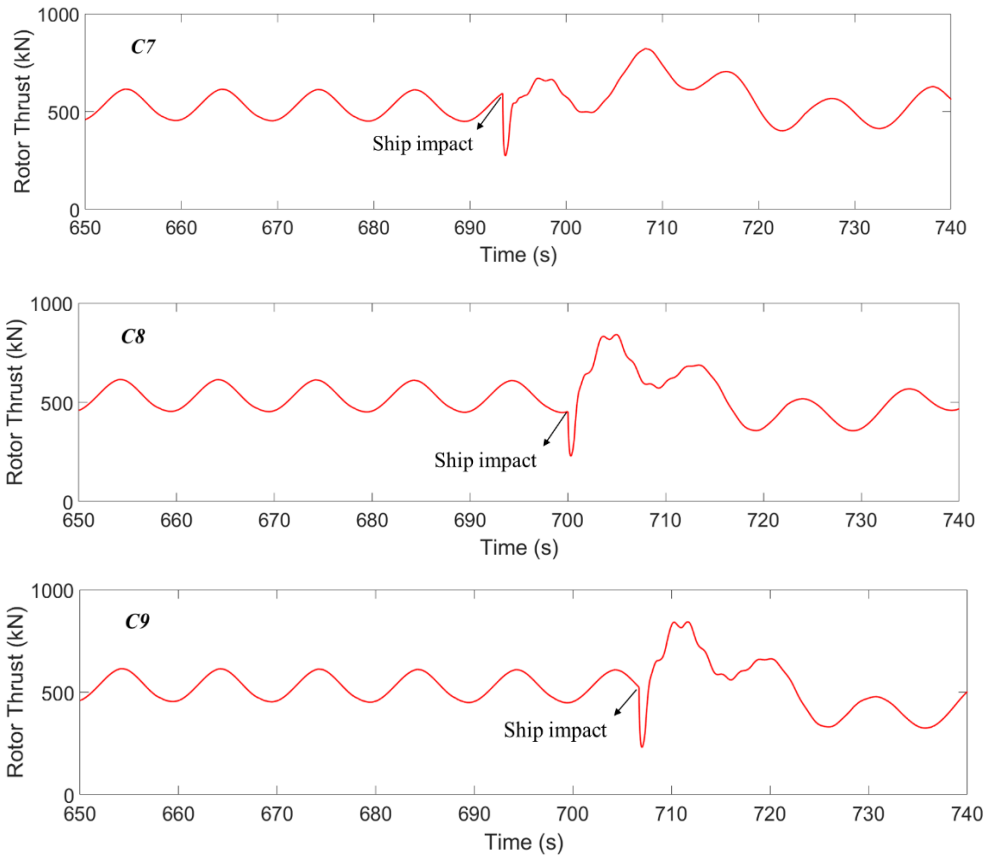

Figure 4-13. Responses of rotor thrust in ship-collision scenarios

4.5.4 Response of the slender structure in FOWT system

Additionally, due to the complicated conditions and ship impact, the responses of flexible-modeled bodies, towers, and blades need to be analyzed. The comparisons of them before and after collisions are listed in Table 4-7. BtDefx and BtDefy refer to the blade tip deformation along the x-axis and y-axis, respectively, which are also called flapwise tip deformation (outside the rotor plane) and edgewise tip deformation (inside the rotor plane). TtDefx represents the tower tip deformation along the x-axis, same as the surge motion. It is noticed that the maximum tower tip deformation in all cases grows after the ship collision. This could be simple to understand because the tower is like a flexible beam that is clamped on the platform and has a lumped mass on the top. Ship collision gives the platform a sudden velocity and motion change, which will induce a large inertia force on the top. Thus, maximum deformation on the top rises. For blade flapwise vibration, they are more obvious than edgewise vibration but the increasing rate of

maximum amplitude after the collision is less than that in the edgewise direction, over 20% in most cases. As the edgewise vibration is mainly governed by the rotor rotation, after the ship collision, the aerodynamic loads acting on the rotor fall rapidly and the rotational speed of the rotor changes accordingly. Due to the sudden change of rotational speed of the rotor, there will be a considerable inertia force acting on blade root in the rotor plane, which results in the large increment of edgewise tip deformation.

Table 4-7. Comparison of blade and tower tip deformation

		Before Collision	After Collision	Increasing rate
C5	Maximum BtDefx (m)	5.9637	6.3548	6.15%
	Maximum BtDefy (m)	0.4955	0.6449	23.17%
	Maximum TtDefx (m)	0.5366	0.7012	23.47%
C6	Maximum BtDefx (m)	5.9637	5.7645	-3.46%
	Maximum BtDefy (m)	0.4955	0.6580	24.70%
	Maximum TtDefx (m)	0.5366	0.6567	18.29%
C7	Maximum BtDefx (m)	5.9916	5.9049	-1.47%
	Maximum BtDefy (m)	0.4955	0.5599	11.50%
	Maximum TtDefx (m)	0.5366	0.6242	14.03%
C8	Maximum BtDefx (m)	5.9916	6.2900	4.74%
	Maximum BtDefy (m)	0.5136	0.6961	26.22%
	Maximum TtDefx (m)	0.5366	0.6075	11.67%
C9	Maximum BtDefx (m)	5.9916	6.1974	3.32%
	Maximum BtDefy (m)	0.5136	0.6782	24.27%
	Maximum TtDefx (m)	0.5366	0.5891	8.91%

4.5.5 Response of nacelle motions

Considering all the loads and structural coupled effects, the maximum accelerations of the nacelle in these 5 cases are presented in Table 4-8. It is noticed that in the wind-wave combined condition plus ship impact, the maximum accelerations at the tower top are extremely large compared with those in still water and wave-only condition. This could be caused by considering the aerodynamic loads. The wind thrust loads are huge enough according to Fig. 4-13 and they mainly act on the rotor plane. Due to the vertical eccentricity, the pitch motion will be enhanced. If the ship impact occurs in this scenario with the same direction of the wind, the transient acceleration at the tower top must be

very large due to the coupling effects of wind thrust loads and ship impact. According to Table 4-8, these accelerations are much larger than the suggested limitation (Echeverry et al., 2019), 0.2-0.3g, where g is the gravitational acceleration. In this case, the equipment in the nacelle might fail to work but the detailed responses cannot be exactly simulated in the current study.Table 4-8. Maximum acceleration at tower top.

Impact scenarios	C5	C6	C7	C8	C9
Maximum acceleration (m/s^2)	14.0387	7.6524	10.9701	10.8619	8.7272

4.6 Summary

In this chapter, the external dynamic responses of a 5MW Hywind Spar-type floating wind turbine in ship collision scenarios are investigated with the newly proposed methods in chapter 3, which is essentially a decoupled method. Some key characteristics are summarized as follows

1) In the still water condition, the impact velocity has a significant influence on the dynamic responses of FOWT. the maximum amplitude in platform motions almost increases proportionally with the impact velocity rising. The responses of the mooring system, as well as accelerations at the tower top, also have huge change but they are still within a safe range even for a head-on collision with an initial velocity of 3m/s.

2) In the wave-only condition, four cases were selected and the platform motions before and after ship collision were demonstrated. The increment of motions in surge and pitch direction after the collision are obvious but smaller than those responses in still water. Additionally, the ship collision can enhance the amplitude of the tower vibration. The maximum tower tip deformation along collision direction changes dramatically, increasing by over 50% in four cases. The maximum axis-accelerations at the nacelle in these four cases are found to be slightly larger than those in still water, but still less than the suggested safe line, 0.2g-0.3g, where g is the gravitational acceleration.

3) In the wind-wave condition, the increments of surge and pitch motion after the collision

are not so large compared with cases in still water and wave-only condition. The mooring line tension and fairlead tension after ship impact have a slightly increased rate, at around 3%-7% but the actual value of mooring line tension has reached almost 3000kN. the wind loads acting on the rotor drop dramatically after the collision. The change of aerodynamic loads further influences the gyroscopic moment, and the yaw motion has obvious change accordingly. The blade tip deformation in the rotor plane is influenced the most by ship impact, owning an overall increasing rate larger than 20%. The axis-accelerations of the generator at nacelle in these cases are found all very huge, mostly larger than 9m/s, meaning that even we ignore the structural damage due to ship impact, the huge accelerations at nacelle may still result in the failure of equipment.

Chapter 5 A coupled method of internal and external dynamics in ship-FOWT collision

5.1 Introduction

In the previous chapter, a decoupled method for external dynamics of FOWT under ship impact is developed. However, ship-FOWT collision is a highly coupled and nonlinear process, the decoupled method has its limitation and is only suitable for certain cases, such as non-critical collision, symmetrical collision. Additionally, the structural deformation and other transient details cannot be accurately captured with the external dynamics method. To further investigate the comprehensive dynamic responses of FOWT in ship-FOWT collision scenarios, this chapter will introduce a newly proposed method which couples the external and internal dynamics based on nonlinear finite element method (NLFEM) technology.

NLFEM has been widely used in the past decades when investigating the internal dynamics in ship collision analysis as it can provide accurate and direct insight on the result of structural deformation. As is introduced before, the external dynamic responses such as 6DOF global motions and local structural dynamic responses may have coupling effects. When a FOWT is impacted by a ship, it may not only get serious local structural deformation but also have 6DOF global motions and the 6DOF global motions can be influenced by the impact loads, wind-wave loads, and mooring loads, which is still a challenge in ship collision analysis. Thus, the method proposed in this chapter is a fully coupled method that considers the wave-wind loads and addresses the external and internal dynamic responses simultaneously.

LS-DYNA, as a general finite element code, is adopted in this study. It is famous for analyzing the highly nonlinear static and dynamic structural responses and has been

widely used in collision and grounding analysis of ships and offshore structures. To consider the wave and wind loads, a powerful tool, the user-defined load subroutine (LOADUD) of LS-DYNA is employed, because the hydrodynamic and aerodynamic loads cannot be defined as time-series loads in the pre-processing stage. They are varying all the time and depend on the motion of FOWT at each moment during the collision. The user-defined load subroutine, LOADUD, exactly provides a possibility for users to define a load as a function of nodal displacements, velocities, accelerations, and other user-defined parameters, as demonstrated by Adoum and Lapoujade (2003). In the following sections, the aerodynamic model, hydro model, and mooring model are introduced, and the detailed coupling algorithm is then demonstrated.

5.2 External loads evaluation

5.2.1 Aerodynamic model

A very famous and common method to calculate the wind loads for an OWT is the blade element momentum (BEM) method (Hansen, 2008) with some aerodynamic corrections, such as Prandtl's tip-loss and hub-loss corrections (Hansen, 2008), Glauert's corrections (Spera, 1994), dynamic wake corrections (Øye, 1991), etc. BEM method is a combination of 1-D momentum theory and 2-D blade element theory. The blades need to be discretized into elements and the total load is obtained by summarizing the aerodynamic loads acting on these elements. The load at each element depends on the relative velocity of wind and element. A significant increment in computational cost will be brought if the BEM method is directly adopted in the coupling analysis because the blade structures need to be detailed modelled and iteration calculation for each blade element will be performed in each LS-DYNA structural analysis time step

To maintain the accuracy and avoid bringing computational burden, the blades are not modeled in a finite element model and the total aerodynamic loads are simplified as a point load acting on the centre of the rotor plane. The calculation procedure for this simplified model is from Nielsen et al. (2006), given as

$$F_T = \frac{1}{2}\rho_a A V_{rel} C_T \quad (5\text{-}1)$$

where ρ_a is the density of air, A is the swept area of rotor and V_{rel} is the relative velocity between the incoming wind and nacelle. C_T is defined as the thrust force coefficient, which is only the function of relative velocity. The C_T curve is shown as Figure 5-1. Note that this curve has considered the influence of a conventional blade-pitch control strategy, which will lead to accurate responses for the whole FOWT system. This control strategy tries to stabilize the power output when the wind speed is higher than the rated speed and maximizes the power output for wind speeds lower than the rated speed.

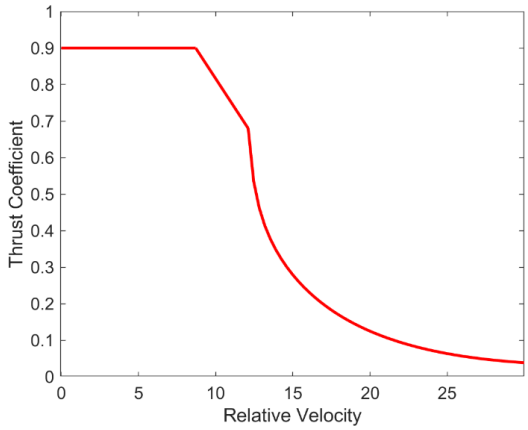

Figure 5-1. Thrust coefficient for different relative velocities (Nielsen et al. 2006)

5.2.2 Hydrodynamic and hydrostatic model

Airy linear wave theory (Faltinsen, 1993) is adopted here to model the wave kinematics and potential-flow theory is used to calculate the hydro force which can be divided into three parts: diffraction, radiation, and hydrostatics (Faltinsen, 1993). Note that the linear wave theory is based on the assumption that the amplitudes of the incident waves are much smaller than its wavelengths as well as the platform motions and this is appropriate for most floating offshore wind turbines in many cases. Before calculating the hydro loads, the 3-D panel-based hydrodynamic analysis program, SESAM/HydroD is utilized firstly to output hydrodynamic and hydrostatic coefficients in the frequency-domain analysis for FOWT. These coefficients are then pre-processed before providing time-domain hydro

loads.

In this model, only unidirectional waves are considered and the wave excitation load of irregular waves in the time domain is expressed as the superposition of harmonic wave components

$$F_W = \Re\left(\sum_{j=1}^{N} g(\omega_j)\zeta_j e^{i\omega_j t}\right) \quad (5\text{-}2)$$

where ω_j is the j^{th} regular wave frequency and $g(\omega_i)$ is the frequency response function associated with ω_j, $\Re$ indicates the real value of the equation. ζ_j is the j^{th} wave amplitude (complex value), obtained by giving a wave spectrum $S(\omega)$.

$$\zeta_j = \sqrt{2S(\omega_j)\Delta\omega} \quad (5\text{-}3)$$

where $\Delta\omega$ is the power spectral densities frequency resolution and $S(\omega_j)$ is the spectral energy density. Currently, we only modelled the JONSWAP (Joint North Sea Wave Project) spectrum (Hasselmann et al, 1973) in the hydro model.

The wave radiation forces are then calculated as

$$F_j^{Radiation}(t) = -\sum_{k=1}^{6}\left\{\mu_{jk}(\infty)\ddot{x}_k(t) + \int_{-\infty}^{t} K_{jk}(t-\tau)\dot{x}_k(\tau)\,d\tau\right\}, \quad j = 1, 2, \dots, 6 \quad (5\text{-}4)$$

where the first term on the right side refers to the added mass force, $\mu_{jk}(\infty)$ is the (j, k) component of the added mass matrix at infinite frequency. The second term on the right side is a convolution integral representing the wave radiation damping. In the radiation problem, the impulse in platform velocity results in a free-surface wave and induces a pressure field, which is the memory effects of the free surface. $K_{jk}(t-\tau)$ is known as the retardation function for the convolution integral considering the free-surface memory effects. The index $j = 1, 2, \dots, 6$ refers to surge, sway, heave, roll, pitch, and yaw,

respectively. The added mass matrix can be directly read from the output files of hydrodynamic coefficients from HydroD and $K_{jk}(t)$ is calculated by knowing damping coefficients in all frequencies, given as

$$K_{jk}(t) = \frac{2}{\pi}\int_0^{\infty} B_{jk}(\omega) cos\omega t d\omega \tag{5-5}$$

where $B_{jk}(\omega)$ is the radiation damping at frequency ω.

Next, the hydrostatic loads including buoyancy are calculated as

$$F^{Hydrostatic} = \begin{pmatrix} 0 \\ 0 \\ \rho g V \\ 0 \\ 0 \\ 0 \end{pmatrix} - C^{Hydrostatic} x(t) \tag{5-6}$$

where the first term on the right side is the buoyancy force, ρ is the fluid density, g is the gravitational acceleration constant and V is the displaced volume of fluid when the support platform is at the un-displaced position. The second term indicates the change in the hydrostatic loads in 6DOF. $C^{Hydrostatic}$ is the linear hydrostatic restoring matrix and $x(t)$ is the platform motion at the moment *t*.

5.2.3 Mooring model

Cable elements in LS-DYNA could be an option to model the mooring system. For catenary mooring lines, the restoring forces from the mooring system are not only from the tension of mooring lines but also from the equivalent gravity loads in the water of those parts of mooring lines not lying on the seabed. Thus, the initial geometry layout of the mooring lines could be important. When establishing the FE model of the catenary mooring system, the length of catenary mooring lines on the seabed should be pre-calculated and the geometry layout in the vertical plane should be correctly modelled. Additionally, the equivalent gravity loads (the true gravity loads minus the buoyancy of

mooring lines) of mooring lines should be applied from the beginning of the simulation. Once the geometry layout is not accurately modelled, the system at the initial state should not be quasi-static and the applied gravity loads will lead to system vibrations, leading to error results. These problems are difficult to solve in practical modelling, so a more efficient way is adopted in this paper. The mooring system is not truly modelled in the FE model and the mooring forces is calculated in the user-defined subroutine.

Jonkman (2007) has mentioned a simplified mooring model, which ignores the mooring inertia and mooring damping in the fluid. The mooring model is linear, and the calculated loads are the contribution from all mooring lines, expressed as

$$F^{mooring} = F_0^{Lines} - C^{mooring} x(t) \tag{5-7}$$

where $C^{mooring}$ is the linearized restoring matrix from the whole mooring system and it combines the elastic stiffness of the mooring lines and the effective geometric stiffness relevant to the weight of the lines in the fluid and $x(t)$ is the platform motion. For catenary mooring lines, F_0^{Lines} is the pre-tension at fairleads from the weight of the cable not lying on the seabed. For taut mooring lines, F_0^{Lines} is the result of pre-tension in the mooring lines from excess buoyancy in the tank when the platform is un-displaced, including the contribution of the weight of the cable in water as well. Note that this linear mooring model may not be accurate enough for a very large amplitude of platform motions.

5.3 Coupling algorithm of hydro-aero-mooring loads and structural analysis

The detailed coupling algorithm is illustrated as Figure 5-2. As is shown in step 1, two types of external files should be prepared in prior, the text files which record the hydrodynamic coefficients output from HydroD and FORTRAN module files which include some necessary data as well as subroutines used for load calculation. Note that in LOADUD, the nodal information can be read only in that current time step and then they will be erased upon moving to the next time step. However, the calculation of radiation

potential damping is a convolution integral and requires velocity history. Therefore, the main purpose of the FORTRAN module files is to store the velocity history. Because any variables declared in a module become the global variables in all subroutines where the module is used so that the history velocities will not be erased when calling LOADUD subroutine in the following time steps in LS-DYNA analysis.

Next, the hydrodynamic coefficients are read and pre-processed in LOADUD to generate the added mass matrix, hydrostatic matrix, retardation functions and so on. These matrices are stored in the module as global variables so that they are not needed for generating again in each time step. By reading the current nodal information, the aero-hydro-mooring loads are evaluated. However, a problem is found when applying the added mass forces. The nodal force on a deformable body brings large vibration and generates weird results, which is not correct. Therefore, a rigid part is planned on the support platform to apply the nodal force, but the nodal acceleration read from a rigid body always shows zero. This problem is also mentioned and discussed by Yu and Amdahl (2016). In this research, we solved the problem by defining a node output history in Keyword file for the nodes we cared for. During the LS-DYNA analysis, there is an output file named 'nodout' recording the nodal information, including accelerations for 6DOF. We let the LOADUD subroutine read this file to obtain the nodal acceleration. It should be noted that the output interval of nodal information and writing interval of nodal information in 'nodout' should be carefully set to ensure accuracy and stability.

Then the LS-DYNA structural analysis will be conducted with the calculated user loads in LOADUD, shown as step 3. To improve the efficiency while guaranteeing accuracy, the user loads from LOADUD are updated every 100 steps and the velocity is also stored every 100 steps. Within every 100 steps, the old value of loads is directly applied, shown as step 4 and step 5. Finally, the results are obtained. The first part is the user loads history which is defined for output in LOADUD, and these results can be used for further verification of the code in LOADUD. The other part is from the coupled simulation results from the LS-DYNA solver, including the 6DOF motion of FOWT and structural

deformation, impact force, energy dissipation, etc.

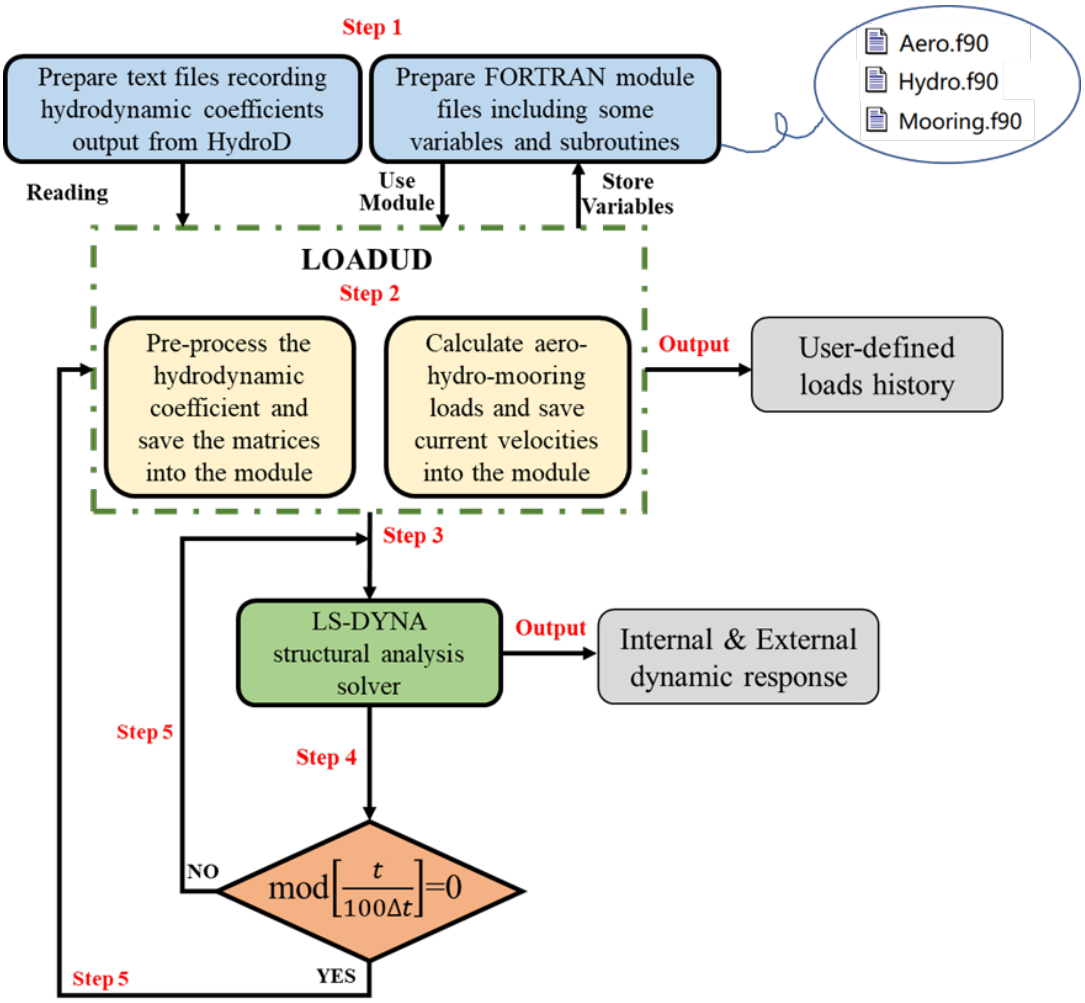

Figure 5-2. Coupling algorithm of user-defined loads and LS-DYNA solver.

5.4 Verification of LOADUD implementation

5.4.1 Model description

A Hywind Spar-type floating platform (Jonkman, 2010) with a 5MW baseline wind turbine (Jonkman et al, 2009) was selected and the main properties are presented in Table 5-1.

Table 5-1. The main properties of 5MW Hywind Spar-type floating wind turbine

5MW Hywind Spar-Type Floating Wind Turbine	
Blade Length	61.5 m
Blades Quantity	3
Nacelle CM Location Above Tower Top	1.75 m

Rated Rotor Speed	12.1 rpm
Elevation to Tower Base (Platform Top) Above SWL	10 m
Elevation to Tower Top Above SWL	87.6 m
CM Location of Tower Above SWL	43.4 m
Total Draft	120 m
Platform Top (Tower Base) Above SWL	10 m
Taper Top Below SWL	4 m
Taper Bottom Below SWL	12 m
Platform Diameter Above Taper	6.5 m
Platform Diameter Below Taper	9.4 m
CM Location of Platform Below SWL	89.9 m
CM Location of whole FOWT System Below SWL	78 m
Number of Mooring Lines	3
Fairleads Below SWL	70 m
Radius To Anchors Form Platform Centreline	853.87 m
Unstretched Mooring Line Length	902.2 m
Total Mass (Including Ballast, Tower, Nacelle, Rotor, Blades)	8066 tons

The FOWT is generally modelled with Belytchko-Tsai shell elements with 4 integration points through the thickness (Hallquist, 2013), shown as Figure 5-3. The ballast tank in the bottom of the platform is modelled as a rigid part and other parts are deformable. A general mesh size of 400mm was used for most parts and a fine mesh of 200mm is applied on the tower top area and the taper area. The catenary mooring cable is not modelled, and the rotor-nacelle assembly is represented by a lumped mass located at the central top of the tower. The node which is assigned the lumped mass is connected to the tower top by a series of rigid beams, shown as Figure 5-4, (a). In the coupled analysis, this lumped-mass node will be selected as the reference point for the aerodynamic calculation.

A global coordinate system is established, of which the origin is located on the centre of SWL along the platform centre line, shown as Figure 5-3. This coordinate system is fixed on the earth and another body-fixed frame is set on the FOWT. This local frame moves with the FOWT and coincides with the global coordinate system when the FOWT is un-displaced. The motion of the platform can then be described with these two frames. In the FE model, a set of rigid cross beams are modelled, and the centre is located on the origin of the body-fixed frame, these beams have a length of 1m and are rigidly constrained with

the rigid tank, shown as Figure 5-4 (b). The kinematic reference point of the platform is on the SWL centre rather than the COG of FOWT and the calculated hydro loads, as well as mooring loads, are all about this reference point where the central node of the beam set is located. However, only nodal force from LOAD can be applied so the moments about the reference point must be transferred into force pairs and applied at other nodes of this beam set.

The FOWT is assigned a high strength elasto-plastic steel with power-law hardening (Yu et al, 2016). The properties are shown in Table 5-2 and the strain rates are not considered. A constant failure strain of 0.3 is adopted regardless of the mesh size for simplicity.

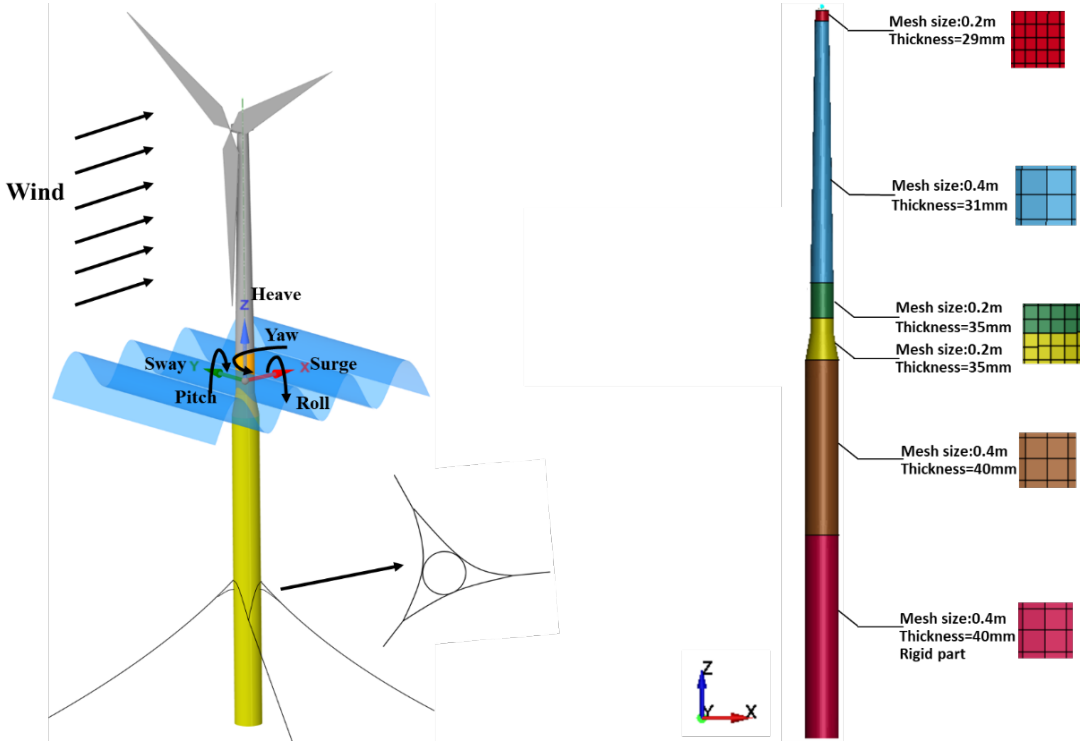

Figure 5-3. Coordinated system and finite element model of the FOWT.

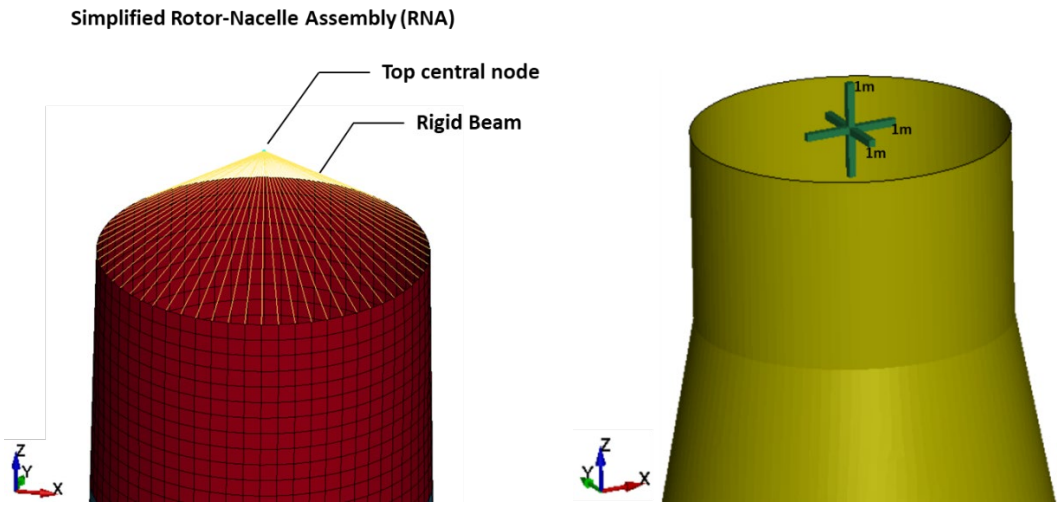

(a) (b)

Figure 5-4. Simplified RNA system and rigid beam set in the FE model

Table 5-2. Material properties of a high strength steel.

Material parameters				
Mass Density	Poisson's ratio	K	n	Yield Strength
7850 kg/m^3	0.3	760 Mpa	0.15	540 Mpa

The $C^{mooring}$ mentioned in equation (5-7) uses the value suggested by Jonkman (2010). These matrices are obtained from the linearization analysis conducted by Jonkman with the FAST code (Jonkman and Buhl, 2005). For the Hywind Spar platform, an additional yaw stiffness of 98340000 Nm/rad is also suggested to add to the mooring model by Jonkman (2010) because the mooring lines attached to the platform via a delta connection, shown in Figure 5-3. To increase the yaw stiffness and the original simplified linearized mooring model doesn't consider this, the revised $C^{mooring}$ is then shown as

$$C^{mooring} = \begin{bmatrix} 41180 & 0 & 0 & 0 & -2.821E6 & 0 \\ 0 & 41180 & 0 & 2.821E6 & 0 & 0 \\ 0 & 0 & 11940 & 0 & 0 & 0 \\ 0 & 2.816E6 & 0 & 3.111E8 & 0 & 0 \\ -2.816E6 & 0 & 0 & 0 & 3.111E8 & 0 \\ 0 & 0 & 0 & 0 & 0 & 1.156E7 + 9.834E6 \end{bmatrix} \quad (5\text{-}8)$$

It should be noted that the nodal acceleration reading in LOADUD always shows zero if this node belongs to a rigid body and this value is obviously not true. Yu et al. (2016) has

also mentioned this problem and they finally estimated the acceleration by using equation $a = (V_n - V_{n-2})/(t_n - t_{n-2})$. In this research, we defined a node output history in *Keyword file* for the nodes we cared about. During the calculation of LS-DYNA, there was an output file named 'nodout' recording the required node information, including displacement, velocities, and accelerations for 6DOF. Next, in LOADUD, we let the program read the file 'nodout' to obtain the nodal acceleration. What needs to be noted is that if this method was adopted, the output interval of the node information and a value called IFLUSH from keyword CONTROL_OUTPUT must be carefully set, otherwise, the reading task from 'nodout' file may not work normally.

5.4.2 Verification

The verification of the hydrodynamic, aerodynamic, and mooring models applied for coupled simulation are made through several steps. Firstly, a free decay test is conducted to verify the correct implementation of the mooring model, hydrostatic model, and hydro radiation model. An initial velocity is defined on the rigid cross beams along the direction we care, and the free decay test results are shown in Figure 5-5. The free decay test in sway and roll motion should be close to surge and pitch motions due to the symmetricity and they are not performed to save computational source. The calculated natural frequency results are compared with the published data of (Jonkman and Musial, 2010) in Table 5-3, and it is shown that the results match very well, indicating that the mooring, radiation, and hydrostatic model can be correctly coupled to LS-DYNA solver for future collision analysis.

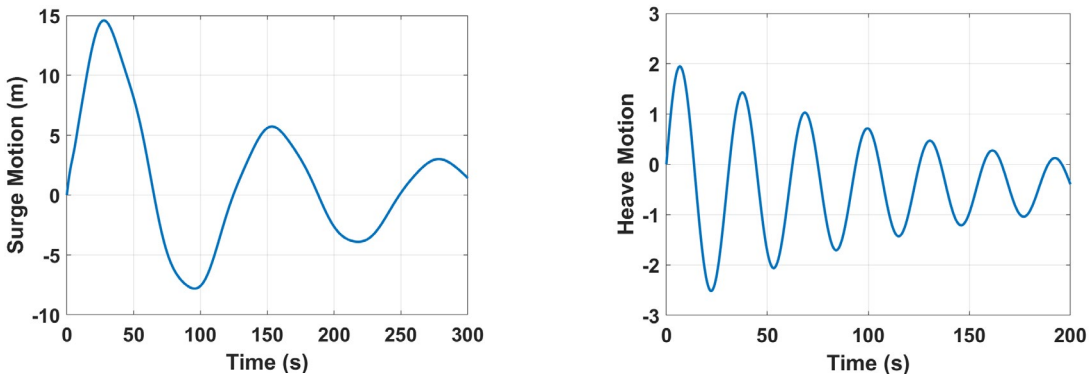

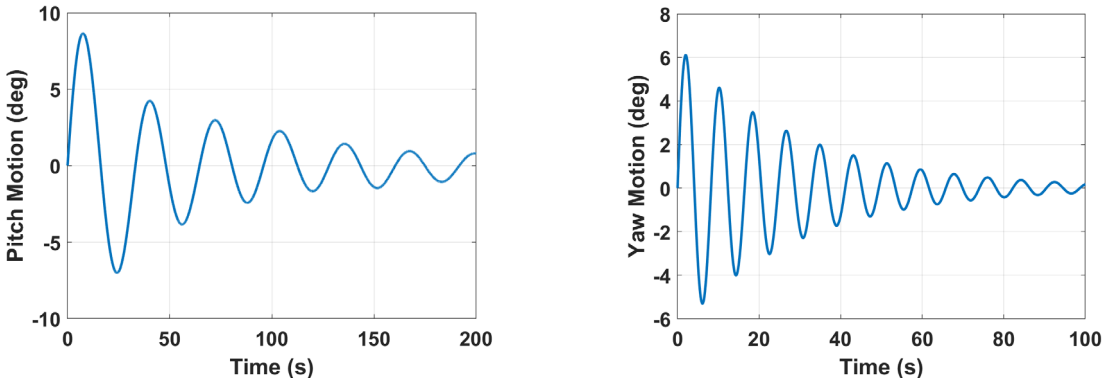

Figure 5-5. Free decay test calculated by LS-DYNA.

Table 5-3. Natural Frequency (Hz) of FOWT

Motion mode	Surge	Heave	Pitch	Yaw
LS-DYNA	0.0081	0.032	0.032	0.12
Published results in the Ref	0.008	0.032	0.034	0.12

Secondly, the aerodynamic model and hydro diffraction model are verified, respectively in wind-only conditions and regular wave conditions. The results from LS-DYNA are compared with those from FAST (Jonkman and Buhl, 2005), a famous simulation tool for offshore wind turbines developed by NREL. As there will be large inertia forces and amplitude of motions when the wind or wave loads are just applied, this start-up process is ignored and only the results after hundreds of seconds are used.

It is found that under the constant wind condition, the FOWT is kept within a relatively stable state away from the un-displaced position after hundreds of seconds, shown as Figure 5-6. The results from the present coupled solver agree well with those calculated by FAST, indicating that the simplified aerodynamic model can be successfully coupled to the LS-DYNA structural analysis. Figure 5-7 gives the motion amplitudes under the three different regular wave conditions. The motions from the present method and FAST reach a good agreement.

Motion response under irregular waves is not compared to save computational cost. As they are treated as a linear summation of numerous regular wave effects, the accuracy of the irregular wave should be guaranteed based on the correct implementation of the

regular wave.

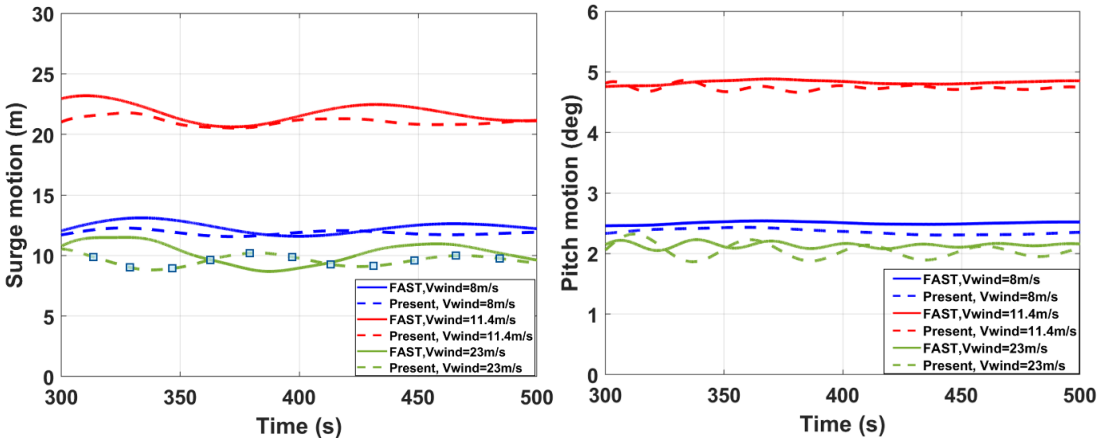

Figure 5-6. Comparison of motions under constant wind.

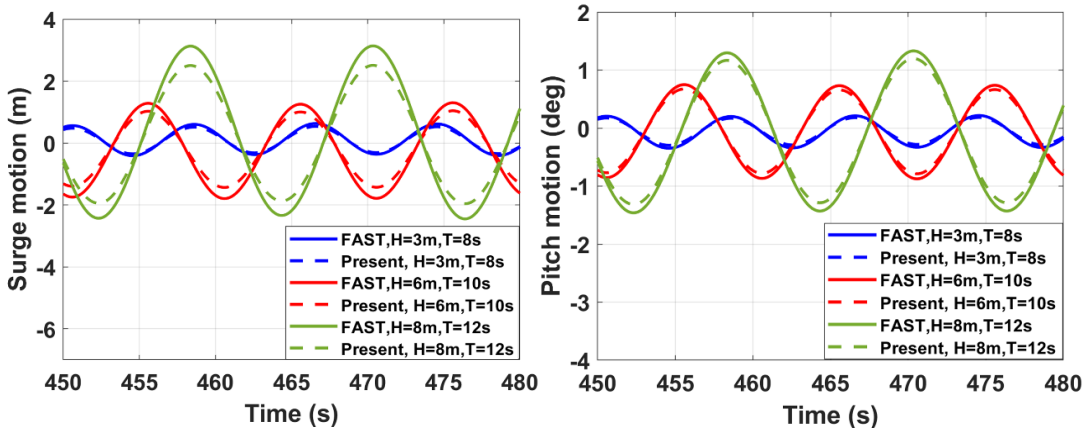

Figure 5-7. Comparison of motions under regular wave.

5.5 Summary

This chapter develops a numerical solver to address the challenge of considering wind-wave loads in the ship-FOWT collision analysis. The user-defined load subroutine, LOADUD, in LS-DYNA is utilized to model the wind, wave, and mooring loads. A simplified aerodynamic model considering blade pitch strategy is used and the hydrodynamic loads are calculated based on the potential-flow theory with linear wave kinematic model. The mooring forces are considered with a linearized model. With the newly developed solver, free decay test, wave-only, and wind-only simulation are performed, and the results are compared with those from FAST (Jonkman and Buhl, 2005).

Good agreements are achieved, implying the developed solver is capable to calculate the wind-wave loads in the structural analysis.

The most advantage of the proposed method is that compared with the conventional ship collision method, it can calculate the external and internal dynamics of FOWT simultaneously so that the possible coupling effect between local structural deformation and 6DOF global motions can be captured. Additionally, the hydrodynamic loads are modelled in an accurate way rather than using a constant added mass or other simplified models. The computation cost of the developed solver is found almost the same as the NLFE analysis with the original structural analysis solver. Therefore, it is still efficient and more accurate compared with the conventional ship collision analysis.

Chapter 6 Discussion on the fully coupled methods

6.1 Introduction

After studying the external dynamic responses of FOWT after ship-collision, the internal dynamic responses of FOWT in ship collision scenarios will be focused on in this chapter with the fully coupled method.

The 5-MW Hywind OC3 Spar-type floating wind turbine and a striking OSV are selected as the objects. The FE model is described and the discussion on various factors such as impact velocity, tower flexibility, the deformability of OSV, and environmental conditions are conducted. The results are expected to be able to supplement or verify the results from the integrated methods as well.

6.2 Cases definition

The offshore service vessels (OSVs) impact risk against OWT has been emphasized (Dai et al, 2013) and therefore, an OSV with a bulbous bow is selected as the striking vessel. The principal scantlings of the OSV are listed in Table 6-1. The striking vessel was not fully modelled and only the bulb bow is modelled and the whole mass of the ship is attached to the bulb bow part to simulate the correct impact energy. Both rigid and deformable models of the bulb bow are modelled, shown as Figure 6-1 and they are used for different cases. The shell thickness of 14mm and 10 mm are used in the bulb and forecastle, respectively. The decks and attached stiffeners are from 7mm to 14mm. The ring stiffeners and breast hooks in the bulb vary between 13mm to 15mm. A general 300mm element size is used for the striking ship and a type of mild steel with power-law hardening is assigned, shown as equation (6-1). The yield stress is 275 MPa, and the

power-law parameters K and n are 746 MPa and 0.24, respectively. A constant failure strain of 0.3 is adopted. The strain rate effect is not considered as well. The FE model of FOWT adopted the model described in section 5.4, which was used for verifying the proposed coupled simulation approach.

$$\sigma = K\varepsilon^n \tag{6-1}$$

Table 6-1. Principal scantlings of the striking OSV

Offshore service vessel	
L.O.A	72.2 m
Beam	16 m
Depth	7.55/11 m
Displacement	4,000 tons

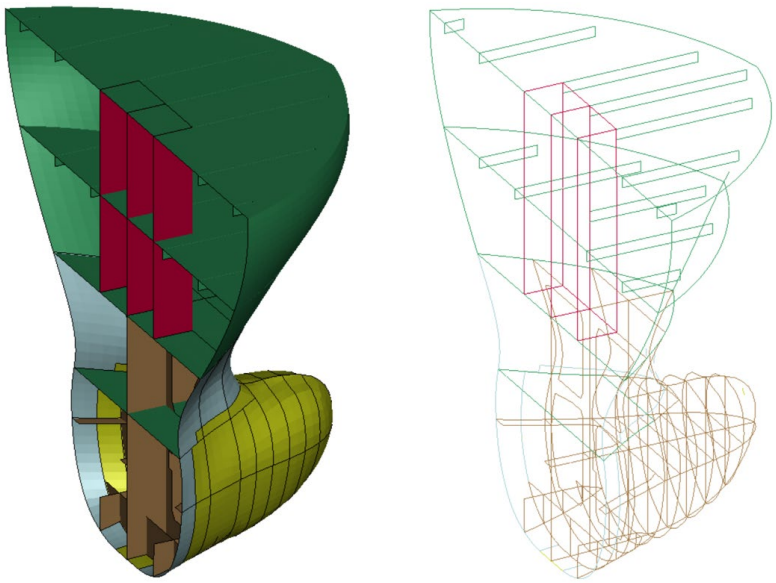

Figure 6-1. The structures of bulbous bow.

Head-on collisions are mainly studied and the FOWT is the major focus so the OSV's responses are not detailed analyzed. The vessel is given an initial velocity forward to the FOWT and its motion is constrained in the direction of velocity. The moving OSV brings the motion of surrounding fluid, and this is represented by the added mass in this study. Petersen and Pedersen (1981) have given an empirical formula for the added mass coefficients of ship used for the ship collision analysis, which depends on the impact

duration. According to the varying range they gave, a constant added mass factor of 0.05 is assigned for the surge motion of the ship, which equals 200 tons in this simulation. The collision height is set at 7m above the SWL. Additionally, structural damping of the tower needs to be considered for the tower in the collision analysis. The damping ratio of 1% critical damping factor for the lowest frequency mode is adopted (Jonkman, 2010). The effects of ship impact velocity, structural deformability, the elasticity of tower and environmental loads in ship-FOWT collisions need to be studied and the cases definition for these scenarios are listed in Table 6-2. Note that the initial kinetic energy may not be the impact energy in some cases because the FOWT are also moving before the collision, such as in wind only, wind-wave combined cases.

Table 6-2. Cases Definition

Case No.	Ship Velocity	Wave			Wind Velocity	Tower Deformability	Ship Deformability	Initial Kinetic Energy of OSV (including added mass)
		H (Hp)	T (Tp)	Wave Type				
L1-2DR	2m/s	-	-	Still Water	0	Deformable	Rigid	8.4 MJ
L1-3DR	3m/s	-	-	Still Water	0	Deformable	Rigid	18.9 MJ
L1-4DR	4m/s	-	-	Still Water	0	Deformable	Rigid	33.6 MJ
L1-5DR	5m/s	-	-	Still Water	0	Deformable	Rigid	52.5 MJ
L1-2DD	2m/s	-	-	Still Water	0	Deformable	Deformable	8.4 MJ
L1-3DD	3m/s	-	-	Still Water	0	Deformable	Deformable	18.9 MJ
L1-4DD	4m/s	-	-	Still Water	0	Deformable	Deformable	33.6 MJ
L1-2RR	2m/s	-	-	Still Water	0	Rigid	Rigid	8.4 MJ
L1-3RR	3m/s	-	-	Still Water	0	Rigid	Rigid	18.9 MJ
L1-4RR	4m/s	-	-	Still Water	0	Rigid	Rigid	33.6 MJ
L2-1DR	1m/s	3 m	8 s	Regular Wave	11.4 m/s	Deformable	Rigid	2.1 MJ
L2-3DR	3m/s	3 m	8 s	Regular Wave	11.4 m/s	Deformable	Rigid	18.9 MJ
L3-3DR	3m/s	3 m	8 s	Irregular Wave	11.4 m/s	Deformable	Rigid	18.9 MJ

6.3 Discussion on the impact velocity

An energy balance analysis for the whole system was conducted at first to help better understand the ship collision process, and it can also help check the simulation validity. The energy transfer analysis for a 2m/s ship impact is presented as Figure 6-2. This figure shows how the energy balance is maintained in ship-FOWT collision scenarios. It is found that almost half of the initial energy is transferred to the internal energy due to ship impact.

Another considerable part of the energy is transferred to the kinetic energy of FOWT. An interesting finding is that the green curve changes later than the blue curve, indicating that there is a motion lag for the struck FOWT compared with the local deformation. This is due to the coupling effect between external and internal dynamics, and this cannot be captured in the conventional decoupled analysis. After reaching the peak, the kinetic energy of FOWT then decreases gradually while the yellow curve is growing. Obviously, the kinetic energy of FOWT is dissipated through the wave radiation and mooring restoring forces.

4 different impact velocities were selected. The impact velocities were all along the positive direction of the x-axis in the global coordinate system. The collision forces in 4 cases with different impact velocities are compared in Figure 6-3. It is observed that the maximum collision forces are influenced by the impact velocity and the value of collision force reached 11.25 MN for an impact velocity of 5m/s, which is more than twice as large as that for the impact velocity of 2m/s. For some cases, it is observed that a second impact scenario occurs, but the collision force value is much smaller than that of the first impact. The first impact in these cases will be mainly studied in the following figures.

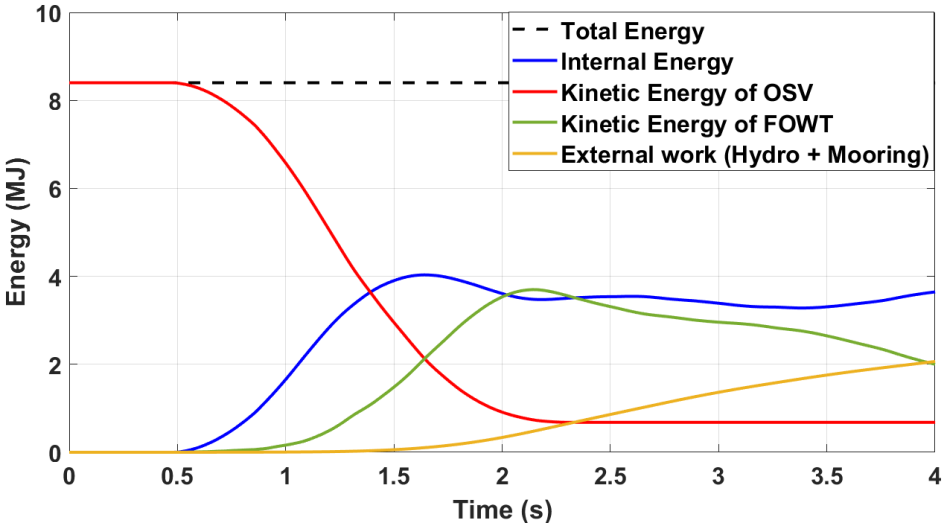

Figure 6-2. Energy balance in time histories. (Impact velocity 2m/s)

It is interesting to find that for the impact velocity of 2m/s, the collision force pattern with respect to time is quite different from the other 3 cases. In the other 3 cases, the collision

forces suddenly fall after they reach the first peak. This can be explained by observing the structural deformation in the collision, which is illustrated in Figure 6-4. Cases L1-2DR and L1-3DR are selected as examples. For case L1-2DR, which has a 2m/s impact velocity, the peak and valley of collision forces occur at 0.98s and 1.06s. It is found that the deformation modes are similar at these two moments. Plastic deformation appears at two small zones, which are crushed by the forecastle and bulb. However, for case L1-3DR, the deformation within a small zone occurs in the beginning and due to the larger impact energy, the structural deformation is not limited within a small zone and large-area indention is found. Then the bulb structure might not get involved in the collision so much because the forecastle is a bit ahead of the bulb. Thus, the collision forces drop quickly at this moment.

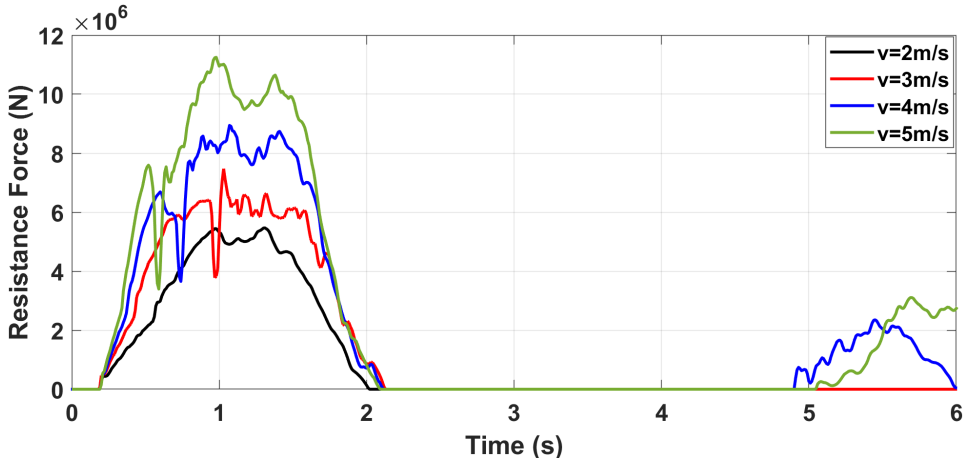

Figure 6-3. Resistance force vs time under different impact velocity.

Figure 6-5 presents the dissipated energy curves during the collision process. Some of the initial kinetic energy of the ship is absorbed by the FOWT to cause structural deformation. Some peak values are found from the 4 curves in the figure, indicating that the ship-FOWT impact includes both elastic and plastic collision. Obviously, the larger impact velocity brings more significant structural deformation, causing more energy dissipated. The maximum dissipated energy reaches 23 MJ under the impact velocity of 5m/s. The energy ratios between dissipated energy and initial kinematic energy of ship before collisions are calculated as 42%, 44.8%, 44.6%, 42.8%, respectively. For head-on collisions, these energy dissipation ratios are not very high due to the floating support

platform because it is flexible and easy to move around under the impact force. A considerable part of the energy should be transferred to the kinematic energy of FOWT..

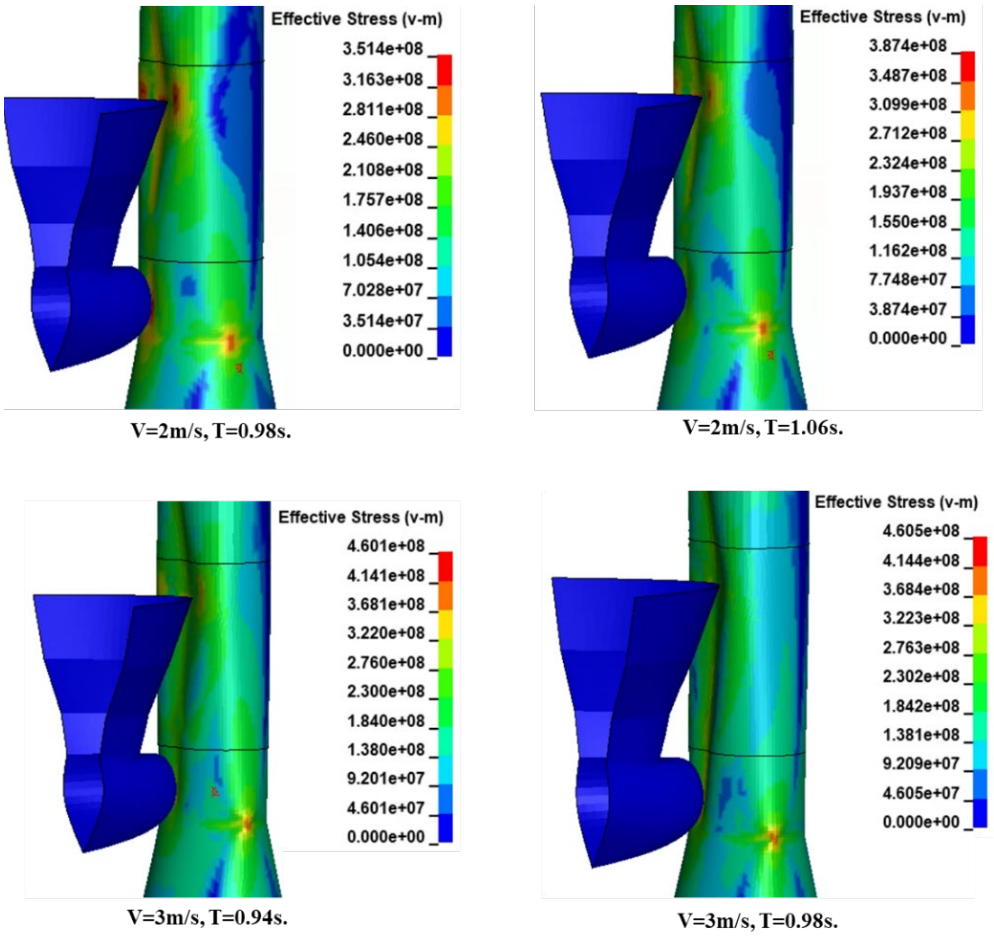

Figure 6-4. Deformation shape of FOWT in ship collision.

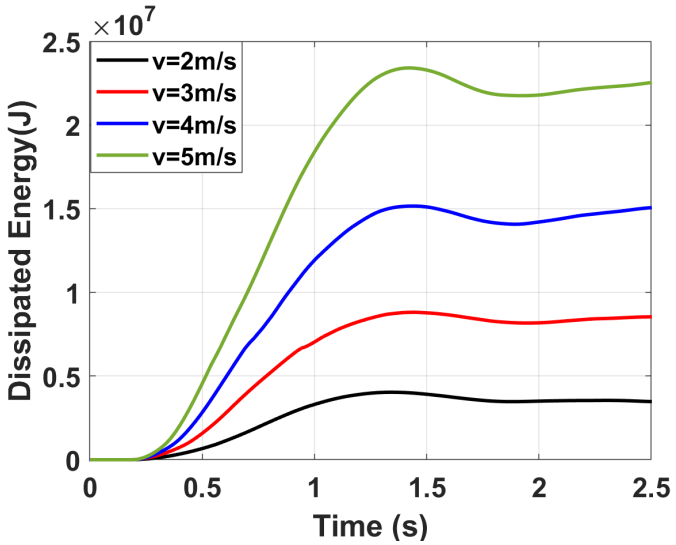

Figure 6-5. Energy dissipation during ship collision.

It should be noted that due to the sudden impact force at the platform and the large mass of nacelle at the tower top, the vibration of the elastic tower will be excited. This phenomenon is also discussed by Bela et al (2017) and by us in Chapter 4. The tower top deflections along the ship impact direction are shown in Figure 6-6. Note that this deflection is under the local body-fixed coordinate systems described before. It is the distance between the deformed tower top and its un-displaced location regardless of the global rigid body motions of the platform. It is found that for impact velocities from 2m/s to 4 m/s, the period and amplitude of tower vibration grow obviously with the increment of impact velocity. The maximum tower top deflection reaches around 5m for an impact velocity of 4m/s. These deflections are then reduced by structural damping. For the impact velocity of 5m/s, serious tower top deflection is found, and then the structure collapse. These different structural behaviors are mainly influenced by the structural residual strength after ship impact. The local indentions at the crushing area are shown in Figure 6-7. Though the impact point is limited on the platform, the structural integrity still influences the bending capacity of the tower due to its slender structure with a lumped mass at the top. As is shown in Figure 6-7, the larger indention is caused by ship impact, the less residual bending capacity remains.

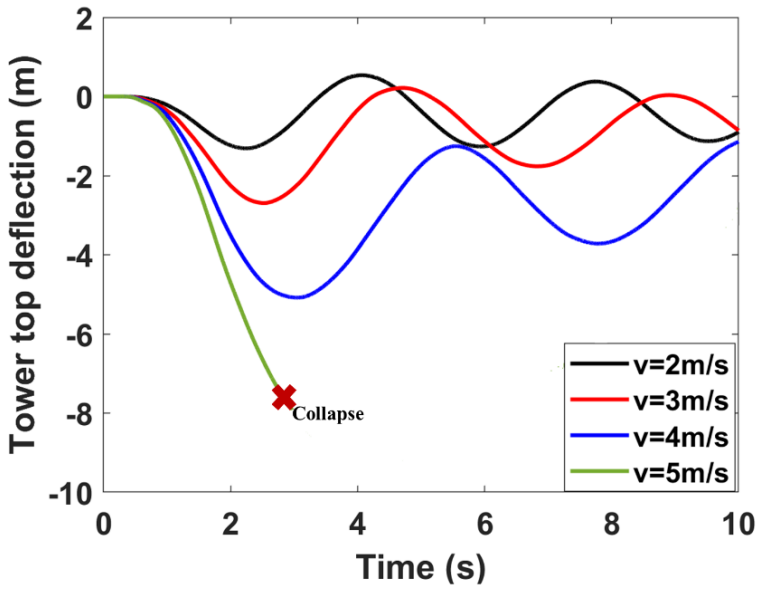

Figure 6-6. Tower top deflection.

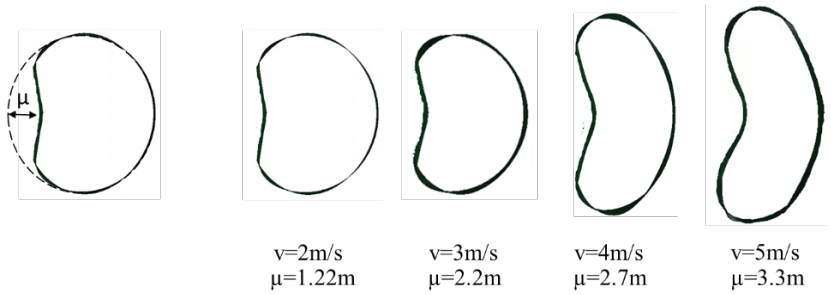

Figure 6-7. Local indention of the FOWT.

In addition to the structural dynamic responses, the external dynamics are also important to be investigated. Because sometimes even though the structure keeps intact, the performance of some components induced by the global motions of the platform still needs to be checked. The global motions of the platform are presented in Figure 6-8. As there are head-on collisions along the surge direction of FOWT, the significant motions can be observed in the surge, heave, and pitch directions. The coupled motion between surge, pitch, and heave direction is found from these results, which is already described by the potential flow theory. It is found that when the impact occurs, rapid growths of all these three motions appear and they are directly caused by the impact force. After the collision (meaning that the contact forces between OSV and FOWT decrease to zero), the surge and pitch motions gradually decay under the hydrodynamic and mooring effects. After several seconds, the maximum pitch angle appears and then started to return to the un-rotated location. If the second impact is not considered, this process happens as a free decay in still water with an initial velocity brought by the first ship impact. These motions should show a periodical pattern if the time-domain results are extended to hundreds of seconds.

The mooring loads are shown in Figure 6-9. These are the total loads contributed by the whole mooring system. The mooring system is mainly used to prevent the platform from drifting away and provide restoring force in the surge, sway motions. As is shown in Figure 6-9, the mooring loads shows a strong linear relationship in surge and heave motions, and a pre-tension of 1.607 MN forward to the negative z-axis can be observed from the figure.

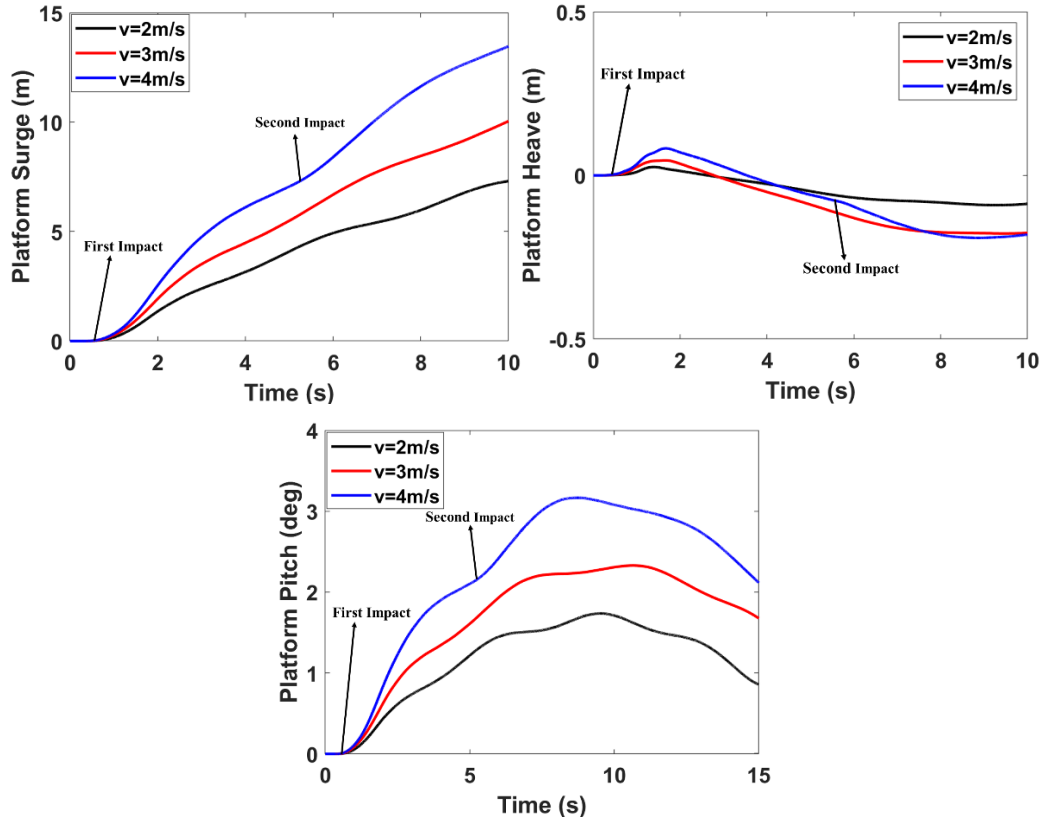

Figure 6-8. Motion amplitudes of FOWT under ship collision.

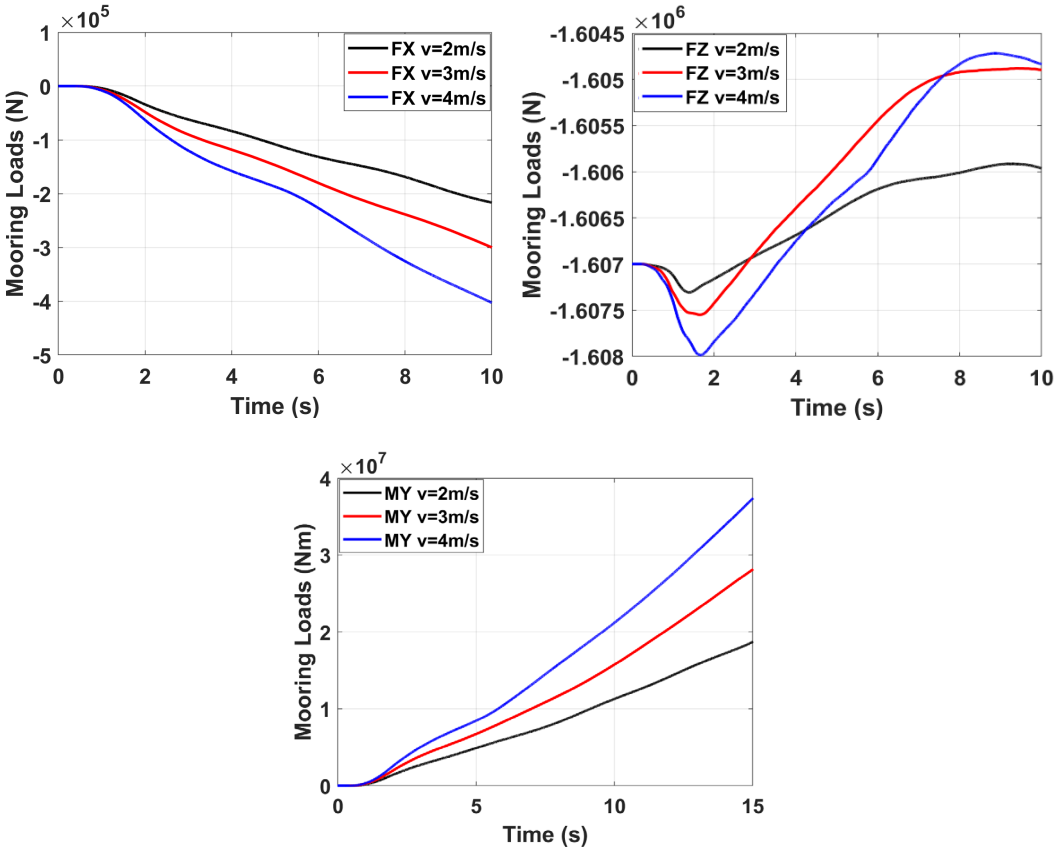

Figure 6-9. Mooring loads from the whole mooring system.

Figure 6-10 gives the maximum tower top acceleration during the collision. As suggested by Bela et al (2017), this value is necessary to investigate as the electrical equipment in the nacelle might be sensitive to this. For those cases in which the structure has collapsed, repair or replacement is obviously needed. However, for those scenarios where minor damage is caused and the whole structure is still intact, the performance of the generator and other equipment in the nacelle are still needed to be checked.

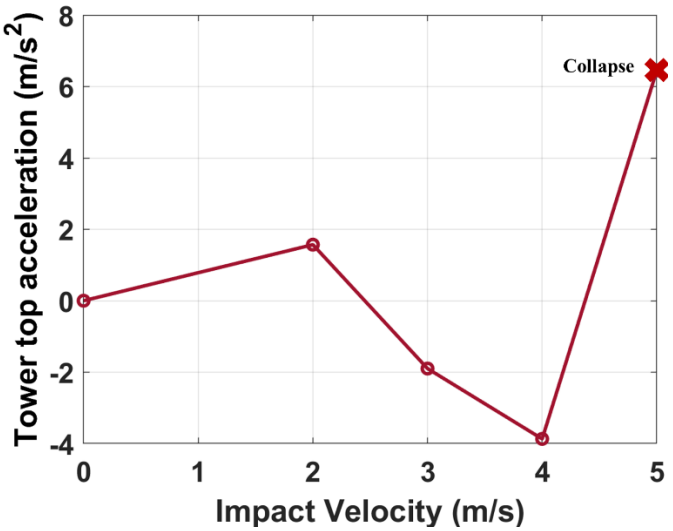

Figure 6-10. Maximum tower top acceleration during collision.

6.4 Discussion on the structural flexibility of the tower

As the FOWT is a long slender structure with a large mass on the top, the ship impact has been found to excite the tower vibration. The influence of flexibility of the tower could be important and is studied in this section. Figure 6-11 shows the energy dissipated by different parts. In the figures, 'Others' refers to the parts except for the tower and in these three cases, they are mainly the crushing area. It is found that though most of the internal energy is from the impact area, the tower still occupies an un-neglectable part of internal energy, which is about 14.2%, 21.7%, 16.7%, respectively in these three cases. The internal energy obtained by the tower mainly comes from several aspects. Firstly, as the impact brings large structural indention, in addition to the gravity effects of the nacelle, the tower bends accordingly, and the internal energy is stored. Also, depending on the impact scenario, the crush area may not only be limited within the contact area between

ship and FOWT, but small plastic deformation could also occur at the tower base.

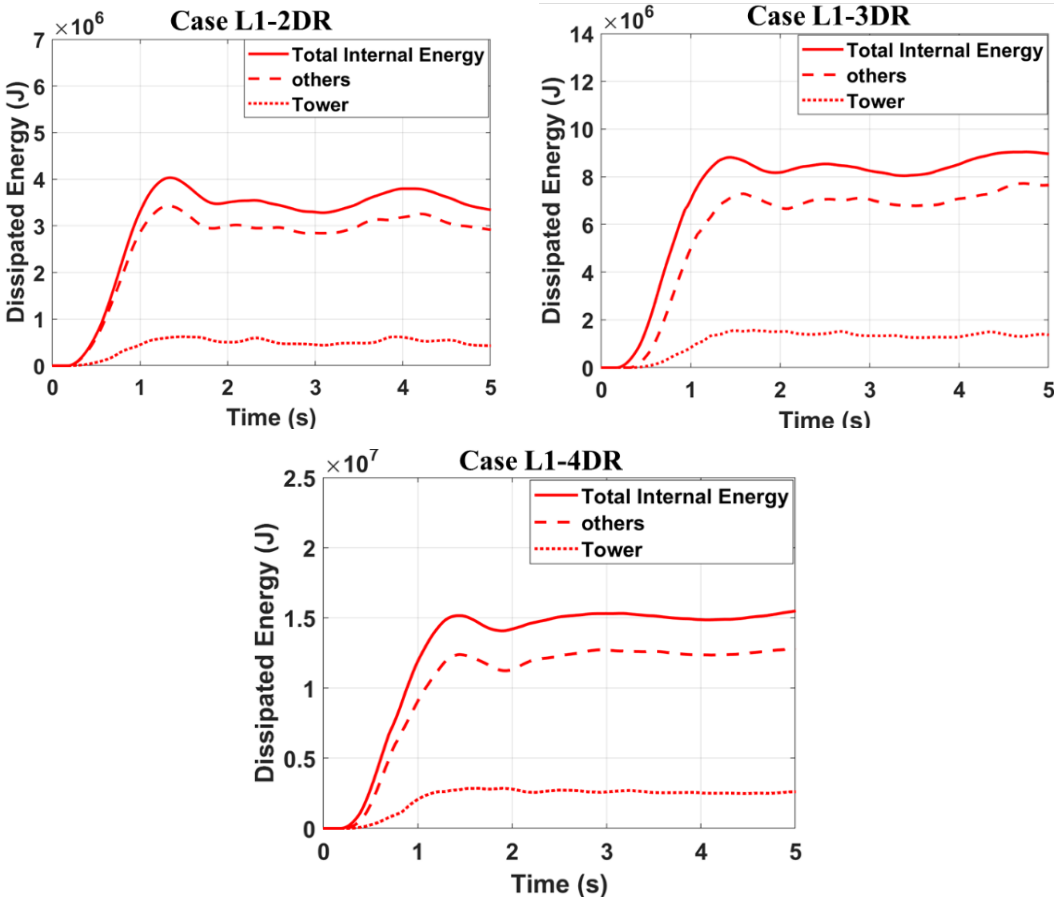

Figure 6-11. Dissipated energy of different parts of FOWT.

The deformability of the tower of fixed bottom offshore wind turbine has also been studied by Pedersen (2013) by numerical simulation and analytical methods. A very interesting finding is that for monopile OWT, the flexibility of the tower can significantly influence the total energy dissipation. Both rigid and flexible towers are modeled and compared, it is found that the flexible tower can greatly lower the energy dissipation, especially for the head-on collision and amidship collision, shown as Figure 6-12.

For a Spar-type floating wind turbine, the effect of the flexible tower is also investigated and the results from 6 cases with rigid and flexible tower models are shown in Figure 6-13. It is interesting to find that for this Spar-type floating wind turbine, the flexibility of the tower rarely influences the energy dissipation of the tower, which is quite different from the fixed-support OWT. This could be explained that for fixed-support OWT, the

platform can rarely move and when the flexibility of the tower is considered, part of the energy transferred to the OWT will be stored as global bending energy in the tower and drive the tower to vibrate in the following seconds after the collision. The global bending motion of the tower can reduce the impact force to cause less indention, so the dissipated energy is reduced. However, for a floating wind turbine, its floating platform is flexible and easy to move around. In that case, the impact force and structure deformation can be mainly relieved due to the floating platform. The global bending motion of the flexible tower will not be the dominant factor to reduce energy dissipation. Considering this finding, it is speculated that the risk of tower structure collapse could be reduced much for FOWTs in the ship collision scenarios compared with fixed-support OWTs.

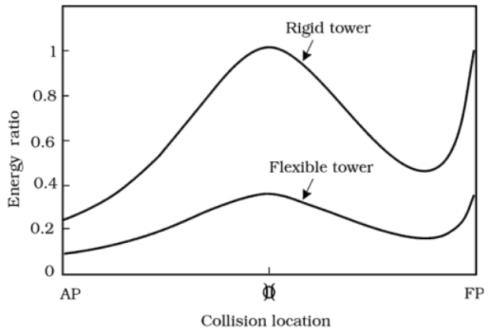

Figure 6-12. Ratio between energy dissipation and the total kinetic energy before collision. (Pedersen, 2013)

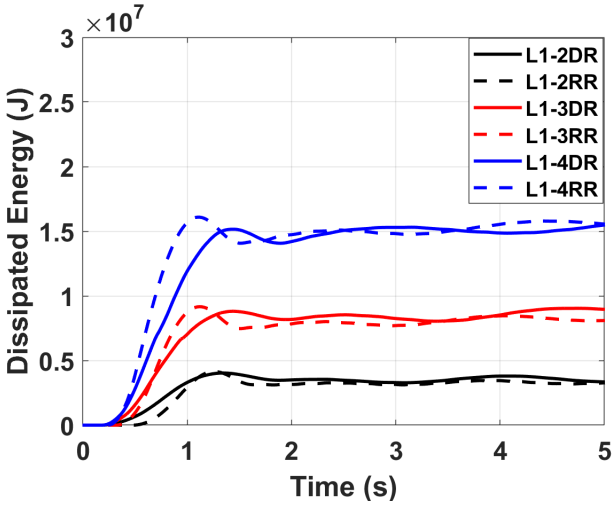

Figure 6-13. The dissipated energy comparison.

6.5 Discussion on the deformability of striking OSV

In the previous calculations, the striking ship is modelled as a rigid body. However, the real striking ship can deform, and the striking energy should be shared by both ship and OSV. In order to better evaluate the dynamic responses of the FOWT, a series of simulations are conducted in still water and the case numbers are shown in Table 6-2. The FE model of the OSV described in section 7.2 is adopted. The bulbous bow is firstly crushed by a rigid wall and the force-deformation curve of the bulbous bow is obtained. It is compared with the design curve in NORSOK N-004 standard (2004), shown as Figure 6-14. The curve from NORSOK (2004) is recommended for a 5000 tons OSV. The difference between these curves should be caused by the difference of dimension of the two ships, e.g., the OSV used in the study is 4000 tons with a bulb and the NORSOK curve is for a 5000 tons OSV. But a similar trend of these two curves is still found.

The collision forces, induced structure indention, and dissipated energy impacted by rigid and deformable OSV are compared to those in Table 6-3. As expected, the collision forces are much lower than those in the cases when the deformable ship bow is applied. According to the results, the resistance force of FOWT impacted by rigid bow is overestimated over 54.41% at the impact velocity of 3 m/s, 7.47 MN, and 3.63 MN respectively. The induced deformations are therefore small, and the reduction is consistent with the crushing force. An average reducing percentage of over 40% is observed for the structural indention.

Note that the energy dissipation listed in Table 6-3 in the case of deformable bow collision is not the total dissipated energy. It is the dissipated energy from FOWT. It is found the energy dissipation is also diminished under the smaller impact force with deformable OSV. The reducing percentages are not so high as the reduction percentage of impact force because the bulbous bow structure is still more rigid than the FOWT and most part of the dissipated energy is contributed by FOWT, and less deformation is caused for the OSV.

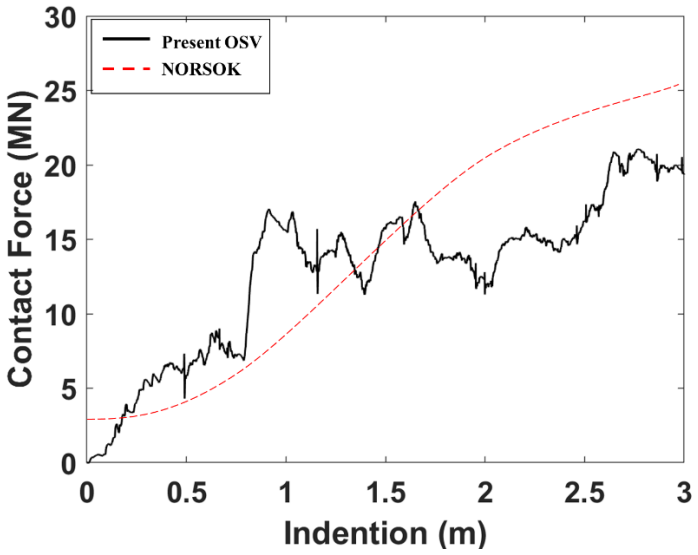

Figure 6-14. Force-deformation curve of the bow structure

Table 6-3. Comparison of maximum collision forces and indentions

		Collision with rigid bow	Collision with deformable bow	Percentage of change
2 m/s	Maximum Impact Force	5.47 MN	3.05 MN	44.24%
	Indention of FOWT	1.22 m	0.67 m	45.08%
	Energy dissipated by FOWT	3.5 MJ	2.98 MJ	14.80%
3 m/s	Maximum Impact Force	7.47MN	3.63 MN	54.41%
	Indention of FOWT	2.2 m	1.12 m	49.09%
	Energy dissipated by FOWT	8.36 MJ	7.25 MJ	13.27%
4 m/s	Maximum Impact Force	8.9 MN	5.74 MN	35.51%
	Indention of FOWT	2.7 m	1.62 m	40.00%
	Energy dissipated by FOWT	14.6 MJ	11.59 MJ	20.62%

6.6 Discussion on the wind-wave influence

In this section, the simulation results of the cases when FOWTs are struck by OSV under wind-wave sea conditions are studied. Two typical sea states and a constant wind velocity are selected as the environmental conditions. The first one is regular wave and the other one is irregular wave (JONSWAP spectrum), defined as case L2-3DR and L3-3DR in Table 6-2. The ship collision is in the same direction as the wind in these cases. When the wind and wave effects are applied on the FOWT, the FOWT will be excited to have large oscillation and will be gradually stabilized within an area. To eliminate the effects of the start-up process (the first few hundreds of seconds) in the simulation, the ship collision is

set to happen after the 350s. In these cases, the computational CPU time should be long enough, so we only use the rigid ship for the simulation with wind or wave conditions to reduce the computational cost.

Figure 6-15 presents the contact forces of these two cases and compared them with the cases in still water. It is found that the collision force in the regular wave is similar to that of still water, and the maximum value reached 7.2 MN, which is a bit larger than the force in irregular wave conditions. However, this difference should not be thought as the influence of sea loads, as the FOWT has an initial velocity and displacement before collision in the wind-wave conditions, and the total initial collision energy and collision height cannot be guaranteed the same in these three cases. The small difference could be caused by the difference in initial collision energy and collision location.

The internal energy of FOWT is shown in Figure 6-16. The figure gives a time history of energy dissipation before, during, and after the collision. It is interesting to find that the whole process contains three different stages. Before the ship collision, a small part of internal energy has been obtained by the FOWT, indicating there are structures deformed. This is simple to understand because under the wind and wave loads, the flexible tower should be kept bending at a certain angle and the internal energy is dissipated. When the collision occurs, the internal energy grows rapidly with the increasing deformation at the crushing area. The dissipated energy should be calculated as the growth of internal energy and a detailed changing process during collision is shown in the right figure of Figure 6-16. It is found that a small drop of internal energy appears after the peak value was reached and this decrease part should be the internal energy from an elastic deformation.

It is interesting to find that the internal energy of FOWT in wave-wind conditions starts to increase after several seconds and the ship collision has ended at that moment. However, this phenomenon doesn’t appear in still water without wind. By demonstrating the snapshots of the ship-collision scenario in Figure 6-17, it is found that this growth of internal energy is caused by the increment of bending moment. It is clearly seen that after

the collision, the supporting platform has been crushed and the overall bending capacity of the structure is significantly weakened. The tower then starts to bend under the wind thrust force as well as gravity effects and finally collapses, shown as Figure 6-17.

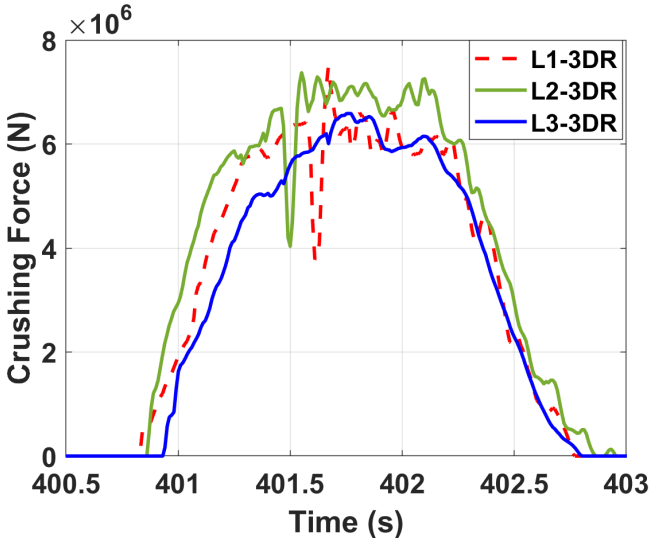

Figure 6-15. Collision forces comparison in different environmental conditions.

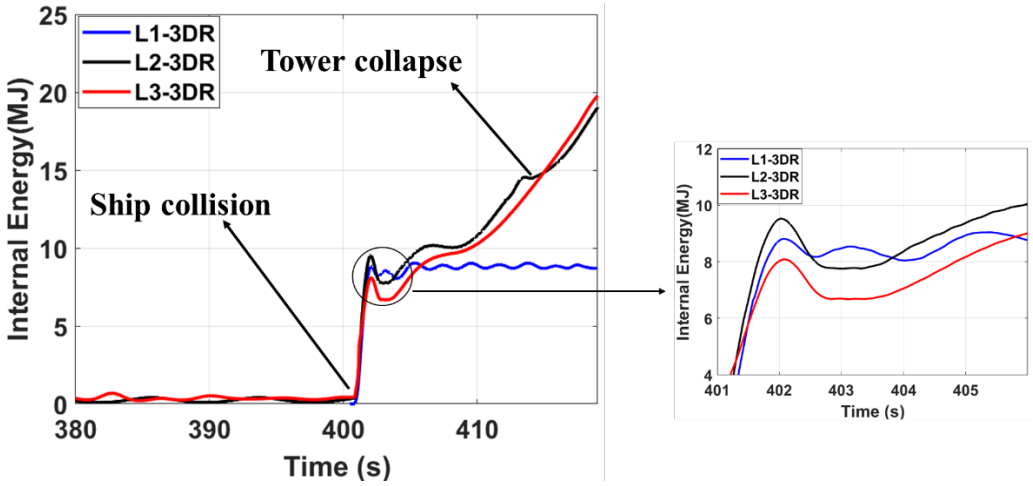

Figure 6-16. Internal energy of FOWT.

Figure 6-18 presents the wind thrust force calculated by user-defined subroutine, LOADUD. It is found that in the wind-regular wave condition, the value of thrust force has shown a periodical variety before the collision, oscillating about 700 KN, and then it drops dramatically to 440 KN. For the thrust force value in wind-irregular wave conditions, an obvious decrease is also observed when the ship impact occurs. This is caused by the sudden change of velocity at the rotor, the lumped-mass node in the FE

model. The aerodynamic thrust force is a function of relative velocity between rotor and wind. When the ship impacts with FOWT, the platform is struck away and the tower top are also moving with the platform. As the striking ship has the same direction as the wind, the relative velocity at the rotor is then smaller than before, leading to a significant force drop. After the ship collision, the platform velocity is reduced under the hydrodynamic damping and mooring system. Then the relative velocity at the rotor grows and the thrust force should be recovered gradually. However, in these two cases, the tower cannot withstand the wind loads after being damaged by the striking ship. So, the thrust force is not observed back to the original level.

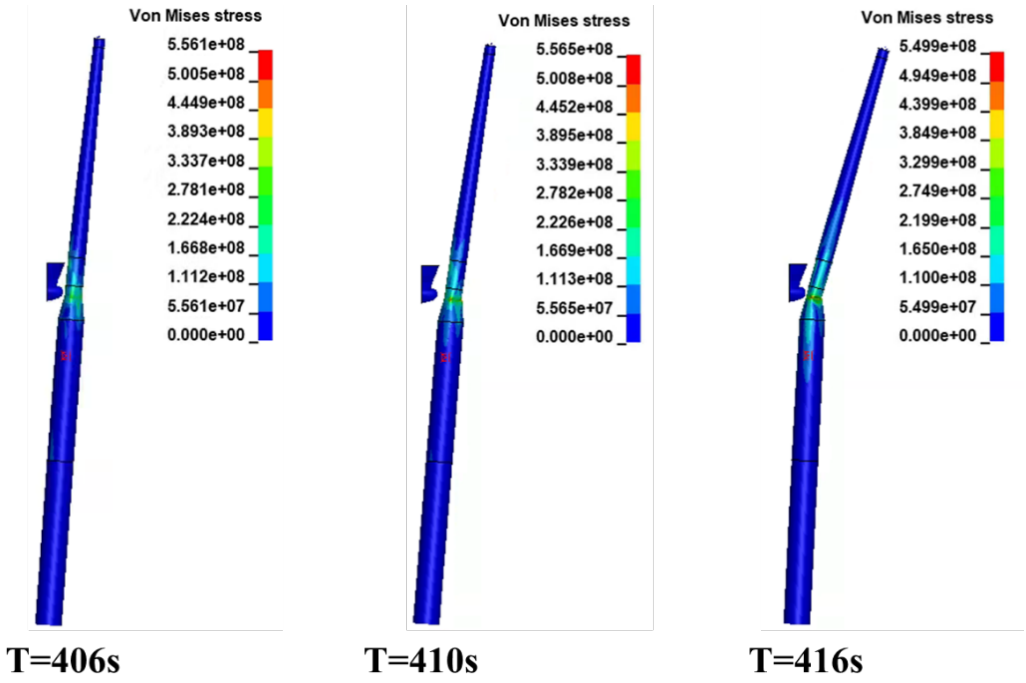

Figure 6-17. Snapshots of the ship-collision scenario in combined irregular wave and wind condition.

The motion amplitudes of surge and pitch are shown in Figure 6-19. Regular and irregular motions are found in regular and irregular wave conditions. Due to the wind force, the platform is drifted away and stabilized at around 21m away from the un-displacement location. A pitch angle of about 3 degrees is observed under the wind effects. Due to the ship impact, both motions grow rapidly under the impact forces. It is observed that the maximum surge motion over 30m and the maximum pitch degree over 5 degrees are

reached and they decrease under the mooring restoring and hydrodynamic loads. Note that these motions are summarized from the reference point at the platform and consider the collapsed tower after 410s.

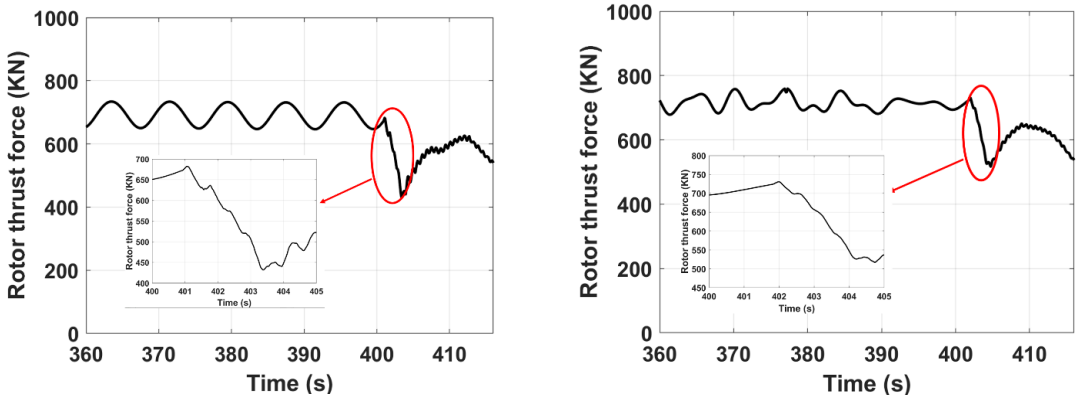

(a) L2-3DR (b) L3-3DR

Figure 6-18. Aero thrust force in the collision scenarios.

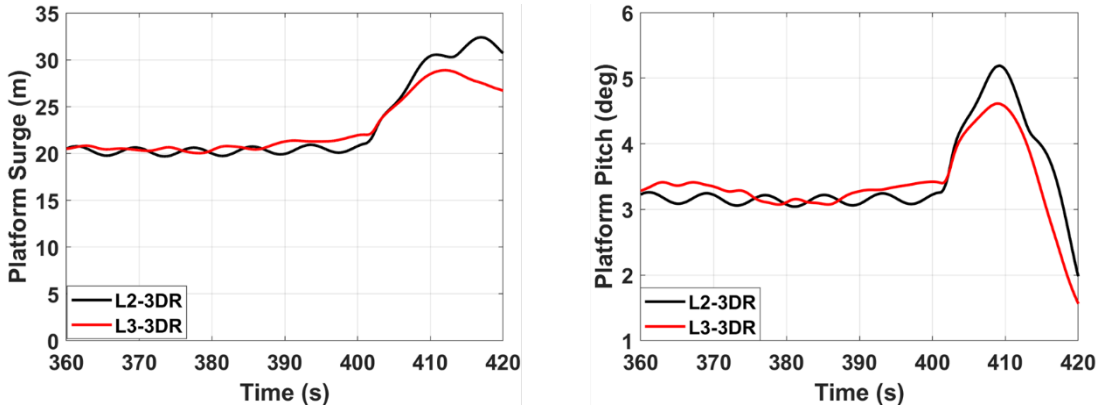

Figure 6-19. Platform motion in the collision scenarios.

6.7 Comparison of coupled and decoupled method

In this section, the motion response in a long period calculated from the hydro-aero coupled solver is compared with the results from the integrated method described in Chapter 5. An analytical collision model and an aero-hydro-servo-elastic coupled simulation tool are combined for ship-FOWT collision analysis. The previous study focuses on the external dynamic responses of FOWT after the ship collision and some transient details during collision cannot be captured in detail. In addition, the decoupled method doesn't solve the problem of structural deformation and global motions simultaneously. But it is still a good reference to study the external dynamics of ship-

FOWT collision.

In the decoupled method, a local coordinate system $(\overrightarrow{n_1}, \overrightarrow{n_2}, \overrightarrow{n_3})$ is established in the common tangent plane at the contact point, shown in Figure 6-20 and the calculation is finished in this local coordinate system. The key point is to find the incremental change in the reaction impulses and a restitution coefficient *e* is introduced to describe the relative velocity of ship and FOWT along $\overrightarrow{n_3}$ direction in the local coordinate system, given as

$$v_3^t = -ev_3^0 \tag{6-1}$$

where v_3^0 is the relative velocity before collision and v_3^t is the relative velocity after collision. Obviously, when *e* equals zero, then the impact is purely plastic and if *e* equals 1, the collision is elastic. Then this analytical model is coupled with an in-house program, which is a fully coupled simulation tool for FOWT. The detailed introduction can refer to Chapter 3.

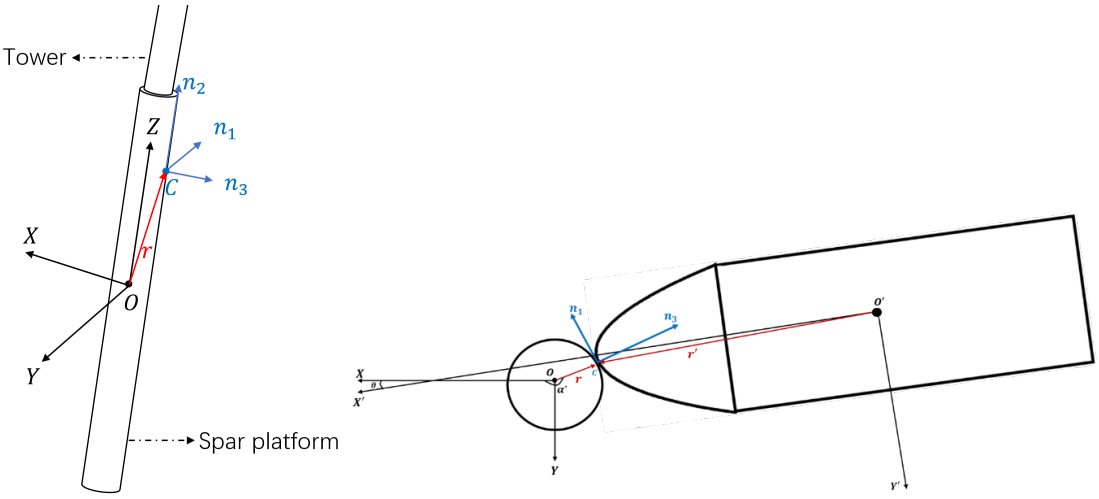

Figure 6-20. An illustration of ship-FOWT collision model in the decoupled method.

Figures 6-21, 6-22, and 6-23 compare the motion response from these two methods. The collision occurs at 0s in the still water without wind and secondary impact is not considered. Three cases are selected to consider the scenarios of low-speed impact, medium-speed impact, and high-speed impact. For the decoupled method in all cases, as the ship impact has transferred a part of kinetic energy to FOWT, the FOWT motion after

the collision is like a free decay with an initial velocity. The period of these regular motions after the collision is also the same as the natural period of FOWT in still water. In the first two cases, the result from the present method matches well. However, in the 3m/s impact scenarios, the gap of results between both methods is enhanced. The amplitude, periods of the motions are quite different from each other. This could be caused by two aspects.

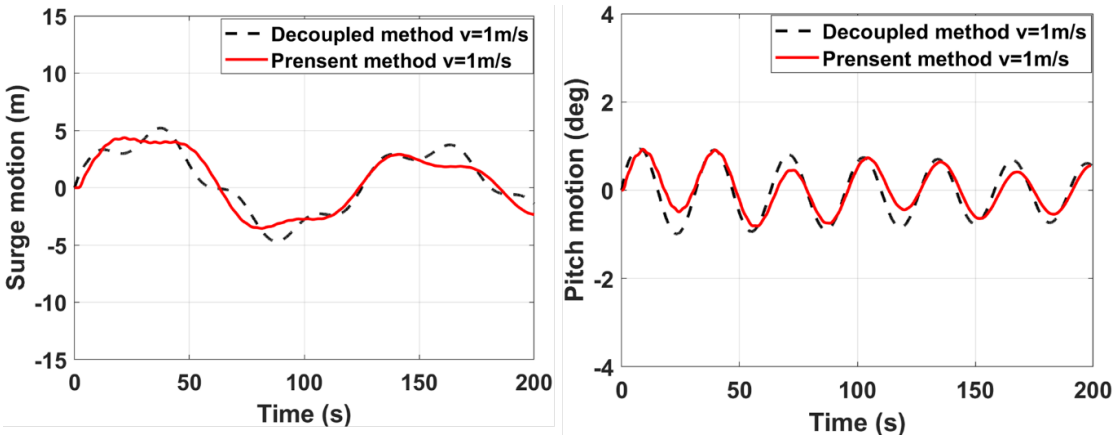

Figure 6-21. Comparison of motion responses of FOWT in a low-speed impact scenario.

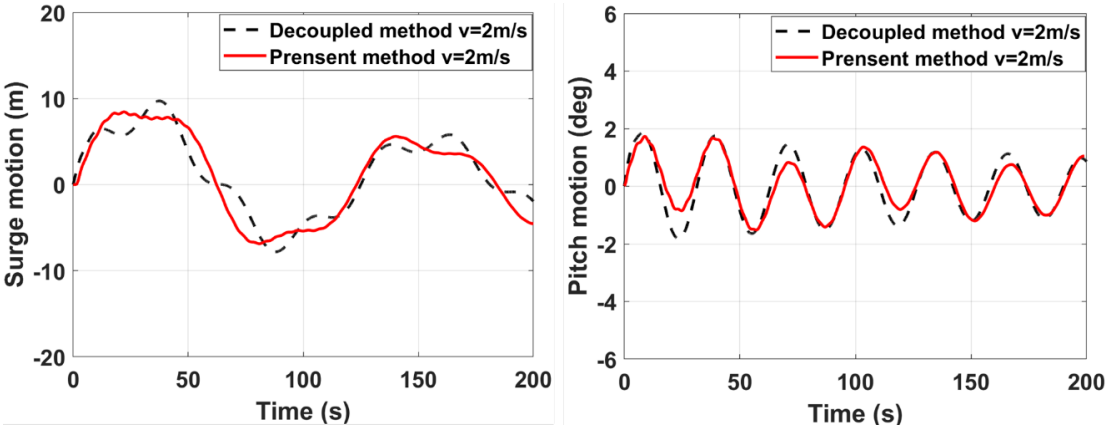

Figure 6-22. Comparison of motion responses of FOWT in a medium-speed impact scenario.

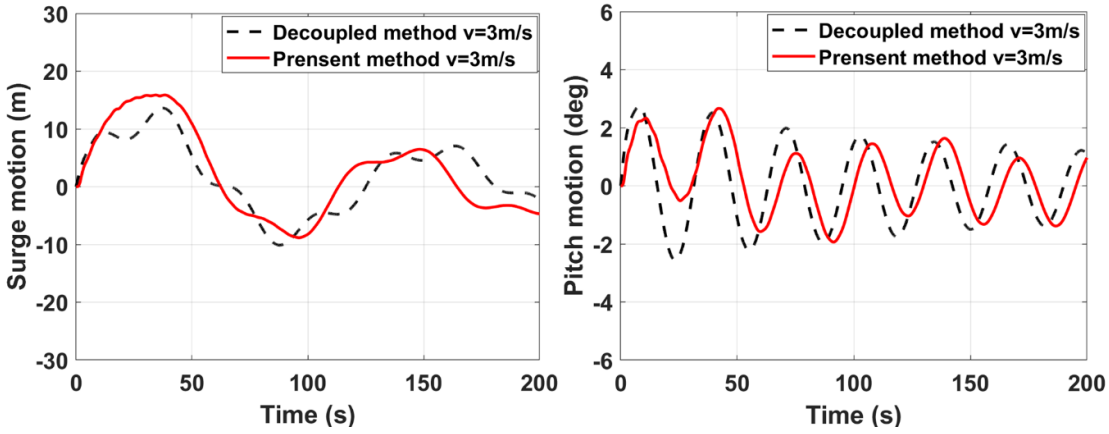

Figure 6-23. Comparison of motion responses of FOWT in a high-speed impact scenario.

First, in the decoupled methods, it is of great importance to adopt the exact value of the restitution coefficient *e* if we would like accurate results. In some theoretical calculations, *e*=0 is adopted to obtain a conservative result. In practical cases, this value might be influenced by many factors such as impact velocity, relative stiffness of the two items, impact angle, and location, etc. If the dissipated energy is obtained, the value of restitution coefficient *e* can be calculated by iterating the external dynamic program with *e* ranging from 0-1. A similar discussion regarding the restitution coefficient can also be found in Yu et al. (2019). In the cases studied in Chapter 4, the empirical value of *e=0.5* is used for case studies. And the measured *e* in the coupled methods for these three cases are shown in Table 6-4. It is found that in the first two cases, the measured restitution coefficient is similar to the value used in decoupled methods, and for the high-speed collision (3m/s), the difference of restitution coefficient between the two methods is quite large. More plastic deformation is caused according to the measured coefficient and the coefficient for the high-speed impact used in the decoupled method needs to be reconsidered.

Table 6-4. Measured restitution coefficient from coupled method

Impact velocity	1m/s	2m/s	3m/s
Restitution coefficient	0.442	0.415	0.28

Secondly, in the decoupled method, some assumptions are made. For example, the

deformation at the contact point is limited in a small zone and collision angles are constant before and after the collision. Based on these assumptions, a unique common plane and a unique normal vector of the common plane can be determined. Then the calculation can be continued. However, the coupled simulation results show that these small deformation assumptions are not suitable for high-speed impact, where large deformation areas are caused according to Figure 6-24. Additionally, as large crushing areas are caused, the tower then bends at a certain angle. The deformed structure will lead to some changes in the CM (centre of mass) location and inertia properties of the whole system. The natural period is still water will change accordingly. Therefore, good agreement isn't achieved between these two methods in the third case.

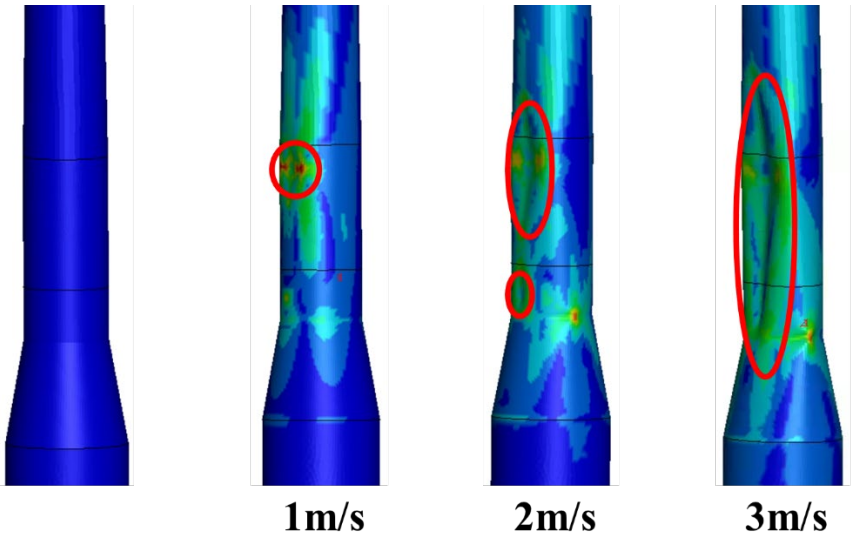

Figure 6-24. Local deformation of FOWT after ship collision.

Next, the motions responses in wind-wave conditions calculated by these two methods are also compared. As a 3m/s impact velocity in the wind-wave condition could lead to tower collapse so that the following motion prediction is meaningless, a low-speed impact velocity 1m/s is then selected. A head-on collision along surge motion is used and the collision height is 6m above the sea surface. The environmental configuration is shown as case L2-1DR in Table 6-2 and the collision moment is set after 400s simulation to reduce the influence of the start-up process.

The surge and pitch motion calculated by these two methods are compared in Figure 6-25. As in the wind-wave condition, a certain drift in surge motion exists under the wind force and the small fluctuations are due to regular waves. When the ship impact happens, and the motions change accordingly. It is observed that the change in pitch motion due to ship impact is very slight but obvious motion responses in surge direction are found. The motion results from the two methods are closed to each other, indicating that the decoupled method is pretty accurate for low-speed impact.

The aero thrust forces acting on the rotor plane are then compared in Figure 6-26. The thrust force from both methods shows a periodical pattern as the platform motion moved regularly before the collision. Due to the impact, the wind forces from both methods drop accordingly because the relative velocity between wind and rotor plane decreases, which has been discussed in section 7.6. Though a similar trend is observed for these two curves during the collision, there still be a gap between the mean value of these two curves. This is caused by the different aerodynamic models used for simulation. In the coupled method, the BEM method with some corrections is adopted and the control strategy is also modelled in detail. In the present coupled method, to efficiently analysing the structural responses and global motions, a simplified aerodynamic model is used, and the control strategy is considered in the thrust coefficient.

In conclusion, the decoupled method can predict the motion responses accurately for a head-on collision at low-speed impact. The main reason should be that in low-speed impact scenarios, minor structure deformation is caused, and the indention is limited within a small area at the contact area. The conditions satisfy the basic assumptions of decoupled methods. However, for collisions leading to serious structural damage or even structural collapse, the decoupled method cannot consider this situation and the coupled method must be adopted.

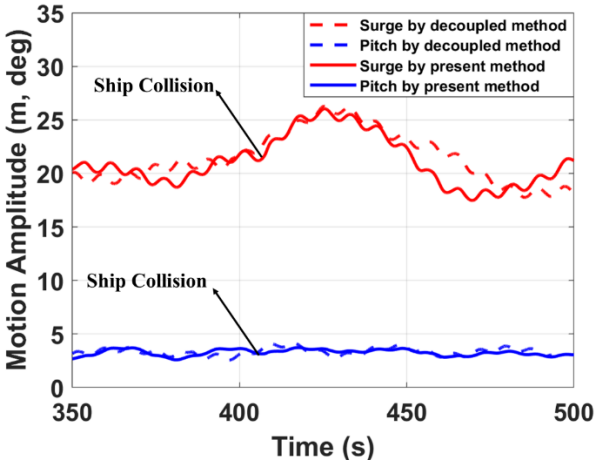

Figure 6-25. Comparison of motion amplitudes

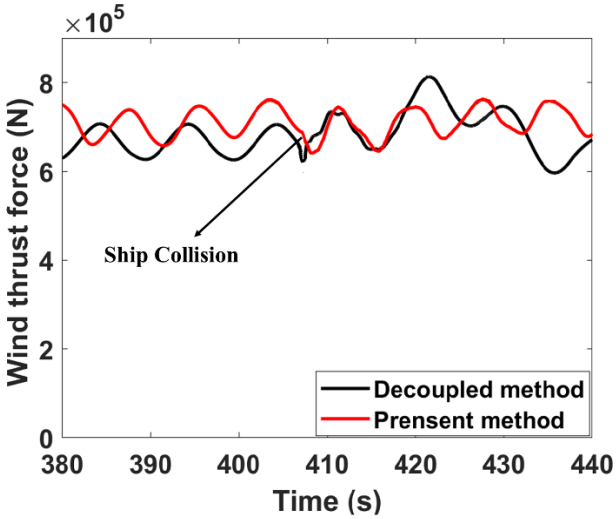

Figure 6-26. Comparison of aero thrust force.

6.8 Summary

This chapter studies the both internal and external dynamic responses of a Spar-type floating wind turbine in ship collision scenarios by using the developed coupled NLFE methods. Some important factors including impact velocity, tower flexibility, ship deformability, and wave-wind loads are studied in detail. Additionally, some results from the coupled method are also compared with the previous results from the decoupled method and some summaries are made as follows.

1). The ship impact velocity greatly influences the structural responses and global motions of the struck FOWT. A high-speed impact with an initial velocity of 5m/s causes serious

local indention, the cross section of platform at collision height dropped over 50% and much bending capacity is lost, leading to a tower collapse. For impact velocity lower than 3m/s, minor damage will be caused.

2). The flexibility of the tower cannot be ignored in structural analysis as it directly influences the responses of the rotor-nacelle assembly on the top. Compared with fixed-support OWT, the tower flexibility is found to influence less on the total energy dissipation for FOWT.

3). For a conservative result and simplicity, a rigid striking ship can be used but the deformability can significantly influence the structural deformation and energy dissipation. It is found that the local indention of FOWT is reduced more than 40% when a deformable striking ship is considered.

4). In the wind-wave conditions, the damage due to ship collision could be more dangerous for FOWT than that in still water conditions. Though the structure can withstand the ship collision at the beginning, the residual strength of FOWT may not be enough to withstand the following wind-wave loads. Therefore, compared with the still water where a 5m/s impact velocity can destroy the FOWT, a smaller impact velocity could cause tower collapse in the wind-wave conditions.

5). This coupled method is also compared with the integrated collision model described in Chapter 3, which is research on external dynamics of ship-FOWT collision. For some low-speed collisions, good agreement has been achieved on the global motions of struck FOWT in still water and wind-wave conditions. However, for higher-speed impact velocity such as 3m/s, the decoupled method has its limitations to accurately predict the dynamic responses because some basic assumptions in the decoupled methods are violated in this scenario.

Chapter 7 Conclusion and future work

Floating offshore wind turbines are experiencing rapid development in terms of quantity and capacity. Like other offshore structures, the ship collision hazard can cause serious economic loss and human injuries, but less attention is paid to this field. The aim of this thesis is to conduct a comprehensive analysis of the ship-FOWT collision problems and understand both external and internal mechanisms of FOWT under the ship collision scenarios. To address the lack of an exact tool for analyzing ship-FOWT collision analysis, two methods were developed in this work.

In this final chapter, some conclusions of this work will be presented, and some limitations will be pointed out for future work recommendation.

7.1 Conclusions

7.1.1 The integrated ship-FOWT collision analysis method

In some scenarios with a short collision duration and low-energy impact, the structural integrity is still kept, and local deformation only appeared with a small zone around the collision point. The performances of the mooring system, tower vibration and rotor-nacelle assembly still need to be checked. An efficient method is proposed to address these aspects. The approach mainly includes two parts, of which the first part is an analytical model for external dynamic analysis of ship collision and the second part is an in-house programme, DARwind, used to predict nonlinear dynamic responses of FOWT in the time domain.

The analytical model is based on previous ship-ship collision studies and can be regarded as a further implementation. Similar assumptions were declared before the derivation.

The analytical model is based on the conservation of momentum principle and the equation of motions of ship and FOWT are transferred into the local coordinate system, which orientates from the collision point. The equations are solved by defining the coefficient of restitution, which gives the relationship between the relative velocity of two items perpendicular to the common plane at collision point before and after ship collision.

DARwind is an aero-hydro-servo-elastic coupled simulation tool for FOWT analysis. The FOWT is treated as a rigid-flexible coupled multibody system in the programme. The platform and nacelle are modeled as rigid whereas the blades and tower are modelled as Bernoulli-Euler beams. The hybrid coordinate dynamical method and Cardan angles are used to describe the translational motion and the rotational movements. For the hydrodynamic aspect, the potential-flow theory and Morison's Equation are adopted and in the aerodynamic module, the blade element momentum method with some aerodynamic corrections are used. The mooring effects are modelled with a quasi-static model. The multibody dynamics are calculated with Kane's dynamical equation.

The external dynamic model is verified and coupled in the DARwind programme and a series of transformation matrices are derived to process the data transfer between these two parts. The integrated method is able to evaluate the global dynamic responses of FOWT before and after collision in time-domain analysis.

With this developed integrated method, some numerical examples of a 5MW Spar-type floating wind turbine impacted by an offshore service vessel were analyzed, including the conditions of still water condition, wave-only condition and wind-wave condition. It is shown that in still water conditions, the ship impact will more obviously change the responses of motions and mooring system, compared with those in wave and wave-wind conditions. In the wave-only condition, these motions responses of the platform are suppressed by wave effects, but the tower vibration and tower top deformation are sensitive to ship collision. For the wave-wind combined condition, the motions increment in surge and pitch due to ship collision becomes smaller than that of wave-only condition,

but the yaw motion has a considerable variation compared with those of the other two conditions. Additionally, the blade tip deformation increment due to ship collision is analyzed and it is found that the edgewise tip deformation gets more obvious increment than that of flapwise direction. To further assess the safety of FOWT, the accelerations at the nacelle are analyzed because some equipment might be sensitive to acceleration. The analysis results indicate that even though the FOWT structure doesn't get critical damage by ship impact, the equipment inside may still fail to work due to the high value of acceleration induced by ship impact.

This method provides fast estimation and should be more suitable in the early designing phase. It is mainly for the low-energy collision with minor structural damage and emphasizes more on the external dynamics and global performances of FOWT components. The structural responses were not analyzed.

7.1.2 The fully coupled ship-FOWT collision analysis method (NLFE method)

From the literature review, it is found that for the high accuracy of structural response prediction, the coupled method (both external and internal dynamics are solved simultaneously) is necessary to be adopted. To analyze the structural responses of FOWT in the ship collision scenarios, a new coupled approach based on nonlinear finite element technology is then proposed.

This method employs a powerful tool, the user-defined subroutine, LOADUD, in LS-DYNA, a general finite element code. The LOADUD subroutine allows the user to define loads according to the node displacement, velocity, acceleration and other user-defined parameters, etc. It provides the probability of modelling mooring, hydrodynamic and aerodynamic loads in the collision duration because these loads are not constant but time-dependent and motion-dependent.

The rotor-nacelle assembly (RNA) structure is simplified, and the aerodynamic loads are evaluated with an existing model from the previous study, which applies the wind force as a point load on the simplified RNA point and considers the conventional pitch control strategy. The hydrodynamic load is calculated by linear potential-flow theory and the mooring effects are calculated with a linear restoring matrix.

The developed method is verified by conducting some free decay tests, wave-only and wind-only analyses and comparing them with the reference values from publications or other numerical programs. The developed method is proved to be able to capture local structural responses and global motions well.

With the developed method and solver, cases of ship collision with a spar-type floating wind turbine are simulated and both local structural deformation and global motions in 6DOF are obtained. The influence of velocity, the flexibility of the tower, deformability of the ship, wind-wave loads is further discussed. It is found that the impact velocity can greatly affect the structural responses and a high-speed impact can directly lead to tower collapse. By comparing the cases of ship-FOWT collision and those collisions with fixed-support wind turbines, the flexibility of wind turbine tower is found to rarely influence the energy dissipation under collision scenario of FOWT, while it is important for the collision scenario of the fixed-support wind turbine. The wind-wave condition can bring more hazards as a smaller impact velocity could lead to structures collapsing because even though the structure can withstand the ship collision, the residual strength may not be enough for the following wind-wave loads. Additionally, the proposed fully coupled method is also compared with the integrated method in the thesis, which is a decoupled method focusing on external dynamics only. The external dynamic results from the two methods are compared and discussed. Good agreement is reached between two methods for low-velocity impact but for high-speed collision or collisions with serious deformation, limitations of decoupled method can be found because some basic assumptions are violated.

7.2 Recommendation for future work.

Though the current work in the thesis addresses the ship-FOWT collision analysis in an innovative way compared with previous studies, some limitations still exist. Thus, some further works, or topics are recommended here for future research.

1) The simplified analytical model used in the integrated method is based on some strong assumptions, thus its validity needs to be assessed before direct use. Additionally, the repeated impact in the integrated model is currently unavailable. A more general model especially the analytical model which addresses the multi-body impact mechanisms is expected to be built.

2) In the fully coupled NLFEM, the hydrodynamic loads including diffraction and radiation forces are included, but the viscous effects of fluid and current are not considered. These effects could be important, and it is expected to be improved to more accurate hydrodynamic loads.

3) In the fully coupled NLFEM, the blades are not modelled in detail and the aerodynamic loads are simplified as a thrust point load. Thus, the rotational effects of blades and the induced loads, such as gyroscopic moment, cannot be captured. The gyroscopic moment is important in the common load analysis for horizontal-axis FOWT. Thus, the importance of the gyroscopic moment is recommended to be investigated in the ship-FOWT collision analysis.

4) 4) In the fully coupled NLFEM, the mooring lines are not modelled, and the mooring loads are simplified as a linear restoring force from the previous study. The accuracy of the mooring model will be lower in the large-motion analysis because the hydrodynamic damping of mooring lines and inertial effects cannot be captured. Thus, the mooring system model used in the ship-FOWT collision can be further improved.

5) Current case simulations mainly study the head-on collision, the oblique collision

especially with small collision angles are advised in the future to investigate the impact mechanisms.

6) For the NLFEM, a power-law hardening material model with constant failure strain is used in the current simulation. It is expected that a more accurate material fracture model should be defined to investigate the internal mechanisms in the future.

7) Current study investigates the Spar-type floating wind turbines under head-on collisions. More types of FOWT are recommended in the future to study the crashworthiness and their characteristics under ship collision scenarios.

References

Abramowicz, W. and Simonsen, B.C., 2003. Effect of fracture on crushing of ship structures. Journal of Ship Research, 47(03), pp.194-207.

Adoum, M. and Lapoujade, V., 2003, May. Examples' manual for* USER_LOADING option. In Proc. 4th European LS-DYNA Users Conference, Ulm, Germany.

Akita, Y., Ando, N., Fujita, Y., & Kitamura, K., 1972. Studies on collision-protective structures in nuclear powered ships. Nuclear Engineering and Design, 19(2), 365-401.

Alsos, H.S. and Amdahl, J., 2009. On the resistance to penetration of stiffened plates, Part I–Experiments. International Journal of Impact Engineering, 36(6), pp.799-807.

Amdahl, J., 1983. Energy Absorption in Ship-Platform Impacts. Dr. Thesis, The Norwegian Institute of Technology, Trondheim.

Bachynski, E.E., Etemaddar, M., Kvittem, M.I., Luan, C. and Moan, T., 2013. Dynamic analysis of floating wind turbines during pitch actuator fault, grid loss, and shutdown. Energy Procedia, 35, pp.210-222.

Bard, J., 2011. HiPRWind: high-power, high-reliability wind technology. In Proc. SET-Plan Conference (Vol. 524).

Bauchau, O.A., 2010. Flexible multibody dynamics (Vol. 176). Springer Science & Business Media.

Bayati, I., Belloli, M., Bernini, L. and Zasso, A., 2017. Aerodynamic design methodology for wind tunnel tests of wind turbine rotors. Journal of Wind Engineering and Industrial

Aerodynamics, 167, pp.217-227.

Belloli, M., Bayati, I., Facchinetti, A., Fontanella, A., Giberti, H., La Mura, F., Taruffi, F. and Zasso, A., 2020. A hybrid methodology for wind tunnel testing of floating offshore wind turbines. Ocean Engineering, 210, p.107592.

Beyer, F., Choisnet, T., Kretschmer, M. and Cheng, P.W., 2015, June. Coupled MBS-CFD simulation of the IDEOL floating offshore wind turbine foundation compared to wave tank model test data. In The Twenty-fifth International Ocean and Polar Engineering Conference.

Blue H Engineering BV, 2017, Blue H Engineering Introduction, available from https://www.energyportzeeland.nl/data/formulieren/uploads/171128%20introduction%20blue%20h%20engineering.pdf

Biehl, F., 2005. Collision safety analysis of offshore wind turbines. In 4th LS-DYNA European Conference.

Biehl, F. and Lehmann, E., 2006. Collisions of ships with offshore wind turbines: Calculation and risk evaluation. In Offshore wind energy (pp. 281-304). Springer, Berlin, Heidelberg.

Bela, A., Le Sourne, H., Buldgen, L. and Rigo, P., 2017. Ship collision analysis on offshore wind turbine monopile foundations. Marine Structures, 51, pp.220-241.

BSH, 2007. Design of Offshore Wind Turbines, Hamburg and Rostock.

Caithness Windfarm Information Forum n.d., Wind turbine accident compilation. Available from: http://www.caithnesswindfarms.co.uk/AccidentStatistics.htm [5 January. 2020]

Carlebur, A. F. C., 1995. Full-scale collision tests. Safety science, 19(2-3), 171-178.

Calle, M.A.G., Oshiro, R.E. and Alves, M., 2017. Ship collision and grounding: scaled experiments and numerical analysis. International journal of impact engineering, 103, pp.195-210.

Cermelli, C., Aubault, A., Roddier, D. and McCoy, T., 2010, May. Qualification of a semi-submersible floating foundation for multi-megawatt wind turbines. In Offshore Technology Conference.

Chen, B.Q., Liu, B. and Soares, C.G., 2019. Experimental and numerical investigation on the influence of stiffeners on the crushing resistance of web girders in ship grounding. Marine Structures, 63, pp.351-363.

Chen, J., Hu, Z., Liu, G. and Tang, Y., 2017. Comparison of different dynamic models for floating wind turbines. Journal of Renewable and Sustainable Energy, 9(6), p.063304.

Chen, J., Hu, Z., Liu, G. and Wan, D., 2019. Coupled aero-hydro-servo-elastic methods for floating wind turbines. Renewable energy, 130, pp.139-153.

Cho, S.R. and Lee, H.S., 2009. Experimental and analytical investigations on the response of stiffened plates subjected to lateral collisions. Marine Structures, 22(1), pp.84-95.

Choung, J., Cho, S.R. and Kim, K.S., 2010. Impact test simulations of stiffened plates using the micromechanical porous plasticity model. Ocean Engineering, 37(8-9), pp.749-756.

Christensen, C. F., Andersen, L. W., & Pedersen, P. H. 2001, Ship collision risk for an offshore wind farm. In Proceedings of the eighth International Conference on Structural Safety and Reliability ICOSSAR., Newport Beach, California. pp. 17-22.

Council, G.W.E., 2021. GWEC| Global Wind Report 2021. Global Wind Energy Council: Brussels, Belgium.

Dai, L., Ehlers, S., Rausand, M. and Utne, I.B., 2013. Risk of collision between service vessels and offshore wind turbines. Reliability Engineering & System Safety, 109, pp.18-31.

DNV GL, 2016. Bladed theory manual version 4.8. DNV GL – Energy.

DNV GL, 2013. Design of Floating Wind Turbine Structures (DNV-OS-J103). Oslo, Norway, May.

DNV GL, 2014. Design of Offshore Wind Turbine Structures (DNV-OS-J101). Oslo, Norway, May.

DNV GL., 2016. Loads and Site Conditions for Wind Turbines (DNV-ST-0437). Oslo, Norway

NORSOK, D., 2004. Standard N-004. Design of steel structures.

Duan, F., Hu, Z. and Niedzwecki, J.M., 2016. Model test investigation of a spar floating wind turbine. Marine Structures, 49, pp.76-96.

Duan, F., Hu, Z., Liu, G. and Wang, J., 2016. Experimental comparisons of dynamic properties of floating wind turbine systems based on two different rotor concepts. Applied Ocean Research, 58, pp.266-280. Duan, F., Hu, Z. and Niedzwecki, J.M., 2016. Model test investigation of a spar floating wind turbine. Marine Structures, 49, pp.76-96.

Echeverry, S., Márquez, L., Rigo, P. and Le Sourne, H., 2019. Numerical crashworthiness analysis of a spar floating offshore wind turbine impacted by a ship. In Developments in the Collision and Grounding of Ships and Offshore Structures (pp. 85-95). CRC Press.

Ehlers, S., Broekhuijsen, J., Alsos, H. S., Biehl, F., & Tabri, K., 2008. Simulating the collision response of ship side structures: a failure criteria benchmark study. International Shipbuilding Progress, 55(1-2), 127-144.

Ehlers, S., Tabri, K., Romanoff, J. and Varsta, P., 2012. Numerical and experimental investigation on the collision resistance of the X-core structure. Ships and offshore structures, 7(1), pp.21-29.

Ellinas, C. P., & Valsgard, S., 1985. Collisions and damage of offshore structures: a state-of-the-art. Journal of energy resources technology, 107(3), 297-314.

Endo, H., Yamada, Y., Kitamura, O. and Suzuki, K., 2002. Model test on the collapse strength of the buffer bow structures. Marine Structures, 15(4-5), pp.365-381.

EWEA European Wind Energy Association, 2013. Deep water: the next step for offshore wind energy. Brussels, Belgium: A report by the European Wind Energy Association.

Faltinsen, O., 1993. Sea loads on ships and offshore structures (Vol. 1). Cambridge university press.

Ferry M. 2002. MCOL user's manual. Principia Marine, technical report. 25 February

Forward, F., 2014. Fukushima floating offshore wind farm demonstration project. Japan: Fukushima Offshore Wind Consortium.

Gao, Z., Hu, Z., Wang, G. and Jiang, Z., 2014. An analytical method of predicting the response of FPSO side structures to head-on collision. Ocean engineering, 87, pp.121-135.

Goupee, A.J., Koo, B.J., Kimball, R.W., Lambrakos, K.F. and Dagher, H.J., 2014. Experimental comparison of three floating wind turbine concepts. Journal of Offshore Mechanics and Arctic Engineering, 136(2).

Gruben, G., Sølvernes, S., Berstad, T., Morin, D., Hopperstad, O.S. and Langseth, M., 2017. Low-velocity impact behaviour and failure of stiffened steel plates. Marine Structures, 54, pp.73-91.

GWEC, 2021. Global wind report 2021. Brussels: Global Wind Energy Council

Hao, E. and Liu, C., 2017. Evaluation and comparison of anti-impact performance to offshore wind turbine foundations: Monopile, tripod, and jacket. Ocean engineering, 130, pp.218-227.

Hagiwara, K., Takanabe, H. and Kawano, H., 1983. A proposed method of predicting ship collision damage. International Journal of Impact Engineering, 1(3), pp.257-279.

Hallquist JO., 2013. LS-DYNA user's manuals version 971, vol. 1 & 2.

Hanhirova, H, 1995. External Collision model, Safety of Passenger/RoRo Vessels. Helsinki University of Technology, Ship Laboratory.

Hansen M.O., Aerodynamics of wind turbines. Routledge; 2008.

Haris, S. and Amdahl, J., 2012. An analytical model to assess a ship side during a collision. Ships and Offshore Structures, 7(4), pp.431-448.

Hasselmann K, Barnett T P, Bouws E, et al. Measurements of wind-wave growth and swell decay during the Joint North Sea Wave Project (JONSWAP) [J]. Ergänzungsheft 8-12, 1973.

Henderson, A.R., Bulder, B., Huijsmans, R., Peeringa, J., Pierik, J., Snijders, E., van Hees, M., Wijnants, G.H. and Wolf, M.J., 2003. Feasibility study of floating windfarms in shallow offshore sites. Wind Engineering, 27(5), pp.405-418.

Heronemus, W.E., 1972. Pollution-free energy from offshore winds. In 8th Annual Conference and Exposition, Marine Technology Society, Sep. 11-13, 1972, Washington, DC.

Hong, L. and Amdahl, J., 2008. Crushing resistance of web girders in ship collision and grounding. Marine Structures, 21(4), pp.374-401.

Ishida, S., Kokubun, K., Nimura, T., Utsunomiya, T., Sato, I. and Yoshida, S., 2013, June. At-sea experiment of a hybrid spar type offshore wind turbine. In International Conference on Offshore Mechanics and Arctic Engineering (Vol. 55423, p. V008T09A035). American Society of Mechanical Engineers.

Ito, H., Kondo, K., Yoshimura, N., Minoru, K., Yamamoto, S., 1984. A simplified method to analyze the strength of double hulled structures in collision. Journal of the Society of Naval Architects of Japan, 156, pp. 283-296

Jia, H. and Moan, T., 2010. January. Global responses of struck ships in collision with emphasis on hydrodynamic effects. In International Conference on Offshore Mechanics and Arctic Engineering (Vol. 49095, pp. 225-236).

Jones, N. (1978). A Literature Survey on the Collision and Grounding Protection of Ships. MASSACHUSETTS INST OF TECH CAMBRIDGE DEPT OF OCEAN ENGINEERING

Jones, N., 2011. Structure impact. Cambridge university press

Jones, N. and Paik, J.K., 2012. Impact perforation of aluminium alloy plates. International Journal of Impact Engineering, 48, pp.46-53.

Jones, N. and Paik, J.K., 2013. Impact perforation of steel plates. Ships and offshore structures, 8(5), pp.579-596.

Jonge, T.D., Laukeland, L., 2013. Collision between a spar platform and a tanker. Collision and Grounding of Ships and Offshore Structures. Amdahl, J., Ehlers, S., Leira, B., (Eds). Taylor & Francis Group, London, ISBN 978-1-138-00059-9.

Jonkman, J.M., 2007. Dynamics modeling and loads analysis of an offshore floating wind turbine (Doctoral dissertation, University of Colorado at Boulder).

Jonkman, J.M., 2010. Definition of the Floating System for Phase IV of OC3 (No. NREL/TP-500-47535). National Renewable Energy Lab. (NREL), Golden, CO (United States).

Jonkman, J.M. and Buhl Jr., M. L. FAST User's Guide, NREL/EL-500-38230 (previously NREL/EL-500-29798), Golden, CO: National Renewable Energy Laboratory, August 2005

Jonkman, J.M, Butterfield, S., Musial, W. and Scott, G., 2009. Definition of a 5-MW reference wind turbine for offshore system development (No. NREL/TP-500-38060). National Renewable Energy Lab. (NREL), Golden, CO (United States).

Jonkman, B. and Jonkman, J.M., 2016. FAST v8. 16.00 a-bjj user's guide. National Renewable Energy Laboratory.

Jonkman, J.M and Musial, W., 2010. Offshore code comparison collaboration (OC3) for IEA Wind Task 23 offshore wind technology and deployment (No. NREL/TP-5000-48191). National Renewable Energy Lab. (NREL), Golden, CO (United States).

Kane, T.R. and Levinson, D.A., 1983. The use of Kane's dynamical equations in robotics. The International Journal of Robotics Research, 2(3), pp.3-21.

Karimirad, M. and Moan, T., 2012. Wave-and wind-induced dynamic response of a spar-type offshore wind turbine. Journal of waterway, port, coastal, and ocean engineering, 138(1), pp.9-20.

Karlsson, U.B., Ringsberg, J.W., Johnson, E., Hoseini, M. and Ulfvarson, A., 2009. Experimental and numerical investigation of bulb impact with a ship side-shell structure. Marine Technology and SNAME News, 46(01), pp.16-26.

Kim, K.J., Lee, J.H., Park, D.K., Jung, B.G., Han, X. and Paik, J.K., 2016. An experimental and numerical study on nonlinear impact responses of steel-plated structures

in an Arctic environment. International Journal of Impact Engineering, 93, pp.99-115.

Larsen, T.J. and Hansen, A.M., 2019. How 2 hawc2, the user's manual (risø-r-1597 ver. 12.8 (en)). Report, Risø National Laboratory, Technical University of Denmark.

Le Sourne, H., 2007. A ship collision analysis program based on super-element method coupled with large rotational ship movement analysis tool. In International conference on collision and grounding of ships (pp. 131-138).

Le Sourne, H., Barrera, A. and Maliakel, J.B., 2015. Numerical crashworthiness analysis of an offshore wind turbine jacket impacted by a ship. Journal of Marine Science and Technology, 23(5), pp.694-704.

Le Sourne, H., Besnard, N., Cheylan, C., & Buannic, N, 2012. A ship collision analysis program based on upper bound solutions and coupled with a large rotational ship movement analysis tool. Journal of Applied Mathematics, 2012

Le Sourne, H., Donner, R., Besnier, F., & Ferry, M, 2001. External dynamics of ship-submarine collision. In Preprints of 2nd International Conference on Collision and Grounding of Ships, Copenhagen

Lehmann, E., & Peschmann, J. (2002). Energy absorption by the steel structure of ships in the event of collisions. Marine Structures, 15(4-5), 429-441.

Le Sourne, H., Pire, T., Hsieh, J.R. and Rigo, P., 2016. New analytical developments to study local and global deformations of an offshore wind turbine jacket impacted by a ship. In Proceedings of the 7th International Conference on Collision and Grounding of Ships and Offshore Structures (ICCGS'16) (pp. 15-18). Ulsan, Korea: University of Ulsan.

Li, Y., Paik, K.J., Xing, T. and Carrica, P.M., 2012. Dynamic overset CFD simulations of wind turbine aerodynamics. Renewable Energy, 37(1), pp.285-298.

Likins, P.W., 1972. Finite element appendage equations for hybrid coordinate dynamic analysis. International Journal of Solids and Structures, 8(5), pp.709-731.

Liu, B., Pedersen, P. T., Zhu, L., & Zhang, S., 2018. Review of experiments and calculation procedures for ship collision and grounding damage. Marine Structures, 59, 105-121

Liu, B. & Soares, C.G., 2015. Simplified analytical method for evaluating web girder crushing during ship collision and grounding. Marine structures, 42, pp.71-94.

Liu, B. & Soares, C.G., 2016. Experimental and numerical analysis of the crushing behaviour of stiffened web girders. International Journal of Impact Engineering, 88, pp.22-38.

Liu, B., Villavicencio, R. & Soares, C.G., 2014. On the failure criterion of aluminium and steel plates subjected to low-velocity impact by a spherical indenter. International Journal of Mechanical Sciences, 80, pp.1-15.

Liu, B., Villavicencio, R. and Soares, C.G., 2015. Simplified method for quasi-static collision assessment of a damaged tanker side panel. Marine Structures, 40, pp.267-288.

Liu, B., Villavicencio, R., Zhang, S. and Soares, C.G., 2017. Assessment of external dynamics and internal mechanics in ship collisions. Ocean Engineering, 141, pp.326-336.

Liu, Y., Xiao, Q., Incecik, A., Peyrard, C. and Wan, D., 2017. Establishing a fully coupled CFD analysis tool for floating offshore wind turbines. Renewable Energy, 112, pp.280-301.

Liu, Z. and Amdahl, J., 2010. A new formulation of the impact mechanics of ship collisions and its application to a ship–iceberg collision. Marine Structures, 23(3), pp.360-384.

Liu, Z. and Amdahl, J., 2019. On multi-planar impact mechanics in ship collisions. Marine Structures, 63, pp.364-383.

Masciola, M., Jonkman, J. and Robertson, A., 2013, June. Implementation of a multisegmented, quasi-static cable model. In The Twenty-third International Offshore and Polar Engineering Conference.

Matha, D., Fischer, T., Kuhn, M. and Jonkman, J., 2010. Model development and loads analysis of a wind turbine on a floating offshore tension leg platform (No. NREL/CP-500-46725). National Renewable Energy Lab. (NREL), Golden, CO (United States).

Matha, D., Schlipf, M., Pereira, R. and Jonkman, J., 2011, June. Challenges in simulation of aerodynamics, hydrodynamics, and mooring-line dynamics of floating offshore wind turbines. In The Twenty-first International Offshore and Polar Engineering Conference.

Minorsky, V.U., 1958. An analysis of ship collisions with reference to protection of nuclear power plants (No. NP-7475). Sharp (George G.) Inc., New York.

Morris, N.F., 1977. The use of modal superposition in nonlinear dynamics. Computers & Structures, 7(1), pp.65-72.

Mostofi, A. and Bargi, K., 2012. New concept in analysis of floating piers for ship berthing impact. Marine structures, 25(1), pp.58-70.

Motora, S., Fujino, M., Sugiura, M., & Sugita, M., 1971. Equivalent added mass of ships in collisions. Selected Papers, J of Soc of Naval Arch of Japan, 7.

Moulas, D., Shafiee, M. and Mehmanparast, A., 2017. Damage analysis of ship collisions with offshore wind turbine foundations. Ocean Engineering, 143, pp.149-162.

Musial, W., Butterfield, S. and Boone, A., 2004, January. Feasibility of floating platform systems for wind turbines. In 42nd AIAA aerospace sciences meeting and exhibit (p.

1007).

Nada, A.A., Hussein, B.A., Megahed, S.M. and Shabana, A.A., 2010. Use of the floating frame of reference formulation in large deformation analysis: experimental and numerical validation. Proceedings of the Institution of Mechanical Engineers, Part K: Journal of Multi-body Dynamics, 224(1), pp.45-58.

Nielsen, F.G., Hanson, T.D. and Skaare, B., 2006, January. Integrated dynamic analysis of floating offshore wind turbines. In International Conference on Offshore Mechanics and Arctic Engineering (Vol. 47462, pp. 671-679).

Ocakli, H., Zhang, S. and Pedersen, P.T., 2004. Crushing of ship bows in head-on collision. International Journal of Maritime Engineering, 146, pp.39-46.

Øye, S., 1991, January. Dynamic stall simulated as time lag of separation. In Proceedings of the 4th IEA Symposium on the Aerodynamics of Wind Turbines (Vol. 27, p. 28). Rome, Italy.

Pawlowski M., 1995. Energy Loss in ship's collisions', Centrum Techniki Okretowej, Poland.

Paik, J.K., Chung, J.Y., Choe, I.H., Thayamballi, A.K., Pedersen, P.T. and Wang, G., 1999. On rational design of double hull tanker structures against collision.

Pedersen, P.T., 2013. Ship collisions against wind turbines, quays and bridge piers. Collision and grounding of ships and offshore structures. CRC Press/Taylor and Francis Group, London, pp.273-280.

Pedersen, P.T., Valsgaard, S., Olsen, D. and Spangenberg, S., 1993. Ship impacts: bow collisions. International Journal of Impact Engineering, 13(2), pp.163-187.

Pedersen, P. T., & Zhang, S., 1998. On impact mechanics in ship collisions. Marine

Structures, 11(10), 429-449.

Pedersen, P.T. and Zhang, S., 2000. Absorbed energy in ship collisions and grounding—revising Minorsky's empirical method. Journal of Ship Research, 44(02), pp.140-154.

Pelastar, 2013. Available from https://pelastar.com/

Petersen, M.J., 1982. Dynamics of ship collisions. Ocean Engineering, 9(4), pp.295-329.

Petersen M.J., Pedersen P.T., 1981. Collisions between ships and offshore platforms. In: Offshore technology conference. Offshore technology conference.

Pill, I., & Tabri, K., 2011. Finite element simulations of ship collisions: a coupled approach to external dynamics and inner mechanics. Ships and Offshore Structures, 6(1-2), 59-66

Pire, T., Le Sourne, H., Echeverry, S. and Rigo, P., 2018. Analytical formulations to assess the energy dissipated at the base of an offshore wind turbine jacket impacted by a ship. Marine Structures, 59, pp.192-218.

Platt, A., Jonkman, B. and Jonkman, J., 2016. Inflowwind users guide. Technical Report.

Popko, W., Vorpahl, F., Zuga, A., Kohlmeier, M., Jonkman, J., Robertson, A., Larsen, T.J., Yde, A., Sætertrø, K., Okstad, K.M. and Nichols, J., 2012, June. Offshore Code Comparison Collaboration Continuation (OC4), Phase 1-Results of Coupled Simulations of an Offshore Wind Turbine with Jacket Support Structure. In The twenty-second international offshore and polar engineering conference.

Popov, Y.N., Faddeev, O.V., Kheisin, D.E. and Yakovlev, A.A., 1969. Strength of ships sailing in ice. ARMY FOREIGN SCIENCE AND TECHNOLOGY CENTER CHARLOTTESVILLE VA.

Presencia, C.E. and Shafiee, M., 2018. Risk analysis of maintenance ship collisions with

offshore wind turbines. International Journal of Sustainable Energy, 37(6), pp.576-596.

Quesnel, L., Bard, J. and Hanssen, J.E., 2011, March. Introducing HiPRWind-high power, high reliability offshore wind technology. In Proceedings of the EWEA Conference (pp. 1-7).

Robertson, A., Jonkman, J., Musial, W., Vorpahl, F. and Popko, W., 2013. Offshore code comparison collaboration, continuation: Phase II results of a floating semisubmersible wind system (No. NREL/CP-5000-60600). National Renewable Energy Lab. (NREL), Golden, CO (United States).

Robertson, A.N., Wendt, F., Jonkman, J.M., Popko, W., Dagher, H., Gueydon, S., Qvist, J., Vittori, F., Azcona, J., Uzunoglu, E. and Soares, C.G., 2017. OC5 project phase II: validation of global loads of the DeepCwind floating semisubmersible wind turbine. Energy Procedia, 137, pp.38-57.

Robertson, A.N., Wendt, F., Jonkman, J.M., Popko, W., Vorpahl, F., Stansberg, C.T., Bachynski, E.E., Bayati, I., Beyer, F., de Vaal, J.B. and Harries, R., 2015, June. OC5 project phase I: Validation of hydrodynamic loading on a fixed cylinder. In The Twenty-fifth International Ocean and Polar Engineering Conference.

Roddier, D., Cermelli, C., Aubault, A. and Weinstein, A., 2010. WindFloat: A floating foundation for offshore wind turbines. Journal of renewable and sustainable energy, 2(3), p.033104.

Santosa, S. and Wierzbicki, T., 1998. On the modeling of crush behavior of a closed-cell aluminum foam structure. Journal of the Mechanics and Physics of Solids, 46(4), pp.645-669.

Sha, Y. and Amdahl, J., 2019. Numerical investigations of a prestressed pontoon wall subjected to ship collision loads. Ocean Engineering, 172, pp.234-244.

Simonsen, B. C., and Lauridsen, L. P., 2000. Energy absorption and ductile failure in metal sheets under lateral indentation by a sphere. International Journal of Impact Engineering, 24(10), 1017-1039.

Simonsen, B.C. and Ocakli, H., 1999. Experiments and theory on deck and girder crushing. Thin-walled structures, 34(3), pp.195-216.

Song, M., Jiang, Z. and Yuan, W., 2021. Numerical and analytical analysis of a monopile-supported offshore wind turbine under ship impacts. Renewable Energy, 167, pp.457-472.

Spera, D.A., 1994. Wind turbine technology.

Stiesdal, H., 2009. Hywind: The world's first floating MW-scale wind turbine. Wind Directions, 31, pp.52-53.

Storheim, M. & Amdahl, J. 2014. Design of offshore structures against accidental ship collisions. Marine Structures, 37, 135-172.

Stronge, W.J. 2004. Impact mechanics. Cambridge university press.

Sun, B., Hu, Z. and Wang, G., 2015. An analytical method for predicting the ship side structure response in raked bow collisions. Marine Structures, 41, pp.288-311.

Tabri, K., 2012. Influence of coupling in the prediction of ship collision damage. Ships and Offshore Structures, 7(1), pp.47-54.

Tabri, K., Broekhuijsen, J., Matusiak, J. and Varsta, P., 2009. Analytical modelling of ship collision based on full-scale experiments. Marine Structures, 22(1), pp.42-61.

Tabri, K., Määttänen, J. and Ranta, J., 2008. Model-scale experiments of symmetric ship collisions. Journal of marine science and technology, 13(1), pp.71-84.

Tabri, K., Varsta, P. and Matusiak, J., 2010. Numerical and experimental motion

simulations of nonsymmetric ship collisions. Journal of Marine Science and Technology, 15(1), pp.87-101.

Tautz, I., Schöttelndreyer, M., Fricke, W. and Lehmann, E., 2010. Experimental investigations on collision behaviour of bow structures. In Ehlers S, Romanoff J. Proc. of 5th International Conference on Collision and Grounding of Ships (pp. 179-183).

Tran, T.T. and Kim, D.H., 2018. A CFD study of coupled aerodynamic-hydrodynamic loads on a semisubmersible floating offshore wind turbine. Wind Energy, 21(1), pp.70-85.

Tupling, S.J. and Pierrynowski, M.R., 1987. Use of cardan angles to locate rigid bodies in three-dimensional space. Medical and Biological Engineering and computing, 25(5), pp.527-532.

Stronge, W. J., 2004. Impact mechanics. Cambridge university press.

Vaughan, H., 1978. Bending and tearing of plate with application to ship-bottom damage. The Naval Architect, 97-99.

Villavicencio, R., Liu, B. and Soares, C.G., 2014. Experimental and numerical analysis of a tanker side panel laterally punched by a knife edge indenter. Marine Structures, 37, pp.173-202.

Vredeveldt, A. W., & Wevers, L. J., 1993. Full scale ship collision tests.

Wan, L., Gao, Z. and Moan, T., 2015. Experimental and numerical study of hydrodynamic responses of a combined wind and wave energy converter concept in survival modes. Coastal Engineering, 104, pp.151-169.

Wan, L., Gao, Z., Moan, T. and Lugni, C., 2016. Experimental and numerical comparisons of hydrodynamic responses for a combined wind and wave energy converter concept

under operational conditions. Renewable Energy, 93, pp.87-100.

Wang, G., 1995. Structural analysis of ships' collision and grounding. Ph.D. thesis, University of Tokyo

Wang, G., Arita, K., & Liu, D. (2000). Behavior of a double hull in a variety of stranding or collision scenarios. Marine Structures, 13(3), 147-187

Wevers, L. J., Vredeveldt, A. W., TNO Building and Construction Research, Netherlands Institute for Maritime Research., 1999. Full Scale Ship Collision Experiments 1998: Test of New Type Ship Side Structure, Royal Schelde, the Netherlands.

Wierzbicki, T., 1995. Concertina tearing of metal plates. International journal of solids and structures, 32(19), pp.2923-2943.

Wind Europe, 2021. Wind energy in Europe 2020: statistics and the outlook for 2021-2025, available at https://windeurope.org/intelligence-platform/product/wind-energy-in-europe-in-2020-trends-and-statistics/#downloads.

Withee, J.E., 2004. Fully coupled dynamic analysis of a floating wind turbine system ,Doctoral dissertation, Monterey California. Naval Postgraduate School.

Woisin, G., 1979. Design against collision. Advances in Marine Technology, pp.309-336.

Woisin, G., 1987. Instantaneous loss of energy with unsymmetric ship collisions. In International Symposium on Practical Design of Ships and Mobile Units, 3rdNorwegian Institute of Technology

Yamada, Y. and Endo, H., 2005. Collapse mechanism of the buffer bow structure on axial crushing. International Journal of Offshore and Polar Engineering, 15(02).

Yamada, Y. and Endo, H., 2008. Experimental and numerical study on the collapse strength of the bulbous bow structure in oblique collision. Marine Technology and

SNAME News, 45(01), pp.42-53.

Yamada, Y. and Pedersen, P., 2008. A benchmark study of procedures for analysis of axial crushing of bulbous bows. Marine Structures, 21(2-3), pp.257-293.

Yamada, Y., Pedersen, P.T. and Endo, H., 2005, June. Numerical study on the effect of buffer bow structure in ship-ship collision. In The Fifteenth International Offshore and Polar Engineering Conference.

Yu, Z. and Amdahl, J., 2016. Full six degrees of freedom coupled dynamic simulation of ship collision and grounding accidents. Marine Structures, 47, pp.1-22.

Yu, Z., Amdahl, J. and Storheim, M., 2016. A new approach for coupling external dynamics and internal mechanics in ship collisions. Marine Structures, 45, pp.110-132.

Yu, Z., Liu, Z. and Amdahl, J., 2019. Discussion of assumptions behind the external dynamic models in ship collisions and groundings. Ships and Offshore Structures, 14(sup1), pp.45-62.

Yu, Z., Shen, Y., Amdahl, J. and Greco, M., 2016. Implementation of linear potential-flow theory in the 6DOF coupled simulation of ship collision and grounding accidents. Journal of Ship Research, 60(03), pp.119-114.

Zhang, S. and Pedersen, P.T., 2017. A method for ship collision damage and energy absorption analysis and its validation. Ships and Offshore Structures, 12(sup1), pp. S11-S20.

Zhang, S., Villavicencio, R., Zhu, L. and Pedersen, P.T., 2017. Impact mechanics of ship collisions and validations with experimental results. Marine structures, 52, pp.69-81.

Zhang, Y., Hu, Z., Ng, C., Jia, C. and Jiang, Z., 2021. Dynamic responses analysis of a 5 MW spar-type floating wind turbine under accidental ship-impact scenario. Marine

Structures, 75, p.102885.

Zhao, Z., Yang, S., Suo, Y. and Zhang, Z., 2020. November. Impact analysis of the dynamic added mass coefficients of ship collision based on the external analytical method. In 2020 Chinese Automation Congress (CAC) (pp. 5742-5747). IEEE.